

Variation in the Juvenile Bony Pelvis

by

Alexandra Nadine Rocca

A thesis submitted in partial fulfillment of the requirements for the degree of

Master of Arts

Department of Anthropology
University of Alberta

© Alexandra Nadine Rocca, 2020

Abstract

The human bony pelvis is important in many anthropological studies of archaeological populations and of human evolution as it balances two important human characteristics: upright walking and the birthing of large-brained infants. While it has been thought that the female pelvis is selectively constrained by these functions, research demonstrates the pelvis is also impacted by developmental plasticity and morphological variation. This thesis studies two archaeological human skeletal collections: Later Stone Age Southern African foragers, and semi-sedentary foragers from Indian Knoll, Kentucky. The sample consists of 60 juvenile individuals from 0-16 years of age as well as 10 adults (5 males, 5 females). The size and age range of the samples offers a look at growth and development in juveniles through maturation. This research explores when in pelvic growth morphological differences arise in the iliac crest and if there are differences between populations. In order to address pelvic growth and variability, geometric morphometric analysis of 3D semilandmark data was used to evaluate shape change during growth. This 3D approach is a novel way of exploring human bone adaptability and constraints in morphological variation. Morphological change was expected to occur between each developmental age cohort. The adult sample was expected to differ based on sex. Comparisons between the mean shape in the two populations was expected to differ based on their distinct geographic locations. When the results of the patterns of shape change were examined, the majority of landmark movement occurred in the mediolateral plane of the iliac crest. The greatest difference in mean shape occurred between the first and fourth developmental cohort, which was expected due to the large difference in age. Correlation tests revealed a positive relationship between shape and size. All results were the same between the two populations. The adult populations did not differ by sex but allowed maturation trajectories to be explored. Both size

and shape maturation demonstrated highly significant positive correlations with age. This research was limited in its analysis by the fact it only examined the iliac crest. This represents only part of the entire human bony pelvis and may have limited the inferences that could be drawn from the results. Future studies should look at the entire shape of the pelvis over maturation and should further explore different populations to better understand the impact of developmental plasticity in different geographic contexts.

Acknowledgements

I would like to thank the Natural Science and Engineering Research Council of Canada for their support of this research through the Alexander Graham Bell Master's Scholarship. I would also like to thank my volunteers Chenee Merchant and Mark Klooster for their time dedicated to this project. Most of all, thank you to the members of my examination committee: Pamela Mayne Correia and Dr. Helen Kurki, who in addition to being on my committee provided support and guidance, and my supervisor Dr. Lesley Harrington for her unwavering support.

Table of Contents

Chapter 1. Introduction and Background	1
1.1 Introduction	1
1.2 Background	2
<i>1.2.1 The Bony Anatomy of the Pelvis</i>	2
<i>1.2.2 Development of the Juvenile Ilium</i>	6
<i>1.2.3 Variability in the Juvenile Pelvis</i>	10
Chapter 2. Geometric Morphometrics in Anthropology	17
2.1 Geometric Morphometrics	19
2.2 Sliding Semilandmarks	23
Chapter 3. Methods	26
3.1 Archaeological Human Skeletons	26
3.2 Estimation of Chronological Age at Death	30
3.3 Methods	32
<i>3.3.1 3D Scanning</i>	32
<i>3.3.2 Landmarking Protocol</i>	34
<i>3.3.3 Statistical Methods</i>	36
<i>3.3.4 Error Analysis</i>	39
Chapter 4. Results	40
4.1 Error Analysis	40
4.2 Patterns of Shape Change	41
<i>4.2.1 Later Stone Age Sample</i>	42
<i>4.2.2. Indian Knoll Sample</i>	45
<i>4.2.3 Combined Samples</i>	49
4.3 Mean Shape	54
4.4 Maturation	57
<i>4.4.1. Size Maturation</i>	59
<i>4.4.2. Shape Maturation</i>	61
Chapter 5. Discussion	63
5.1 Results in Context	63
<i>5.1.1 Error Analysis</i>	63
<i>5.1.2 Morphological Shape Change</i>	63
<i>5.1.3 Correlation Between Shape and Size</i>	67
<i>5.1.4 Maturation Trajectory</i>	69
5.2 Adult Shape Variation	71

5.3 Obstetric Dilemma Hypothesis	75
5.4 Revisiting the Question: Differences Between Populations	78
5.5 Research Evaluation	83
Chapter 6. Conclusion and Future Directions	88
Works Cited	91
Appendix A: Tables and Figures	102
Appendix B: R Code	116
Appendix C: Sliding Average Approach	131

List of Tables

Table 1.1 Typical developmental stages of the juvenile and adult ilium.	10
Table 3.1 Summary of the 60 juvenile skeletal individuals included in this study.	32
Table 4.1 Euclidean distance for 12 error specimens.	40
Table 4.2 Variance explained by the first three Principal Components.	41
Table 4.3 Results of correlation tests in Later Stone Age sample.	43
Table 4.4 Results of correlation tests in Indian Knoll sample.	47
Table 4.5 Results of correlation tests in combined sample.	51
Table 4.6 Results of correlation tests in adult sample.	58
Table 4.7 Results of independent samples t-tests between sex and centroid size in adults.	59
Table 4.8 Results of two sample t-test comparing male and female shape in adult sample.	59

List of Figures

Figure 1.1 Anterosuperior view of the mature bony pelvis.	4
Figure 1.2 Detailed bony anatomy of the ilium.	5
Figure 1.3 Lateral view of the three juvenile pelvic bones.	8
Figure 3.1 Map of region of South African cape from which LSA samples were recovered.	28
Figure 3.2 Map of regions Indian Knoll samples were recovered.	30
Figure 3.3 Example of ilium with 100 landmarks on the iliac crest.	35
Figure 4.1 A comparison between the extreme positions shape outlines of PC1 in LSA.	42
Figure 4.2 A comparison between the extreme positions shape outlines of PC2 in LSA.	44
Figure 4.3 Principal Component Analysis of the LSA sample along PC1 and PC2.	45
Figure 4.4 A comparison between the extreme positions shape outlines of PC1 in IK.	46
Figure. 4.5 A comparison between the extreme positions shape outlines of PC2 in IK.	48
Figure 4.6 Principal Component Analysis of the IK sample along PC1 and PC2.	49
Figure 4.7 A comparison between the extreme positions shape outlines of PC1 in combined sample.	50
Figure. 4.8 A comparison between the extreme positions shape outlines of PC2 in combined sample.	52
Figure 4.9 Principal Component Analysis of the combined sample along PC1 and PC2.	53
Figure 4.10 Images depicting shape change between the means of each age cohort	56
Figure 4.11 Principal Component Analysis LSA and IK adults along PC1 and PC2.	57
Figure 4.12 Principal Component Analysis combined adult sample along PC1 and PC2.	58
Figure 4.13 The percent size maturity of each individual in the combined sample.	60
Figure 4.14 The percent shape maturity of each individual in the combined sample.	61
Figure 4.15 Comparison between shape and size maturation trajectories.	62

Chapter 1. Introduction and Background

1.1 Introduction

This thesis explores the shape of the juvenile bony ilium in two archaeologically derived human skeletal samples. This study focuses on growth of the pelvis, which is composed of three pelvic bones (the ilium, ischium and pubis); however, only the ilium will be examined. This study is focused specifically on the iliac crest because previous research has demonstrated its potential use in the biological profile of juveniles (e.g. Schutkowski 1993; Wilson et al. 2008, 2011, 2015). Four primary questions are used to investigate morphological changes that occur during growth and development. 1) What changes in morphology occur in the iliac crest? 2) What is the average shape of the iliac crest at particular developmental stages? 3) What is the maturation trajectory in each population? and, 4) Is there a difference in the patterns of growth between two different populations? The first three questions relate to the importance of the human bony pelvis as it facilitates two uniquely human characteristics: upright walking, and the birthing of large-brained infants. The iliac crest plays a role in the formation of the birth canal while also being an important site for muscular attachments during bipedal locomotion. The interplay of these two functions, termed the obstetrical dilemma hypothesis (Dunsworth et al. 2012, Dunsworth and Eccleston 2015; Roberts and Thorpe 2014; Rosenberg and Trevathan 1995; Washburn 1960), has traditionally been viewed as a balance between selective pressures acting on the female pelvis to facilitate successful childbirth and the biomechanical adaptations required for efficient bipedal locomotion. This interplay has been invoked as the explanation for pelvic morphological differences between males and females; however, recent studies have shown that this relationship may be influenced by additional environmental factors during growth, including nutrition and activity levels (Dunsworth 2018; Wells et al. 2012; Wells 2016).

In order to address pelvic variability during growth, this study examines two archaeological human skeletal collections. Individuals were divided by age groupings (0-1.99 years, 2-6.99 years, 7-10.99 years and 11-15.99 years) based on biological stages of childhood development. The skeletons studied are non-sedentary foragers from Later Stone Age South Africa and the site of Indian Knoll, Kentucky. Both samples include immature individuals spanning development and were selected for comparison based on assumptions of distinctive ancestries and activity patterns of people from different geographic locations of the two populations. This allows the exploration of the question of whether people from different places have different growth patterns in iliac crest shape. Adaptive responses during growth, also termed “developmental plasticity” (Betti 2017; Hochberg et al. 2011; Moczek et al. 2011; Wells et al. 2012; Wilson et al. 2015), is an understudied component influencing the variability observed in pelvic form (Humphrey 1998; Wilson et al. 2015; 2017). Therefore, it is essential to consider the pelvis’ response to external factors in order to better understand the variability observed in the bony pelvis. Three-dimensional (3D) data are used as they more accurately represent shape than 2D representations of a 3D object. This thesis analyzes the shape of the iliac crest using 3D geometric morphometrics in order to understand the development of the ilium, particularly the shape of the iliac crest, and the variables that potentially impact its adult morphology.

1.2 Background

1.2.1 The Bony Anatomy of the Pelvis

The endpoint of juvenile pelvic growth is the mature bony pelvis; therefore, it is important to understand and consider typical adult pelvic form. The adult morphology of the

pelvis demonstrates considerable variability within and between populations (Betti et al. 2013; LaVelle 1995; Ruff 2002; Tague 1989); however, in order to understand when and how such variability arises during growth, it is important to comprehend the process of normal development and the characteristics that are used to estimate biological parameters. This section will briefly discuss the pelvis in general, followed by its normal growth and development. The focus will be on the ilium. The ischium and pubis will not be discussed in detail as neither element is considered in the analysis.

The pelvic girdle is composed of two *ossa coxae* and the sacrum (Figure 1.1). Each *os coxa* is comprised of three separate bones - the ilium, the ischium, and the pubis - that fuse at the triradiate cartilage of the acetabulum during puberty. Anteriorly and medially, the two *ossa coxae* articulate through a cartilaginous joint at the pubic symphysis. Posteriorly, each *os coxa* articulates with a cartilaginous synovial joint at the sacrum. Laterally, each half of the pelvis articulates with the femoral head at the acetabulum. The pelvic inlet is the primary space bounded by the promontory and alae of the sacrum, the iliopectineal lines, and the pubic crest and symphysis (Cunningham et al. 2016).

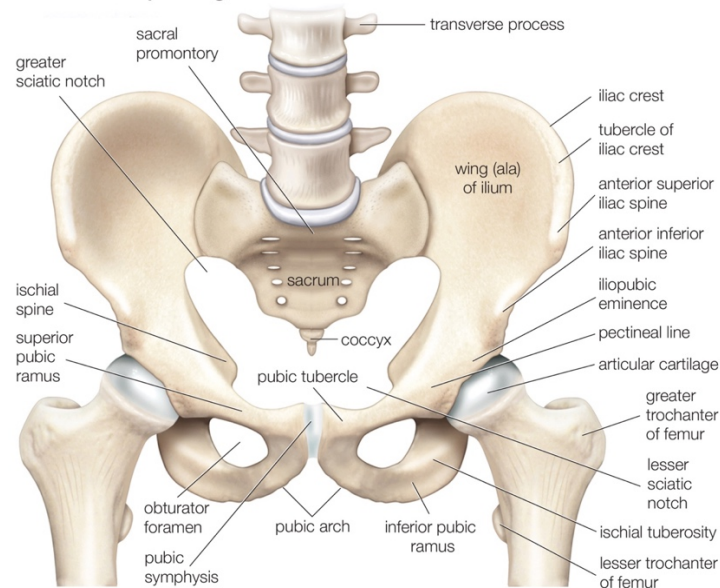


Figure 1.1. Anterosuperior view of the mature bony pelvis. Image from Encyclopedia Britannica, Inc. (Editors of Encyclopedia Britannica 2019; <https://www.britannica.com/science/pelvic-girdle/media/449463/197299>)

The ilium creates the iliac crest of the pelvis as well as the upper two-fifths of the acetabulum (Cunningham et al. 2016) (Figure 1.2). The iliac crest runs superiorly in a sinuous curve from the anterior superior iliac spine (ASIS) to the posterior superior iliac spine (PSIS). When viewed superiorly, the anterior two-thirds of the ilium display an inner concavity, called the iliac fossa, with a corresponding lateral (gluteal) convexity at the side of the iliac tubercle (Cunningham et al. 2016). At the border of the auricular surface, the sinuosity changes direction so that the posterior third of the iliac crest is concave laterally and convex medially at the non-articular sacroiliac region (Cunningham et al. 2016). Several major muscles of the trunk insert on the iliac crest demonstrating its importance in muscular function (Cunningham et al. 2016).

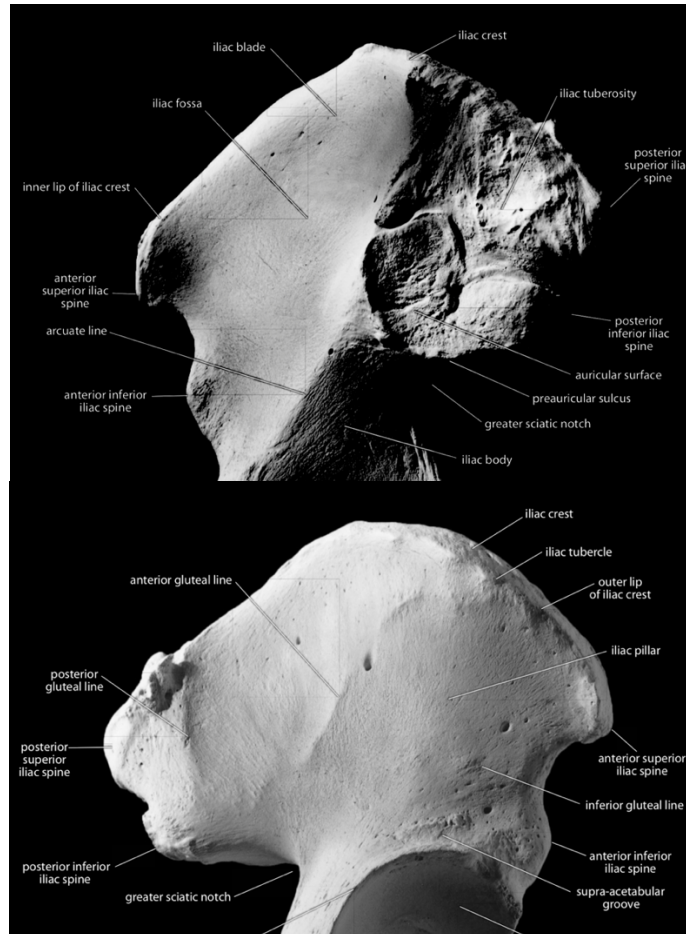


Figure 1.2. Detailed bony anatomy of the ilium. Top: lateral aspect of the ilium. Bottom: medial aspect of the ilium. Figure from White et al. (2011).

The gluteal surface is buttressed between the iliac tubercle and upper border of the acetabulum due to musculature responsible for erect posture and bipedal locomotion (Aiello and Dean 1990; Cunningham et al. 2016). The lowest part of this surface becomes continuous with the posterior ischium and demonstrates the site of union between the two bones in adolescence (Cunningham et al. 2016). The sacro-iliac joint has limited movement due to strong ligamentous attachments; however, increased joint movement in this region, as well as at the pubic symphysis, is associated with parturition. Both of these ligamentous attachment sites are often used in age estimation due to progressive bony degeneration (Brooks and Suchey 1990; Buckberry and Chamberlain 2002; Lovejoy et al. 1985; Todd 1920).

As previously mentioned, the female pelvis in particular must balance two biological processes: bipedalism and successful parturition. Researchers have argued that since bipedalism predates encephalization in human evolution, the primary modifications of the pelvis are related to optimal body weight transfer in efficient upright walking through the sacroiliac joint, the acetabulum, and the femoral heads (Cunningham et al. 2016). The pathway of weight transfer is supported by pressure lamellae in the pelvis, of which there are three: lower auricular surface to superior acetabulum, upper auricular surface to inferior acetabulum, and ischial tuberosities (Cunningham et al. 2016). These provide buttressing against compressive forces, such as sitting and shearing (Cunningham et al. 2016). Moreover, for these systems to be in place in adulthood, locomotion-related strains at specific sites would likely occur during normal growth. While this addresses the role of the pelvis in locomotion and weight-bearing, for females, the variable of obstetrics is also important to explore. Biomechanical effects of body weight transfer in addition to earlier female puberty result in pelvic dimension variability and sex-based differences (Cunningham et al. 2016). Sexual dimorphism in the pelvis supports that selection has acted on pelvic shape, resulting in different functional requirements; however, the variability highlighted by Dunsworth (2018) in modern pelvic bony anatomy emphasizes that other factors, such as metabolic constraints, health and disease, and activity during growth and adulthood impact adult pelvic morphology. Therefore, considering the adaptive responses of the juvenile ilium may help to explain adult variability that differs from patterns of sexual dimorphism.

1.2.2 Development of the Juvenile Ilium

With a basic understanding of the endpoint of growth, the adult bony pelvis, it is now important to consider the development of the juvenile ilium specifically (Table 1.1), and most

importantly, the different variables that may impact its morphology. The early development of the pelvic bones will be briefly discussed, followed by an analysis of the timing of ossification and typical growth timelines of the ilia. Variability in the juvenile pelvis will be further explored considering external variables and their impact on normal growth.

The pelvis is developed from the lower limb bud at approximately 28 days in utero, which initially creates a mass of mesenchymal cells in the border of the ectoderm (Cunningham et al. 2016). Chondrification begins in the blastemal structures between weeks 6 and 7 in utero, and first appears in the iliac mass near the acetabulum (Cunningham et al. 2016). By 9 weeks in utero, ossification has spread covering the internal and external surfaces of the iliac blade; this ossification continues as a radiating fan creating an internal and external shell of bone (Cunningham et al. 2016). By the beginning of week 12 in utero, the cartilaginous pelvis is nearly complete (Cunningham et al. 2016). Between 12-13 weeks in utero, the primary centre of ossification for the ilium appears in the roof of the acetabulum near the greater sciatic notch (Cunningham et al. 2016). By 4-5 months in utero, the ilium is recognizable due to the formation of the sciatic notch and the shells of bone (Cunningham et al. 2016).

At birth, the primary ossification centres of all three pelvic bones are developed and identifiable (Cunningham et al. 2016) (Figure 1.3). Their morphology does not initially change significantly; however, rapid growth occurs in the first 3 months followed by slowing development until 2-3 years old (Cunningham et al. 2016). The rate of growth decreases further after this age range until puberty and the adolescent growth spurt (Cunningham et al. 2016; Yusof et al. 2013). This study includes individuals spanning a wide range of ages (infancy to late adolescence) in order to examine morphological change that occurs over growth and development, known as ontogenetic variability.

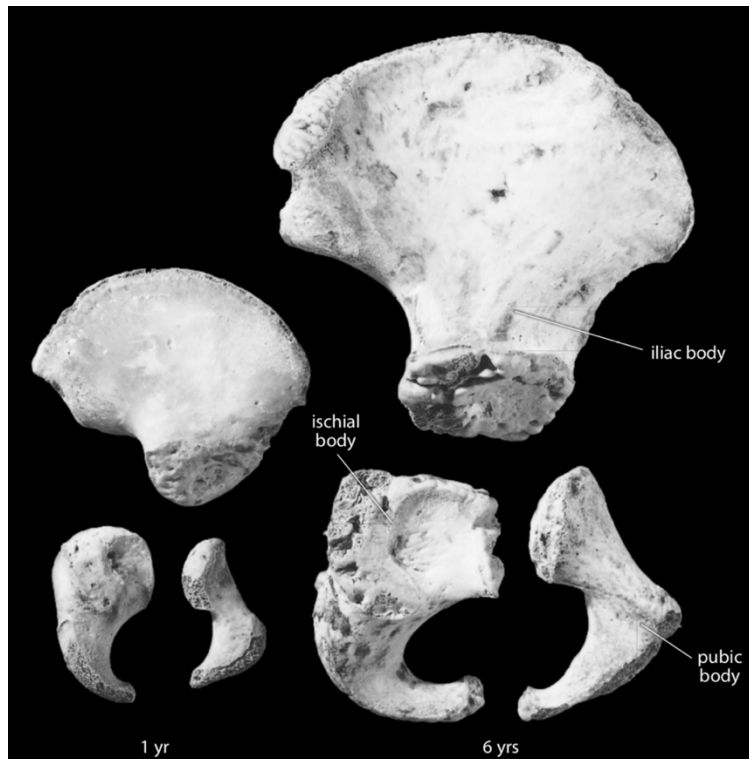


Figure 1.3. Lateral view of the three juvenile pelvic bones: ilium, ischium and pubis. The left images depict the bones of a one-year old. The right images are of a six-year old. This image demonstrates that the fetal ilium is recognizable at an early age and also depicts the size and shape differences that occur between the two ages. Image from White et al. (2011).

Secondary centres of ossification of the ilium appear in the proximal crest and distal acetabulum (Cunningham et al. 2016). Growth of the acetabulum will not be discussed in detail as this region is not explored in this thesis. Briefly, the acetabulum develops through a triradiate cartilage from each of the three bony elements and begins to fuse at approximately 11-16 years in females and 11-18 years in males (Cardoso 2008; Cunningham et al. 2016). This union and the wide age range of fusion times can impact growth patterns, focusing areas of pubertal changes to other epiphyseal regions.

Following fusion of the triradiate cartilage, the secondary epiphyses of the pelvis fuse in the subsequent order: AIIS, iliac crest, ischial tuberosity, pubic symphysis. The AIIS begins to form between 10-13 years and fuses between 16-20 years (Cunningham et al. 2016). The crest

epiphysis itself is thin, long, and curved, assuming the shape of the iliac crest (Cunningham et al. 2016). Ossification of the crest begins at approximately 12-13 years in females and 14-15 years in males, with the anterior half forming first (Cunningham et al. 2016). Timing of fusion is variable; initially the anterior and posterior halves fuse to form a unified crest. Fusion begins anteriorly at the ASIS and progresses posteriorly, with the region of the superior sacroiliac joint typically fusing last (Cunningham et al. 2016). Partial fusion of the iliac crest can be seen between 14-26 years in females and 15-24 in males (Cunningham et al. 2016). This section has summarized the general timeline of pelvic development; however, it is important to consider how and when variation arises, and why it develops in certain regions given the expected patterns of growth.

Table 1.1. Typical developmental stages of the juvenile and adult ilium (Adapted from Cunningham et al. 2016.)

Timing	Process
Prenatal Month 2-3	Ilium commences ossification
Birth	Primary bony components represented
6 Months	Ilium prominence on acetabular extremity formed by iliopectineal line
2 Years	Anterior border ilium bent forwards in vertical plane
3-4 Years	Demarcation of iliac and ischial articulation sites defined on pubis
4-5 Years	Non-articular acetabular area well defined on ilium
5-16 Years	Fusion ischiopubic ramus
9-10 Years	<i>Os acetabuli</i> and ossific island in triradiate cartilage
10-13 Years	Centre appears for AIIS
11-16 Years	Acetabulum commences and completes fusion in females
12-15 Years	Superior acetabular epiphysis appears, and iliac crest commences ossification in females
14-18 Years	Acetabulum commences and completes fusion in males; iliac crest commences ossification in males; iliac crest commences fusion in females
18 Years	AIIS fused
17-20 Years	Iliac crest epiphysis commences fusion in males
20-23 Years	Iliac crest completes union

1.2.3 Variability in the Juvenile Pelvis

Excluding individual variation, growth typically occurs in a predictable sequence due to biological signals. It is for this reason phenomena such as tooth eruption can be used for age estimation of juveniles; there is a predictable pattern and rate of growth for the dentition. This study will focus on the pattern and rate of growth for the pelvis, specifically the ilium. Before

being able to explore growth among the individuals in the study populations, it is necessary to understand what is known about “normal” pelvic growth patterns.

An aspect of pelvic growth that cannot be ignored is the role of sexual dimorphism; it is a by-product of hormone-driven growth and development of the pelvis. Due to resultant sex differences in the pelvis, many researchers have focused on growth of the pelvis in this context. For example, Coleman (1969) examined longitudinal pelvic growth in 14 males and 16 females, aged 9 to 18 years using 2D fixed landmarks to explore variation in growth during the adolescent growth spurt, particularly related to sexual dimorphism. Excluding individual variability, Coleman (1969) concluded that many differences between male and female pelvis shape are due to the relationship of total growth in the internal acetabular and pubic regions in comparison to the total growth in other regions. In particular, females show greater total growth in inner regions than males. The pubertal growth spurt starts from approximately 10-14 in females and 14-19 in males (Rissech and Malgosa 2005) and coincides with an increase in growth hormone secretion initiated by the gonadal steroid hormone and adrenal androgens (Fischer and Mitteröcker 2017). The patterns of pelvic growth observed may be due to the earlier onset of puberty in females, allowing this region to diverge from male patterns of growth earlier, totalling a greater degree of differential growth. Different functional regions will develop according to energetic constraints on the production and maintenance of different tissues in tandem with developmental stages in a child (Humphrey 1998). For example, the skull demonstrates sexual dimorphism through differential growth duration (Rogers 1991, 2005); however, the pelvis is unique in that sex-specific traits are primarily due to different growth patterns, which reshape and remodel bony regions (Coleman 1969).

Humphrey (1998) found overlap in all skeletal dimensions between male and female values, emphasizing the relatively low levels of sexual dimorphism in modern humans compared to other great apes. Humphrey (1998) concluded that pelvic growth occurs later than long bone length growth, and fits in the category of intermediate-late growth (categories defined by Humphrey 1998). For both the minimum and maximum iliac breadth, 70% of adult size was achieved by approximately 9 years old, and 90% was reached by 17-18 years old (Humphrey 1998). The increasing trend found in the mean level of sexual dimorphism over the growth categories, especially upon achieving 90% of adult size, suggests the influence growth has on the development of sexual dimorphism (Humphrey 1998). Early growing skeletal elements may not display as much sexual dimorphism as later growing parts, such as the pelvis, due to the functional growth trajectory as well as different growth rates. An early-growing skeletal element may complete growth prior to divergence of growth trajectories at puberty (Humphrey 1998). Both growth rate and duration were identified as important factors in the development of pelvic variability specifically, as a continuum of traits over time; however, differences in growth rates and growth patterns were emphasized as the driving factor of sexual dimorphism in the pelvis (Humphrey 1998; Rogers 1991, 2005). Therefore, it is important to consider both growth rates and patterns of growth when examining pelvic variability. It is also reasonable to expect a majority of this growth is achieved slightly later in development, at approximately 9 years of age. This later growth may help to explain why the pelvis displays variability more than other skeletal regions as it is susceptible to environmental influences over its maturation.

With respect to regional patterns of the ilium, the mean total growth of the anterior crest is larger in males than in females while the mean growth of the posterior region is slightly larger in females (Coleman 1969). The difference between these means has not demonstrated statistical

significance in studies. The region with the greatest growth differentiation is the point of most pelvic height and pelvic breadth (Coleman 1969). Equal growth in the middle one-fourth of the iliac crest is present, with superior and lateral movements (Coleman 1969). The pattern of growth is slightly different between sexes. In earlier years, the direction of male growth is more lateral than superior, which reverses with time, while females have the opposite growth pattern (Coleman 1969). The point of greatest pelvic breadth moves in the superolateral direction, approximately 50-70 degrees from the vertical (Coleman 1969). Overall, females demonstrate a greater final lateral shift in this measurement (Coleman 1969). The anterior superior iliac spine (ASIS) also displays sex-specific growth patterns. The male ASIS moves superolaterally 60-70 degrees from the vertical, and as previously mentioned, this movement is initially lateral followed by superior shifting (Coleman 1969). In females, the direction of growth is similar, but 60% of females in the study by Coleman (1969) displayed movement laterally without superior displacement. The posterior superior iliac spine (PSIS) differs slightly between sexes with males 0-20 degrees superolateral from the vertical, and females 20-30 degrees (Coleman 1969). This results in a wider and broader female pelvic shape with less prominent ischial spines and a narrower subpubic arch in males (Lewis et al. 2017). The female inlet is wider, the iliac blades shorter, the subpubic angle larger, and the sacrum is also shorter and more outwardly projecting (Fischer and Mitteröcker 2017). While these observations provide information on sex-specific growth patterns, the analysis was conducted on 2D radiographs in Coleman's study (1969), which may have impacted the interpretations by limiting observations to a single plane. Humphrey (1998) found that there are insignificant sexual differences, specifically for the measurement of maximum iliac breadth. These results are also supported by Coleman (1969).

Other pelvic regions explored by Coleman (1969) did not result in significant of a difference between sexes. With respect to the acetabular region, individual variation was present; however, no significant sex differences were apparent in acetabular growth (Coleman 1969). The ischial tuberosity and ischiopubic ramus showed no significant sex differences for total growth, although females did have slightly extended growth in the ischiopubic ramus (Coleman 1969). As supported by other studies (e.g. Rissech and Malgosa 2005) the only sex-based difference in the pubis was total length, with many females showing a greater length, but it was not statistically significant (Coleman 1969). Regarding the greater sciatic notch, which is often used in adult sex estimation, Coleman (1969) stated that growth varied heavily based on individuals, with the only significant difference in juveniles at the ischial spine. Overall, Coleman (1969) emphasized that the pelvis demonstrates considerable overlap in the direction of growth, which is partially due to large individual variation.

While it is clear that there is differential growth and a general understanding of how variability is expressed in the ilium between sexes, it is important to understand what causes these local changes. Coleman (1969) states that the driving force of local change is the yearly pattern of directional growth, as the male and female patterns typically contrast. As discussed above, in males the growth is more superior later in growth whereas in females growth is mainly lateral (Coleman 1969; Koļesova 2014). Considering overall pelvic shape rather than specific regions, it has been theorized that males have greater external dimensions, while females have greater internal dimensions to facilitate childbirth (Coleman 1969). One reason for this that has been proposed is males have a slightly larger pelvic complex before the adolescent growth spurt. On the other hand, it may be attributed to the earlier age at which the growth spurt occurs in females; this ceases growth in females earlier than in males, allowing for continued growth in

males (Coleman 1969). Coleman (1969) emphasizes that differences in the pelvic inlet are due to functional demands, since lower iliac height in females is directly related to the obstetric role of the pelvic complex. Studies have shown that overall inlet shape is similar between males and females (Kolesova 2014; Kurki 2013; Tague 1989). Instead, dimorphism is the most pronounced in the lower part of the pelvic cavity (Kolesova 2014; Kurki 2013; Tague 1989).

Wilson et al. (2015) expanded on the analysis of growth in the pelvis using geometric morphometrics and the ilium, specifically the shape of the greater sciatic notch, auricular surface, and iliac crest. In their results, females were found to have a shorter shape trajectory (the relationship between time and shape growth patterns) than males, but both sexes demonstrated shape change correlated with age. Wilson et al. (2015) found that the auricular surface demonstrated considerable shape variability throughout ontogeny. Wilson et al. (2015) also concluded that at younger ages, the shape between males and females were more similar. Regarding maturity of size and shape, males were more size mature, achieving adult size at a quicker rate, in the iliac crest. On the other hand, females had a greater maturation rate in the greater sciatic notch and auricular surface (Wilson et al. 2015). Therefore, it is evident that maturation impacts shape and size in both males and females, resulting in adult dimorphism. Females mature at a quicker rate; however, males accumulate greater change (Wilson et al. 2015). Moreover, as found by Humphrey (1998), accuracy of sex estimation increased with age, further demonstrating the role of growth and maturation on pelvic shape variability. While the above study was a 2D approach to pelvic shape analysis, Wilson et al. (2016) elaborated on the method by using 3D geometric morphometrics on the juvenile iliac crest. The authors concluded that curvature of the crest was more pronounced in males than females in each age group. Moreover, the sinuosity of the iliac crest, especially the anterior half, increased with age in both

sexes (Wilson et al. 2016). Older juvenile females were found to have a similar iliac crest shape as younger males; however, the male shape diverged through growth from the female shape, especially between 5-9.99 years of age. This increased sinuosity on the posterior section was present when compared to females of all age groups (Wilson et al. 2016). Despite the results of this study and those done previously, Wilson et al. (2016) emphasize that sexual dimorphism during growth of the juvenile pelvis is still poorly understood, requiring further research.

Overall, this section demonstrates the role of sexual dimorphism in pelvic variability. While it is an aspect of pelvic growth, this variable was not known in this study. By examining two populations of unknown sex, this study is unique by exploring if there are detectable differences in the ontogeny of ilium shape without considering the direct impact of sexual dimorphism.

Chapter 2. Geometric Morphometrics in Anthropology

Geometric morphometrics is widely becoming more popular in anthropology for the analysis of morphology especially when considering human origins and evolution (Slice 2007). Several human skeletal elements have been landmarked in 2D and 3D including the scapula (Scholtz et al. 2010), the ribs (Gayzik et al. 2008), the skull (Bastir et al. 2011; Smith et al. 2013), and the pelvis (Bytheway and Ross 2010; González et al. 2007). Fragments of skeletal elements have been studied using geometric morphometrics, demonstrating its applicability in human paleoanthropology and archaeology (Bytheway and Ross 2010). Geometric morphometrics is a powerful statistical tool in anthropology because it considers maximum variation, but more importantly, the methodology provides visualization tools to demonstrate shape changes (Slice 2007). While it is clear this methodology has wide applications in various skeletal elements in both ancient and modern humans, Lycett and von Cramon-Taubadel (2013) emphasized that the pelvis is of particular importance to study due to its significance in exploring human evolution. This is because pelvic size and shape are impacted by variables such as obstetric constraints, environmental conditions, locomotion, overall body size, and the complex anatomy of the 3D pelvis itself, which is comprised of three fused bony elements. While many visual methods have been developed to examine pelvic morphology for sex-estimation (e.g. Buikstra and Ubelaker 1994; Phenice 1969; Sutherland and Suchey 1991) or the evolution of the pelvis (e.g. Hammond et al. 2018; Lycett and von Cramon-Taubadel 2013), the subjective nature of visual assessments result in both inter- and intra-observer error (Bytheway and Ross 2010). In order to objectively assess physical attributes, geometric morphometrics can be applied. This methodology results in a quantifiable set of measurements, which increases repeatability and statistical value (González et al. 2009). Geometric morphometrics allows for the precise

quantification of size and shape and the ability to compare between different subgroups. Such a method allows curves and protrusions to be quantified, which may be missed in other morphological assessments (González et al. 2009; Steyn et al. 2004). The objectivity in combination with its powerful visualization of morphological change make geometric morphometrics an effective technology for the analysis of juvenile shape and its variability.

Several studies have successfully used geometric morphometrics in the exploration of ontogeny and sexual dimorphism in the juvenile pelvis (e.g. Mokrane et al. 2013; Wilson et al. 2011, 2015, 2016; Wilson and Humphrey 2017). Initially, Wilson et al. (2011, 2015) used 2D geometric morphometrics in their analyses. Of particular importance in this research is the work of Wilson et al. (2015) as it provided a methodological base from which this thesis expanded upon. In their study, Wilson et al. (2015) used 2D outline-based geometric morphometrics of three traits (greater sciatic notch, auricular surface, iliac crest) on ilia of known sex and age from London, England and Lisbon, Portugal in order to explore differences in shape over postnatal ontogeny. A total of 50 equally spaced semilandmarks were placed on the outline of the greater sciatic notch and auricular surface, with 100 semilandmarks on the iliac crest. Due to the ability of geometric morphometrics to separate size from shape, Wilson et al. (2015) were able to explore three potential ontogenetic trajectories to determine how and when male and female size and shape maturations diverge. In later research, Wilson et al. (2017) quantified curvature in the iliac crest using 3D geometric morphometrics. The 3D use of geometric morphometrics is a powerful tool for shape analysis because it facilitates shapes to be interpreted in 3D instead of imposing 2D structures or measurements on a 3D shape. While this thesis primarily follows the methods of Wilson et al. (2015), it differs in its use of 3D landmarks. Furthermore, it expands on the research of Wilson et al. (2016) by not only looking at ontogeny in 3D but also exploring the

potential influence of population variation. It is evident geometric morphometrics can be used in the analysis of ontogeny in juvenile ilia; however, it is important to better understand the basics of this methodology and why it is a powerful tool in such analyses.

2.1 Geometric Morphometrics

While this is not a comprehensive summary of the theory and methodology of geometric morphometrics, it is important to have a general understanding of how shape is isolated and studied when using this method. In geometric morphometrics, measurements can be obtained through lengths, ratios, angles, open or closed curves, or landmark data in either two or three dimensions using Cartesian coordinates. Landmarks are precisely located points on a specimen that are homologous, and therefore comparable, between individuals in the study population (Webster and Sheets 2010). This thesis employed landmark data due to its successful use in previous literature on the juvenile and adult pelvis. It also facilitated the analysis of a curved feature, which is often problematic. The necessity of choosing landmarks on the basis of homology has been debated as many anatomical regions lack discrete landmarks (Baab et al. 2012). However, through the use of semilandmarks, such typically featureless surfaces that would be challenging to quantify can be accurately captured and measured. This problem will be addressed below in the discussion of semilandmarks.

While powerful and informative, there are several limitations to consider in landmark data. In some methodologies precise points are selected based on anatomical features. This choice results in the potential loss of important information depending on the anatomical region and condition of the specimen. Therefore, landmark selection must be carefully considered to understand the limitations of the study and how best to collect data. Three different types of

landmarks are defined: Type One, Type Two, and Type Three (Bookstein 1991; Zelditch et al. 2012). Type One landmarks represent the meeting of different margins (i.e. the coronal and sagittal sutures). Type Two landmarks represent points of maximum or minimum curvature (i.e. medial and lateral curvature of the iliac blade). Type Three landmarks represent an extreme point in a dimension (i.e. the most anterior point). Once each specimen has been landmarked with the same points, analysis can continue in order to isolate shape as the morphometric of interest.

Before conducting such analyses, it is important to understand how size and shape are defined and isolated in geometric morphometrics. Size and shape have specific definitions when considered in geometric morphometrics. Size is the scale of an object, while shape is the proportion of the object apart from scale (Bookstein 1989; Klingenberg 2013; Mitteröcker and Gunz 2009); in other words, shape is the arrangement of the parts relative to each other in a given object. Most importantly, shape does not consider size, location, or orientation (Bookstein 1989; Klingenberg 2013). It is necessary for size, location, and orientation to be omitted in geometric morphometric analysis so that the landmarks between different specimens are comparable between one another, leaving shape as the only variable to assess. The process that isolates shape from the variables size, location, and orientation, is called Procrustes superimposition (Mitteröcker and Gunz 2009). In this process, landmarks of the specimens are shifted to a common position by scaling to a standard size and rotation until the best fit to a standard is reached. Centroid size, which is the square root of the sum of the squared distances of all landmarks from the center of gravity of the specimen, is often used to standardize in generalized Procrustes superimposition (Zelditch et al. 2012). In this process, all specimens are scaled to a centroid size of one and then shifted to coordinate (0,0) (Zelditch et al. 2012). The final step is the rotation of the landmark configurations of each specimen around the centroid

until an overall best fit is achieved (Zelditch et al. 2012). In generalized Procrustes superimposition, pair-wise fits for each specimen are configured to a common or target consensus. Following this application, the original landmark coordinates are now Procrustes coordinates (Rohlf and Slice 1990; Zelditch et al. 2012). With the data in this format, Procrustes distance can be calculated in order to quantify shape difference. Procrustes distance is the sum of the squared coordinate differences between corresponding landmarks and represents shape in geometric morphometrics (Zelditch et al. 2012).

Another benefit of geometric morphometrics is the visualization of shape change. Several visualization methods can be used including a scatter plot, landmark displacement graphs, or thin-plate spline analysis (Webster and Sheets 2010). Shape change is the relative displacement of landmarks, which can be visually represented (Klingenberg 2013). The process of Procrustes superimposition creates what is termed the “morphospace,” which is a multidimensional space in which the shape of the specimens from the landmark configurations are situated relative to one another to demonstrate shape change. A drawback to this visualization is that multiple dimensions are required and therefore it is too complicated to properly visualize shape change in this space. Therefore, the tangential space is used. Klingenberg (2013) outlines that this process is similar to projecting Earth’s globe on to a map; the points representing shapes in the data are projected onto the tangent space at the point of mean shape allowing visualization of shape change and parametric statistical analysis (Baab et al. 2012; Klingenberg 2013).

The most common method used to visualize variation in shape is principal component analysis (PCA) in order to look at overall total variation rather than subgroup structures. This analysis is often first used when exploring variation as the variables from the Procrustes superimposition are uncorrelated with each other and therefore account for the maximum

possible amount of variation (Mitteröcker and Gunz 2009). The Procrustes superimposition links to the shape space, allowing shape change to be visualized; however, it is important to remember not all shape changes will be biologically relevant (Klingenberg 2013). It is for this reason the actual drivers of variation in each axis must be explored further. The resultant Procrustes coordinates (PC) derived from the PCA represent the dimensions of greatest shape variation. The axes of the PCA are aligned with the main axes of variation in the data, producing an ellipsoid (in 3D) with the long axis principal component 1 (PC1) and the shorter axis principal component 2 (PC2). Typically, PC1 represents the most variance in the data, with PC2 representing the next greatest portion of the leftover variance, in a 2D scenario. In both 2D and 3D analyses there are multiple dimensions and therefore multiple principal components that must be explored. PC1 is still associated with the most variance, with the following PCs representing the remaining variance in decreasing amount of variation. The principal components are derived from the PCA and are the same as the sum of the variance (Mitteröcker and Gunz 2009). PC scores are important because they represent the pattern of variation in data, which are computed as a linear combination of the original variables and are the weighted sum of the variables (Mitteröcker and Gunz 2009). The PC coefficients represent the effects of the change in a given PC with weighting of the different variables (Mitteröcker and Gunz 2009). In other words, it indicates how close a given PC axis is aligned with the original coordinate axis and the change associated in the original variables with change in the PC scores. The PC scores produced from such analyses can be used in statistical tests to determine if there are significant correlations or differences between shape and other variables of interest.

In its traditional use, geometric morphometrics has been shown to be a powerful statistical tool; however, there are limitations to which bony elements it can be applied.

Traditional landmarks used in geometric morphometrics require homologous and identifiable structures between all specimens in a sample (Webster and Sheets 2010). Curves, borders, and surfaces, which are present on many bony elements, challenge this traditional approach since such features often do not have easily identifiable landmarks (Gunz and Mitteröcker 2013). Therefore, new approaches using sliding semilandmarks have been developed to accommodate for difficulties in selecting numerous homologous landmarks. Semilandmarks offer a solution to this problem by incorporating information about morphological structures not included using traditional landmarks (Perez et al. 2006).

2.2 Sliding Semilandmarks

The concept of semilandmarks was first introduced by Bookstein in 1991. Its use in 2D analysis was explored in 1996 by Bookstein, with advances in 3D methods by Gunz et al. (2005). Initially Bookstein referred to these landmarks as “quasilandmarks” and they were used where points do not have local definitions. The model underlying quasilandmarks was that variation tangential and normal to the outlines must be weighted equally, and group differences were modelled as equally plausible regardless of the direction they were in space (Bookstein 1996). Data are produced through a preliminary relaxation of points on a flexible curve, which is termed spine relaxation. This allows curves as a whole to be analyzed through semilandmarks, which describe a relation to a template (Bookstein 1996). Semilandmarks still follow the rule of homology as they are bound by set fixed homologous landmarks; however, the curve or surface is comparable between specimens (Perez et al. 2006).

The two computational approaches in the analysis of semilandmarks are the same as traditional landmarks: Procrustes superimposition or thin-plate spline (Gunz and Mitteröcker

2013). The first stage in analysis is distributing the same number of semilandmarks on the required curve or surface in each specimen. The number and order of placement is important and since the semilandmarks will slide relative to each other, their exact position is less critical. The second step is allowing the spacing of the semilandmarks to be optimized by allowing them to slide (Gunz and Mitteröcker 2013). After this step, the semilandmarks are treated in the same statistical manner as traditional landmarks in analysis (Gunz and Mitteröcker 2013).

The number of semilandmarks placed on a curve or surface depends on the complexity of the feature. Gunz and Mitteröcker (2013) emphasize that oversampling by placing dense semilandmarks is essential in effectively visualizing the shape and estimating any missing portions. This is further supported by Gunz et al. (2005), who state more semilandmarks than specimens is often required in order to create detailed morphometric data sets. However, many multivariate methods require an excess of specimens over variables, and therefore dimension reduction may be required later in analysis (Gunz and Mitteröcker 2013). Some geometric approaches have involved placing equidistant points along a curve; however, this can lead to statistical and visual artifacts as the space is arbitrary (Gunz and Mitteröcker 2013). Allowing the semilandmarks to slide removes the arbitrary spacing by optimizing the semilandmark positions with respect to the average Procrustes shape coordinates (Gunz and Mitteröcker 2013).

The following steps outline the process of sliding semilandmarks, as outlined by Gunz and Mitteröcker (2013). Semilandmarks slide relative to an arbitrary template from which a Procrustes superimposition is conducted. The semilandmarks slide with respect to the average Procrustes shape along the tangent structure (Gunz et al. 2005). The Procrustes average configuration is then computed, and all new tangents are created. The specimens are then relaxed

against the Procrustes average configuration (Gunz et al. 2005). While the theoretical background behind semilandmarks is complicated, it has been shown to be an effective method of geometric morphometrics in the analysis of featureless curves and surfaces, such as the juvenile pelvis (Wilson et al. 2015, 2016). This computational approach facilitated the examination of a relatively featureless curve of the pelvis: the iliac crest.

Chapter 3. Methods

3.1 Archaeological Human Skeletons

One of the two samples included in this study were Later Stone Age (LSA) foragers from South Africa. The skeletal remains studied were recovered from archaeological sites located throughout the coastal foregrounds of the Cape Fold Mountains of South Africa (Figure 3.1) in a region known as the Greater Cape Floristic Region (GCFR) (Pfeiffer and Harrington 2018). This region spans 80 000 km² and includes a high degree of floral diversity including underground storage organs, terrestrial plant and mammal food resources, and coastline marine resources (Deacon and Deacon 1999; Pfeiffer and Harrington 2018). Research has shown that an understanding of the region and the resources available would require skills in hunting and gathering as well as connectivity throughout the region socially (Pfeiffer and Harrington 2018). Both skeletal and paleodemographic characteristics support trekking for resources to exploit plant and animal resources through hunting and tool use (Pfeiffer and Harrington 2018). The human burials were found in rock shelters and sand dunes, and typically were individual internments (Harrington 2010; Pfeiffer and Harrington 2018). Uncalibrated radiocarbon dates have placed the burials to approximately 8000-800 years before present in the Later Stone Age, which has also been confirmed by customary LSA hunter-gatherer mortuary customs (Deacon 1976; Harrington 2010; Mitchell 2002). Genomic evidence dates the populations in the region to as early as 160 000 to 110 000 BP (Nielsen et al. 2017) with homogenetic traits in cranial shape, dental size and shape, and diverse skeletal dimensions that support the existence of humans in the region for many millennia and the LSA sample descending from these earlier populations (Pfeiffer and Harrington 2018).

The skeletal elements studied come from collections of Later Stone Age human remains curated by several South African institutions: Albany Museum (ALB), National Museum of Bloemfontein (NMB), University of Cape Town (UCT), Iziko South African Museum (SAM), and McGregor Museum (MMK). Individuals in the burial population were small in body size with no individuals greater than 178 cm tall (Pfeiffer and Harrington 2018). Most importantly, when juvenile growth trajectories were studied, there was no indication of delay in the tempo of stature growth indicating this selection was stable and not due to disrupted development and poor health impacting growth in children (Pfeiffer and Harrington 2018). Considering the pelvis, the bi-iliac diameter indicates a low body mass. The women of LSA had narrow bi-iliac breadths but relatively large pelvic mid-planes and outlet canal planes (Pfeiffer and Harrington 2018). This indicates adaptive allometry due to selective pressures in these populations (Kurki 2017; Pfeiffer and Harrington 2018). Physical activity in the LSA population is indicated through plastic responses in cortical bone. For example, the lower limbs are strong relative to body size, which supports high levels of terrestrial mobility (Pfeiffer and Harrington 2018). While women of the LSA had balanced upper arm cortical bone, dominance asymmetry was found in males, indicating the different roles in hunting and gathering based on sex (Pfeiffer and Harrington 2018).

Considering the juveniles of the population, there are no signs of stress or deprivation impacting growth, or the evidence of chronic infection or disease (Pfeiffer and Harrington 2018). Patterns of lower limb strength are seen in adolescence and may be due to sexually dimorphic activities (Harrington 2010; Pfeiffer and Harrington 2018). Linear enamel defects do demonstrate children of the LSA population may have experienced regular minor interruptions in growth, but there is no marker of intense, long-lasting illness or malnutrition (Pfeiffer and

Harrington 2018). In the absence of such evidence, it is likely the juveniles' early mortality is due to acute events. Overall, the skeletons of LSA show the expected patterns of immediate-return hunter-gatherers whom were mobile people but maintained a diverse and nutritionally balanced diet (Pfeiffer and Harrington 2018).

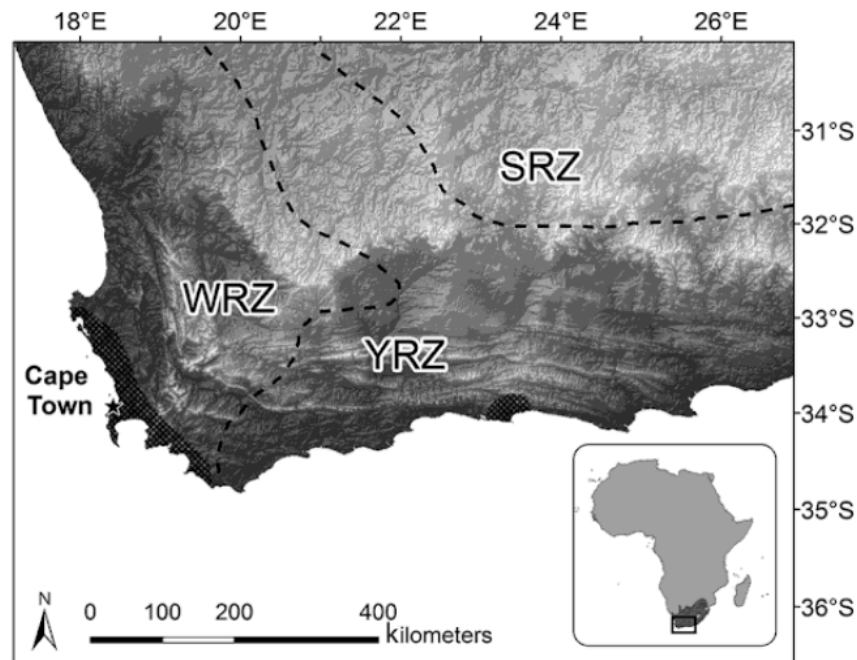


Figure 3.1. A map indicating the region of the South African cape from which samples were recovered from Later Stone Age sites. Zones of winter (WRZ), summer (SRZ) and year-round (YRZ) rainfall are indicated. Image from Pfeiffer and Harrington (2018).

The Indian Knoll sample were hunter-gatherers buried in association with prehistoric shell middens on the Green River in Kentucky, United States (Figure 3.2). The various sites have produced abundant cultural artifacts, and more than 1000 human skeletons (Claassen 2018; Johnston and Snow 1961; Snow 1948; Webb 1946). Of these skeletal individuals, 880 documented burials are conserved at the University of Kentucky Museum of Anthropology and were originally excavated by Webb (1946). Carbon-14 dating has placed the average age of the sites between 4508 ± 365 to 6100 ± 315 before present (Johnston and Snow 1961; Rothschild 1979). Individuals at these sites are classified as hunter-gatherers due to artefacts, food remains,

and the lack of defined permanent villages (Johnston 1962; Rothschild 1979). Burials were found in all stages of the midden formation, and were typically independent but closely spaced, sandy burial pits (Webb 1946).

The Indian Knoll site likely represents 500 years of occupation based on midden debris (Snow 1948). It is situated on a natural levee that at one time historically was the main bank of the Green River (Snow 1948). The land bordering the site consisted of rolling hills, steep bluffs, and was likely mostly forested containing small mammals for hunting (Snow 1948).

Hypertrophy of the leg muscles indicates dynamic movement in the population through hunting and gathering freshwater clams as well as plant sources such as walnuts, hickory nuts, and acorns (Snow 1948; Webb 1946). Habitual squatting was also common practice in food gathering or preparation due to the high presence of squatting facets in the population (Snow 1948). The skeletal individuals consisted of 706 subadult individuals; 46% of the entire sample are infants indicating a high mortality rate at birth (Johnston 1962). Of the adults present, their body type was described as slender to medium but short (153.2-165.6 cm in height) (Snow 1948).

Compared to their body proportions the adult individuals had relatively longer lower arms and lower legs (Snow 1948). This body stature may be due to depressed growth rate due to environmental factors; however, genetics cannot be ruled out as acting in conjunction with external factors such as health (Johnston 1962). With respect to the pelvis, Snow (1948) emphasized less sexual dimorphism than expected in a modern population. His metric findings indicated males were only slightly larger than females, with the greatest sex-based difference in the bi-ischiatic and inter-spinous diameters (Snow 1948).

Considering the high infant mortality of the population, investigations were made into the general health of the Indian Knoll population. Snow (1948) found across millennia there were

many striking similarities and low statistical variability, indicating homogeneity. A total of 60% of the adult population had lumbar arthritis. Moreover, Snow (1948) hypothesized their gritty diet contributed to the extreme dental wear found in the population and may have resulted in infectious dental abscesses. Abundant osteoporosis indicated dietary deficiencies as well (Snow 1948).

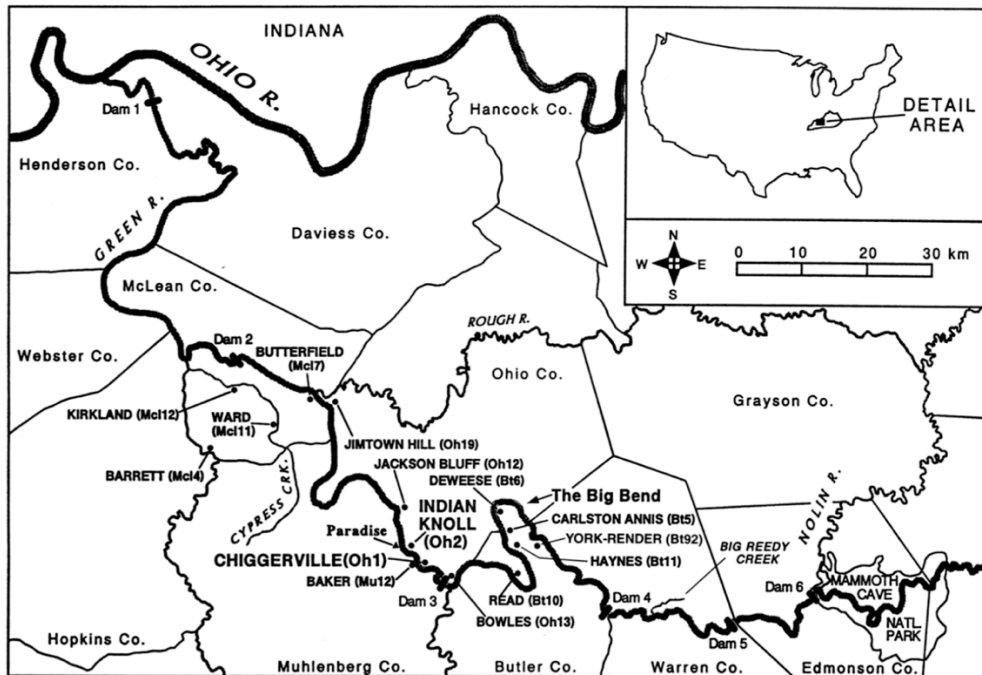


Figure 3.2. A map of regions from which Indian Knoll individuals have been collected. Image from Morey et al. (2002).

3.2 Estimation of Chronological Age at Death

This thesis focuses on how growth and variation contribute to pelvic variation, therefore the skeletal elements selected for study are those from sub-adult individuals. A developmental restriction was placed on individuals in the study; an ilium was excluded if there was any fusion of the iliac crest epiphysis. Partial fusion can begin as early as 14 years in females and 15 years in males (Cunningham et al. 2016). This step was taken to ensure the iliac crest was comparable

between all individuals in the study as partial fusion of the iliac epiphysis may have impacted landmark location.

The sample collected of the LSA individuals ranged from perinatal infants to young adults (Table 1; Table A1). Chronological age at death was estimated (Harrington 2010) by examining dental development using the methods of Smith (1991) and Liversidge and Molleson (2004). The dental age of an individual was calculated by averaging the scores of all observable teeth. If an individual did not have dentition, regression formulas were generated using the dentally aged individuals and long bone lengths (Harrington 2010). The equations were then applied to the long bones of the individuals without recordable dentition to predict dental age. The same protocol was used to estimate the dental age of the Indian Knoll Individuals and was conducted by Libby Cowgill (2010) (Table 1; Table A2). This resulted in a total study sample of 60 sub-adult individuals (Table 1; Tables A1, A2).

In addition to the 60 juvenile individuals, 20 mature individuals were included to create the “adult” state of size and shape maturity (Table A3). In order to be considered mature, an individual had a fused or fusing epiphysis on the iliac crest. A total of 10 individuals were sampled from both LSA and IK, five males and five females from each. The adult sample is young to middle aged adults without pathologies and an equal representation of sex. These sex estimations were performed by Dr. Helen Kurki and are estimations based on morphological observations of each pelvis. A pelvis was only included if the iliac crest was intact and a sex estimation had been conducted on the individual.

Table 3.1. Summary of the 60 juvenile skeletal individuals included in this study. Each column under the sample represents the number of individuals from the specific age grouping. A total of 26 individuals were included from IK and 34 from LSA.

Age (years)	LSA	IK	Number of Individuals
0-1.99	3	7	10
2-6.99	15	8	23
7-10.99	8	7	15
11-15.99	8	4	12
Total Number of Individuals	34	26	60

3.3 Methods

3.3.1 3D Scanning

Scanning was completed for a larger research project under the direction of Drs. Lesley Harrington and Helen Kurki. A Konica-Minolta Virtuoso 3D scanner was used for the Indian Knoll sample and most of the LSA sample; the remaining LSA specimens were scanned using a NextEngine Desktop Scanner. The Konica is a structured light system, and the NextEngine uses laser triangulation; both produce highly accurate and comparable surface scans (Slizewski et al. 2010; Villa et al. 2015). Both the Konica scanner and NextEngine scanner were calibrated each time the scanner was set up. Each bone was scanned in 2-3 orientations using a 360-degree scan rotation to ensure the scanner sufficiently captured the complete morphology of each bony element. A total of 6-8 scans were taken from each orientation.

The majority of the raw scans were then loaded into Geomagic Design X (3D Systems Inc. 2019). For the individuals scanned with the NextEngine scanner fusion of the models occurred in ScanStudio (NextEngine, Inc. 2015). A protocol was followed to fuse the scans into a single 3D model in Geomagic Design X. The function “Mesh Buildup Wizard” was used (3D Systems Inc. 2019). In this function “Fix Erroneous Data” was selected to improve the quality of

the final fused model. In the data editing stage, all of the background noise was removed. This included any scanned image that was not bone. The models were carefully examined at this stage and if a portion was too difficult to discern as bone or not, it was left for later stages of editing. The third stage was to pre-align the data based on a picked point. This manual process was chosen to ensure as accurate alignment as possible instead of allowing the program to automatically guess the alignment. Using the picked point alignment is more common with juvenile bones as they are more amorphous, and it is therefore more difficult for the auto function to locate unique landmarks. Each set of 6 scans was aligned with each other to create a complete model. Distinct areas and features of the bone were chosen when selecting landmarks to ensure they could be replicated on all of the scans. Different portions of the bone were covered to ensure higher accuracy in fusion. Approximately 7 landmarks were placed for each alignment. In the fourth stage, best-fit aligning was used to ameliorate any potential issues that occurred in the manual alignment. Each scan was highlighted and set to “moving”. The sampling ratio for this stage was left on “auto” at 25%; this lower percentage indicates lower alignment accuracy from the manual process. Once this stage was complete the data was merged, which fuses the aligned scans. The “Geometry Capture Accuracy” was set to 7/10. A higher accuracy was chosen because accurate models are an assumption in morphometric analysis. This means more poly-faces were used to create the shape, portraying features accurately and smoothing the model shape. However, setting the ratio to 10/10 created too large models that required decimating for loading into other programs. Even at 7/10, some models were too large to load into Landmark Editor or R, and did require decimating in Design X. In this final stage “Remesh And Fill All Holes To Create Watertight Mesh” was selected and the final product was a fused 3D model from the initial scans. Sometimes this process would result in small outliers or fragments

surrounding the perimeter that required removal. The function “Healing Wizard” was used to automatically detect abnormalities on the model. In the event any erroneous data were missed, any remaining edits were done manually at the data editing stage of the “Mesh Buildup Wizard”. If any bone was accidentally trimmed in this process, or if small holes in the mesh were noticed, they were filled using the “Healing Wizard”, “Fill Holes” function. This was only applied to small anomalies; if there was a large portion missing on the iliac crest of an individual it was excluded from the study rather than filled in using this function. The final stage was exporting the fused model as an “Ascii PLY file” for use in the Geomorph function in R as this function can only read ascii formats.

3.3.2 Landmarking Protocol

Following the selection of the appropriate individuals for landmarking, the left ilium was used except in cases where it was lacking, in which the right ilium was reflected to create a left using Landmark Editor (D. Wiley and the IDAV 2006). Each ilium was examined at this stage to ensure no significant damage was present on the iliac crest. If there was damage or disruptions to the iliac crest, the individual was omitted and replaced by an individual of the same age where possible. Each ilium was subsequently imported into RStudio as a .ply file, which was the statistical software used for subsequent analyses (RStudio Team 2016). The package Geomorph version 3.1.0 (Adams et al. 2019) was used once the .ply files were loaded into R (Appendix B). The code used and described in the subsequent paragraph can be found in Appendix B. The function “digit.fixed” was used to create a 3D outline of each iliac crest by placing 100 semi-landmarks along the iliac crest (Figure 3.3; Appendix B). This high number of landmarks was chosen so that a nearly complete outline of the iliac crest could be derived from the landmarks. The 3D model was rotated into anatomical position so that the most anterior point (the ASIS) on

the iliac crest could be identified. This was the first landmark and the only fixed homologous landmark between models. Anatomical position was then used to identify the medial and lateral aspect of the crest. The remaining landmarks were placed starting on the medial aspect of the crest, moving posteriorly.

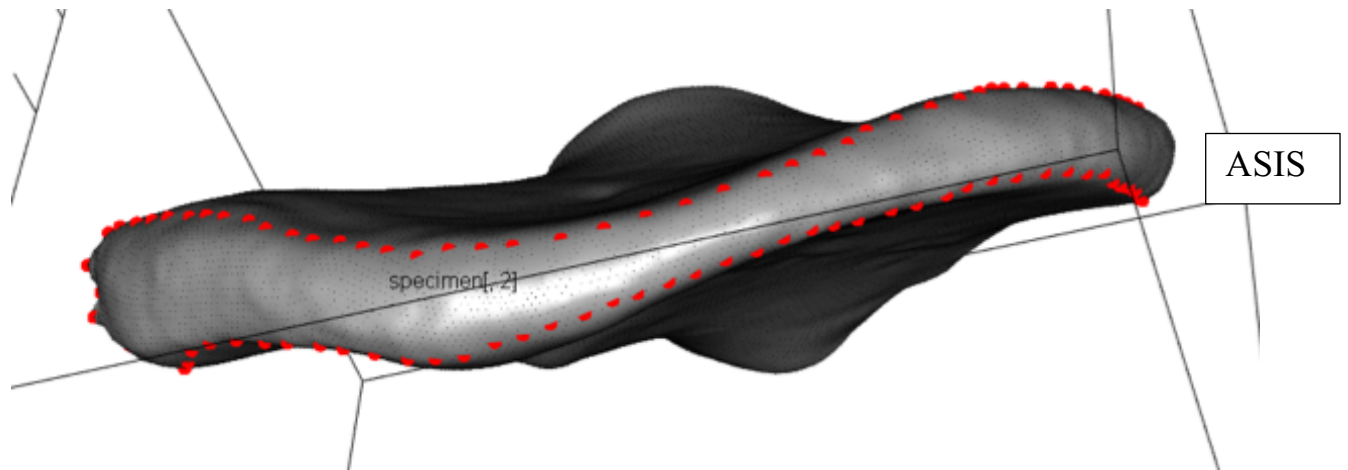


Figure 3.3. Example of ilium once the 100 landmarks had been placed on the iliac crest.

A total of 50 landmarks were placed on the medial and lateral aspects respectively with the 50th landmark on the most posterior position (PSIS) (Figure 3.3; Appendix B); however, the exact placement of landmarks 2-100 were not of strong concern as this step in the process was aimed at obtaining an overall outline of the iliac crest from which the semilandmarks could be derived from the `digit.curves` function in Geomorph version 3.1.0 (Adams et al. 2019). Each was placed as equally spaced as possible on the iliac crest border to maximize accurate outlining of the iliac crest from which the semilandmarks would be derived from the `digit.curves` algorithm. Studies have indicated it is better to have more landmarks in the outline of the item from which semilandmarks are derived and a dense number of semilandmarks in order to increase the accuracy of the shape captured (Gunz et al. 2005; Gunz and Mitteröcker 2013); therefore, a total of 81 semilandmarks were derived from the original outline of 100 landmarks as per

semilandmaking protocol using the function `digit.curves` and Procrustes distance minimization. Once all ilia from a sample had been landmarked, data were compiled into a .csv file for the remaining analyses. The data were converted into a matrix and then a 3D array, which is the required format for Generalized Procrustes Analysis (`gpagen` function) in Geomorph version 3.1.0 (Adams et al. 2019) (Appendix B).

3.3.3 Statistical Methods

Using the 3D array of landmark data, a Generalized Procrustes Analysis (GPA) was conducted for three separate groups: LSA, IK, and the two samples combined (Appendix B). All of the analyses were performed on each sample independently as well as in the combined dataset. This step was taken so that patterns could be observed in each separate sample. If similar patterns of change with age occurred, combining into one dataset would increase the statistical power of the analysis. However, if different patterns of ontogenetic change were observed, the samples would need to be compared and contrasted rather than combined. This allowed the impact of shape variation in each sample to be explored in addition to statistical tests in the pooled dataset. A customized PCA plot was produced for each sample, visually identifying the individuals by age groupings (0-1.99 years, 2-6.99 years, 7-10.99 years and 11-15.99 years) (Appendix B). These plots were created to demonstrate clustering of the individuals in the PCA based on the shape variation represented by the PCs that were visually separated in colour by age groups. The PCA captures the major axes of shape variation in the sample in multidimensional space. While the PCAs conducted on LSA and IK could only visually be differentiated by age, the combined samples PCA was also divided by sample to visually represent variation according to sample in addition to age. Pearson correlation tests were performed between PC scores and

two variables (age and centroid size) in each sample separately and then in the combined sample. Centroid size is the square root of the sum squared distances of all landmarks in an object from their centre and provides an overall size measure for each individual (Klingenberg 2016). A correlation was performed between the dental age of each individual and the Principal Component scores of the first two or three axes of variation, depending on the sample (Appendix B). Only the first two or three axes were explored as they accounted for more than 50% of total variation (Appendix A). A correlation between centroid size and the PC scores of the selected PC axes was completed. Finally, a correlation test between age and centroid size in the combined sample was performed (Appendix B).

The next step in the analysis involved exploring and comparing the mean shape of age cohorts and samples. Mean shape was calculated by determining the average shape in each developmental cohort. This mean was then compared between successive age groups and between the youngest and oldest group (Appendix B). The results of the correlation tests dictated which Principal Components to explore in more detail with respect to shape. The diagnostic criteria for further exploration was a correlation p-value of <0.5 . The minimum and maximum shapes on PC axes correlated with age were explored. The minimum shape was plotted as graphs against the maximum shape to provide a visualization of shape change (Appendix B).

In order to investigate the process of maturation, Generalized Procrustes Analysis and Principal Component Analysis were performed on the 20 adult individuals using Geomorph version 3.1.0 (Adams et al. 2019) (Appendix B). A Pearson correlation test was performed on the first two Principal Components with centroid size. A t-test was also conducted on the PC scores of all the females versus the PC scores of all the males to determine if there was a difference between the females and males for each PC to determine if the mean shape difference between

the sexes was significant. This analysis was performed on the LSA, IK, and combined samples (Appendix B). The mean shape of the 20 adults combined was determined for maturation analyses. The mean shape of the five youngest in each sample was also determined in order to create a starting point for a shape maturity trajectory. This process followed that outlined by Wilson et al. (2015) (Appendix C). In order to explore size maturity, the results from the GPA and PCA in the combined dataset were used. The centroid sizes calculated in the GPA were re-expressed as a percentage of the combined adults mean centroid size (100% maturity). The trajectory of size maturation was then graphically plotted to explore the trajectory of growth with respect to size.

In order to explore shape maturation, the Procrustes distances (PD) between successive individuals were calculated (Appendix B). This analysis was based on the process conducted by Wilson et al. (2015) (Appendix C). The mean shape of the five youngest individuals was used as the starting point. The PD was then calculated between the mean of the five youngest and the first individual, then between the first individual, and second individual, and so on. This was repeated with the last PD measured between the oldest juvenile and the mean shape of the adult sample, which represented 100% maturity. These PDs were then summed to create the cumulative trajectory length. Following the protocol conducted by Wilson et al. (2015) a sliding average approach was used in determining the maturity trajectory. This method prevents over-estimating the length of the trajectory under the assumption that an individual must pass through each shape of the individual before it. This was also an important step in this analysis as age was estimated and could have impacted the trajectory if errors are present. Groups were created by averaging the age and Procrustes distance of every five individuals, with an overlap of two individuals in the previous cohort (e.g. group 1 is the mean of individuals 1-5, group 2 is the

mean of individuals 3-7, group 3 is the mean of individuals 5-9, and so on). Each group average was then re-expressed as a percentage of the cumulative Procrustes distance calculated above. This resulted in two vector averages for the groups, one for age and the other for shape as represented by Procrustes distance, from which the trend of shape maturity could be graphically represented.

3.3.4 Error Analysis

In order to check the reproducibility of geometric morphometric landmark placement, 12 juvenile individuals were randomly selected to be landmarked again. The same protocol was followed, placing 100 landmarks on the crest with the ASIS as the only fixed homologous landmark. The new 82 sliding semilandmarks were then derived from this outline. A Procrustes ANOVA in MorphoJ (Klingenberg 2011) was used to compare the placement of the 82 derived semilandmarks. Measurement error was quantified using the ratio of the two variance components using the following equations (Zelditch et al. 2012). MS is the mean square value of the given component and 2 is the number of replicates.

$$\text{Individual Variance} = (\text{MS}_{\text{individual}} - \text{MS}_{\text{error}})/2$$

$$\text{Total Variance} = \text{MS}_{\text{error}} + \text{individual variance}$$

$$\text{Repeatability} = \text{individual variance}/\text{total variance}$$

$$\text{Percent Error} = 1 - \text{repeatability}$$

To compare the placement of the first landmark, inter-landmark error was calculated following Lewton (2010):

$$\text{Error} = \sqrt{(x_2 - x_1)^2 + (y_2 - y_1)^2 + (z_2 - z_1)^2}$$

Chapter 4. Results

4.1 Error Analysis

Landmark error for the first landmark placed was calculated by determining the difference between the XYZ coordinates of the original and error trial following the calculation of Lewton (2010): $\text{Error} = \sqrt{(x_2-x_1)^2 + (y_2-y_1)^2 + (z_2-z_1)^2}$. The results of this calculation can be seen in Table 4.1. The average error across the 12 specimens was 3.121 units of Euclidean distance. A Procrustes ANOVA was run in MorphoJ (Klingenberg 2011) to quantify measurement error of the 82 semilandmarks placed. The results indicated a repeatability of 0.96 (4% error).

Table 4.1 Results of the Euclidean distance between the first landmark for the 12 error specimens.

Individual	Euclidean Distance
inkn0022512	0.274
inkn0051512	1.102
inkn0082613	0.678
inkn0003311	28.582
inkn0006211	2.306
lsaa00138r2	0
lsaa00152r4	0.928
lsaa00175r2	1.702
lsaa00181r2	1.024
lsaa0029911	0.287
lsam00230r3	0.566
lsas0605212	0.000000513

4.2 Patterns of Shape Change

Principal Component Analysis was used to explore patterns of shape change in each sample separately as well as in a combined sample. The first 2 or 3 principal components were explored based on the percentage of variation explained by these components (Table 4.1; Figures A1-3, Tables A4-6). For LSA and IK, PC1 and PC2 explained more than 50% of the variation; however, for the combined sample PC3 was required to reach 50% of the cumulative variation (Table 4.2). Since size and age were of concern, each principal component was tested against centroid size, a proxy for size in Procrustes superimposition, and age of the individuals. Each description of shape, as represented along a PC axis, began with the first landmark, which was positioned at the anterior-most aspect of the iliac crest (ASIS). Shape was then described moving posteriorly on the medial border until the most posterior aspect (PSIS). The description then continued on the lateral border moving anteriorly. Where possible, movement of the semilandmarks was related back to anatomical landmarks on the iliac crest to assist in visualization of shape movement. All movements were compared from the minimum (negative) shape to the maximum (positive) shape, which are the shapes represented at the two extremes of shape variation on a PC axis.

Table 4.2. Variance explained by the first three principal components in the Later Stone Age sample, Indian Knoll sample and combined samples.

	PC1	PC2	PC3
LSA	28.0%	22.5%	13.2%
IK	34.3%	17.9%	10.3%
Combined	28.1%	17.0%	12.7%

4.2.1 Later Stone Age Sample

When comparing the two end points of the shape change outline of PC1, at the medial aspect of the ASIS there is shifting in the superior direction from minimum to maximum shape (Figure 4.1). Moving posteriorly along the medial border of the iliac crest, there is an inferior shift in landmarks, as well as medial movement. The posterior region demonstrated little movement. Moving anteriorly on the lateral border, significant lateral shifting from minimum to maximum shape was observed. This movement progresses to medial movement along the crest and back to medial movement approaching the lateral aspect of the ASIS. PC1 was not significantly correlated with centroid size or age (Table 4.2).

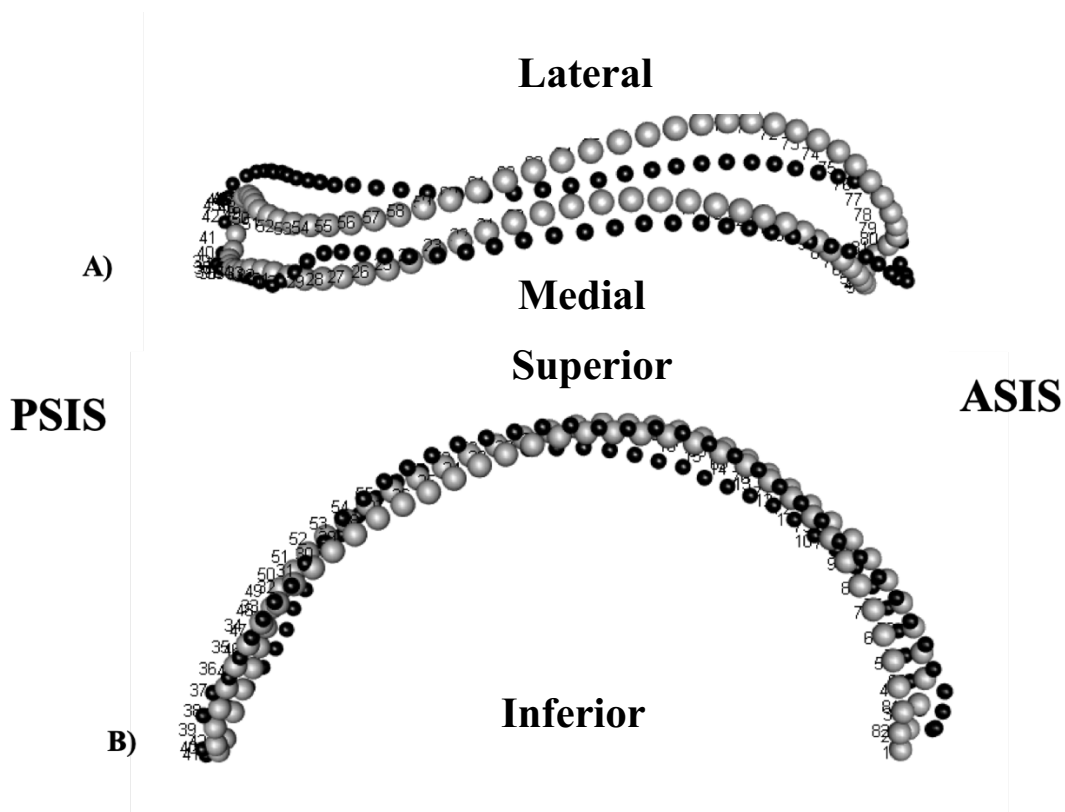


Figure 4.1. A comparison between the extreme positions shape outlines of PC1 in LSA; grey dots represent the minimum (negative) and the black dots represent the maximum (positive) shapes along the axis. The points represent the location of the semilandmarks and are labelled in order of placement with the first on the anterior-most aspect of the crest then continuing posteriorly along the medial aspect. The **A)** view of the superior aspect of the iliac crest; **B)** view of the lateral aspect of the iliac crest, viewed from the medial border.

Table 4.3. P-values of correlation tests in Later Stone Age sample (sample size of 34 individuals). The first two principal components were analysed with respect to age and centroid size as a proxy for size. The significant correlations are bolded.

	PC1	PC2
Centroid Size	r = 0.311 p-value = 0.073	r = -0.6 p-value = <0.001
Age	r = 0.002 p-value = 0.992	r = -0.5 p-value = <0.001

PC2 is correlated with both size and age significantly (Table 4.3), demonstrating the extremes in shape in these dimensions. This is indicating a high degree of correlation between size and age on the axes. Beginning at the medial aspect of the ASIS medial movement can be seen from the minimum to maximum shape dimension (Figure 4.2). Moving along the medial border in the posterior direction this movement progresses to lateral shifting of the semilandmarks. However, this movement changes to significant medial movement until the medial aspect of the PSIS is reached, where movement becomes lateral once again. On the lateral aspect of the PSIS and surrounding area, the movement is once again in the lateral direction. However, this movement continues to oscillate from the medial to the lateral direction until reaching the lateral aspect of the anterior end, where it is predominantly medial once again. This shape change likely represents the development of the sigmoid iliac crest with age.

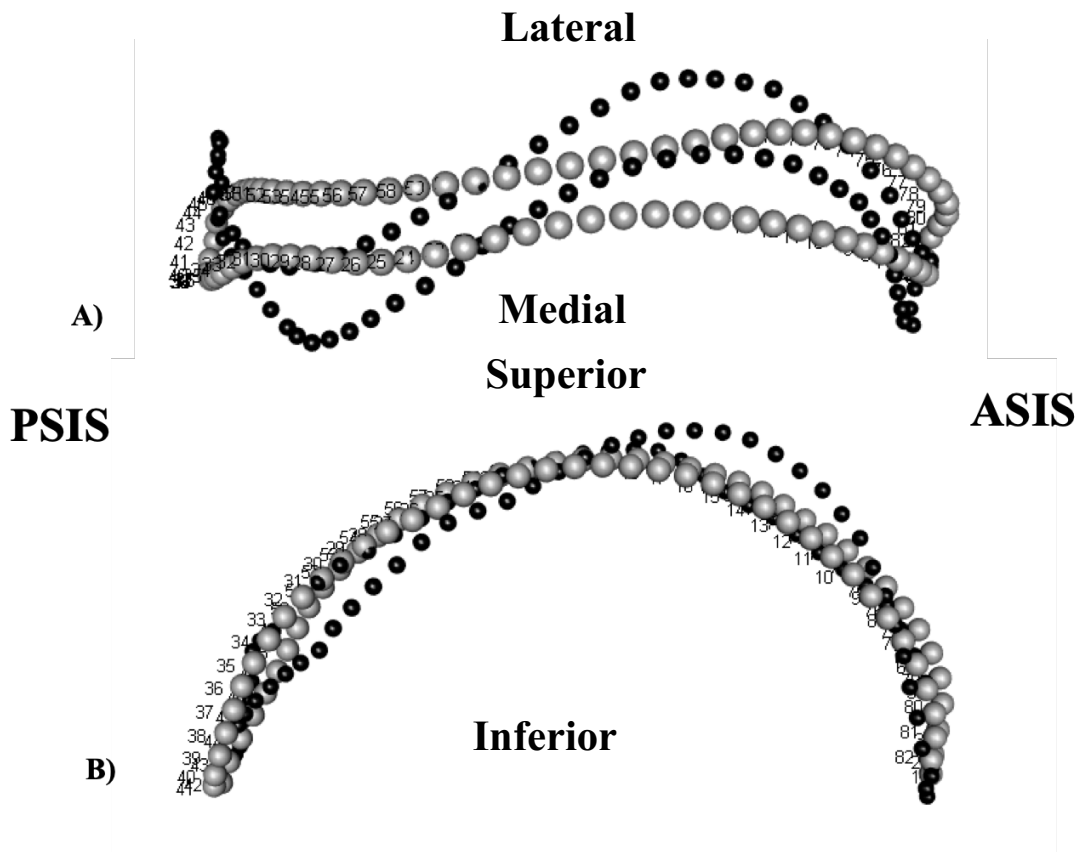


Figure 4.2. A comparison between the extreme position shape outlines of PC2 in LSA; grey dots represent the minimum (negative) and the black dots represent the maximum (positive) shapes along the axis. The points represent the location of the semilandmarks and are labelled in order of placement with the first on the anterior-most aspect of the crest then continuing posteriorly along the medial aspect. The **A)** view of the superior aspect of the iliac crest; **B)** view of the lateral aspect of the iliac crest, viewed from the medial border.

The results of the correlation tests aforementioned (Table 4.2) demonstrate that PC1 is not correlated with either size or age. PC2 is highly correlated to both centroid size and age. A scatter plot of PC scores for PC1 vs. PC2 can be seen in Figure 4.3.

Principal Component Analysis of Later Stone Age

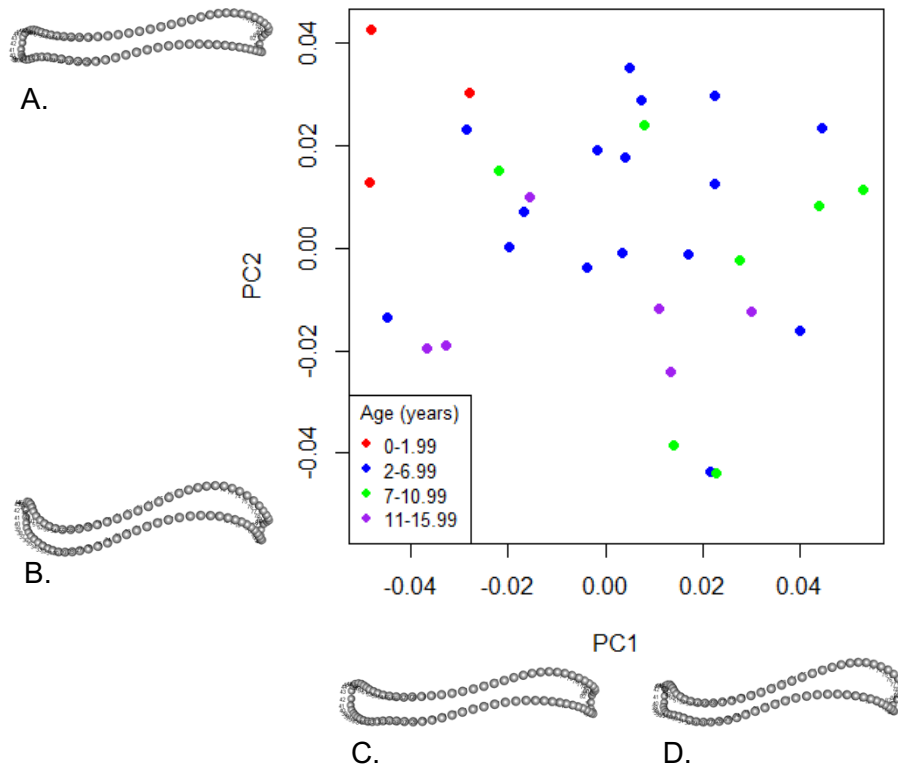


Figure 4.3. Principal Component Analysis of the Later Stone Age sample visualizing shape change along the first two principal components. The extreme shapes on each principal component were displayed with **A.** representing the positive shape outline of PC2, **B.** representing the negative shape outline of PC2, **C.** the negative shape outline of PC1 and **D.** the positive shape outline of PC1.

4.2.2 Indian Knoll Sample

As with LSA, movement will be described moving from the minimum to maximum dimensions of shape change on each PC axis. At the medial ASIS on PC1, the landmarks shift inferiorly and laterally, differing from the trend observed in LSA PC1 (Figure 4.4). Moving along the medial border in the posterior direction landmark movement begins to shift medially but progresses to lateral shifting as the posterior section is approached. At the PSIS and surrounding area there is slight inferior and medial shifting that progresses to significant lateral movement moving along the lateral border in the anterior direction. This movement continues to oscillate along the crest progressing to significant medial movement until reaching the lateral

aspect of the anterior section, at which lateral and superior movement of the landmarks is evident. PC1 is significantly correlated with centroid size (Table 4.4). These landmark movements may be demonstrating variation driven by size.

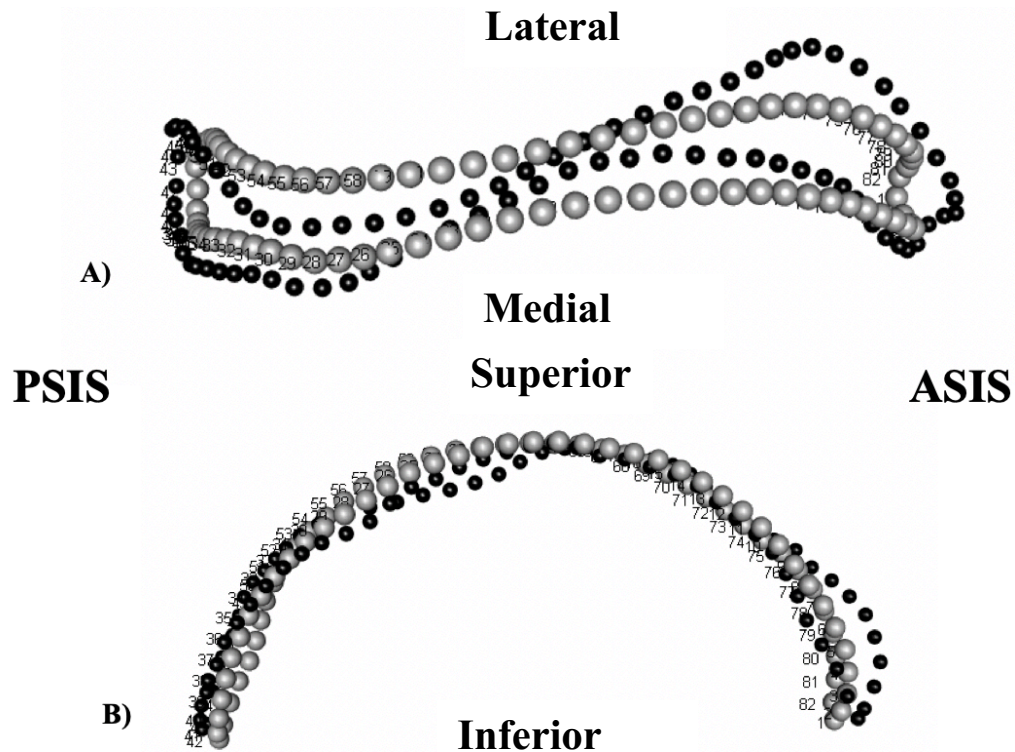


Figure 4.4. A comparison between the extreme positions shape outlines of PC1 in IK; grey dots represent the minimum (negative) and the black dots represent the maximum (positive) shapes along the axis. The points represent the location of the semilandmarks and are labelled in order of placement with the first on the anterior-most aspect of the crest then continuing posteriorly along the medial aspect. The **A)** view of the superior aspect of the iliac crest; **B)** view of the lateral aspect of the iliac crest, viewed from the medial border.

Table 4.4. P-values of correlation tests in Indian Knoll sample (sample size of 26 individuals). The first two principal components were analysed with respect to age and centroid size as a proxy for size. The significant correlations are bolded.

	PC1	PC2
Centroid Size	r = -0.4 p-value = 0.041	r = -0.6 p-value = <0.001
Age	r = -0.3 p-value = 0.070	r = -0.5 p-value = 0.004

PC2 is correlated with both size and age significantly, as in LSA PC2 (Table 4.4). Very similar trends were observed in the movement of PC2 in IK as in LSA. At the anterior aspect moving posteriorly along the medial border, landmark shifting begins as lateral movement, progresses to medial movement along the crest, and back to lateral shifting approaching the posterior and medial aspect of the PSIS (Figure 4.5). At the medial aspect of the PSIS, the semilandmark shifting is medial once again. This medial trend continues along the lateral aspect of the PSIS. However, an oscillating pattern is observed once again with shifting movement from the initial medial direction to lateral then back to medial before reaching the lateral aspect of the ASIS where lateral movement is observed.

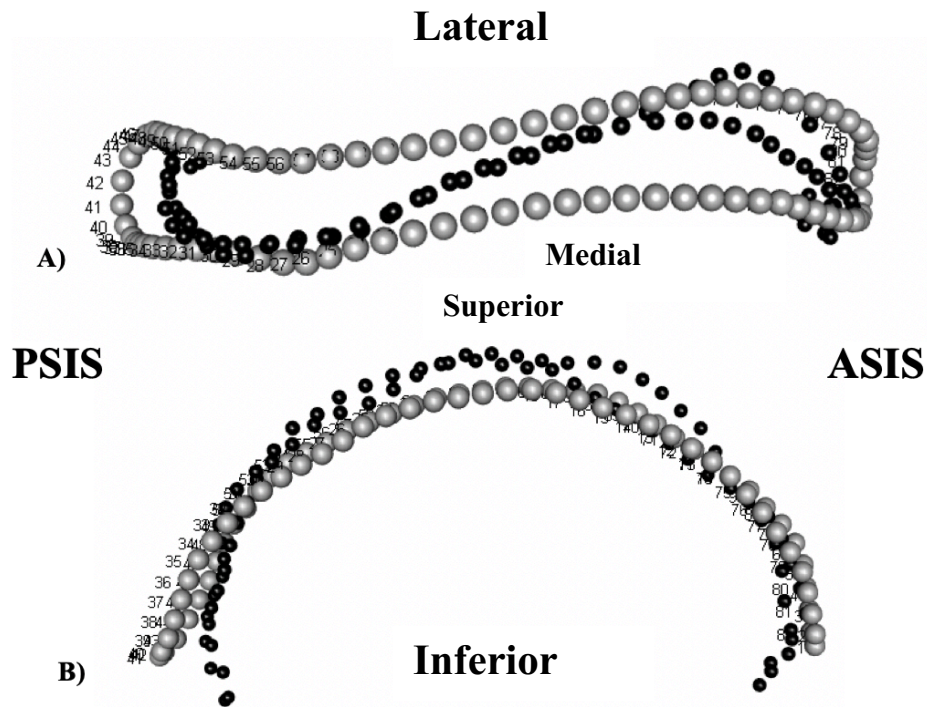


Figure 4.5. A comparison between the extreme positions shape outlines of PC2 in IK; grey dots represent the minimum (negative) and the black dots represent the maximum (positive) shapes along the axis. The points represent the location of the semilandmarks and are labelled in order of placement with the first on the anterior-most aspect of the crest then continuing posteriorly along the medial aspect. The **A)** view of the superior aspect of the iliac crest; **B)** view of the lateral aspect of the iliac crest, viewed from the medial border.

The results of the correlation tests in Table 4.4 demonstrate PC1 is correlated with size while PC2 is correlated with both size and age. This latter pattern is also observed in LSA. A scatter plot of the PC scores for PC1 and PC2 with the iliac crest shapes at the extremes of each axis can be seen in Figure 4.6.

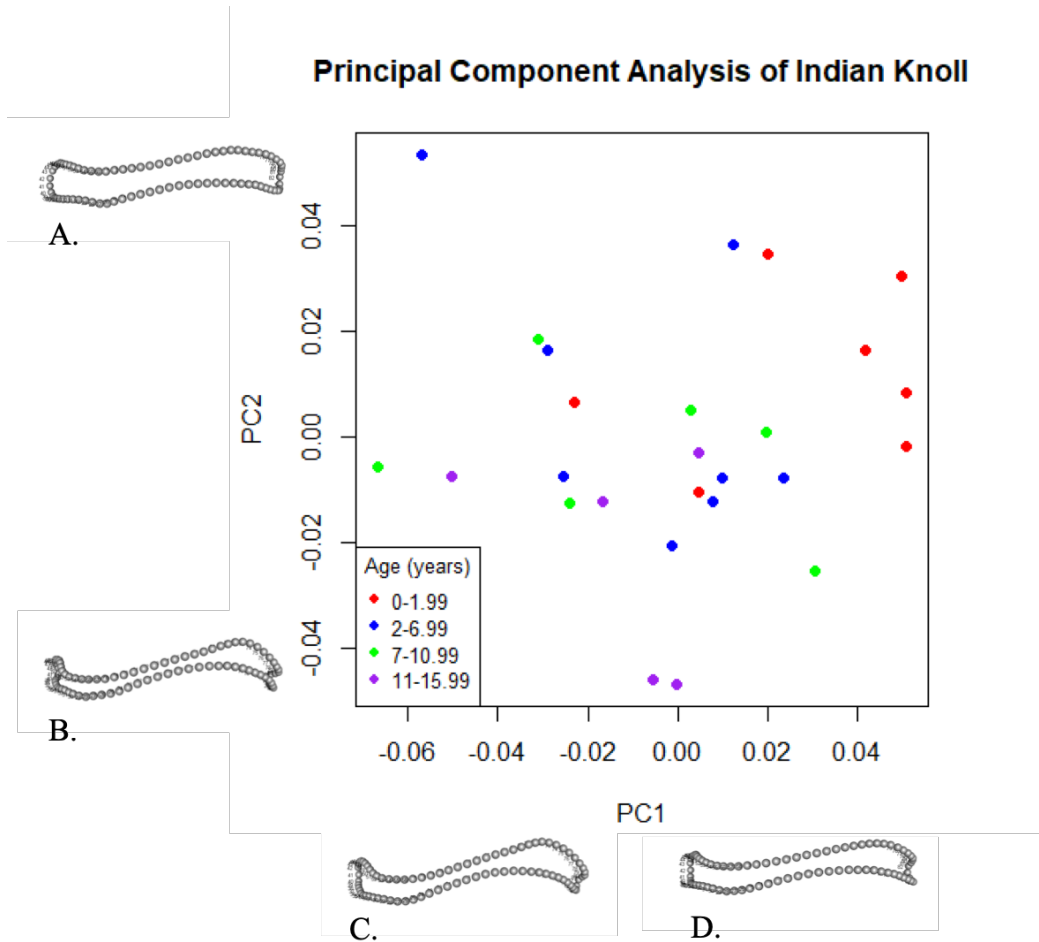


Figure 4.6. Principal Component Analysis of the Indian Knoll sample visualizing shape change along the first two principal components. The extreme shapes on each principal component were displayed with **A.** representing the positive shape outline of PC2, **B.** representing the negative shape outline of PC2, **C.** the negative shape outline of PC1 and **D.** the positive shape outline of PC1.

4.2.3 Combined Samples

The extreme dimensions of PC1 and PC2 were also explored in the combined sample after assessing how the two samples were similar or different through sample-independent analysis. Beginning at the medial ASIS on PC1, the landmarks demonstrate inferior and slightly medial movement (Figure 4.7). Moving along the medial border in the posterior direction, this medial movement progresses to slight lateral shifting. At the PSIS and surrounding region, shifting begins as medial on the medial aspect and transitions to lateral on the lateral aspect. The

trend along the lateral border demonstrates significant lateral movement initially, which is similar to the observed movement in the samples when analysed separately. This trend then progresses to medial shifting while moving anteriorly and finishing at the lateral aspect of the anterior section with slight lateral shifting. As in IK, PC1 is significantly correlated to size, demonstrating the impact of size on shape variation on this axis (Table 4.5).

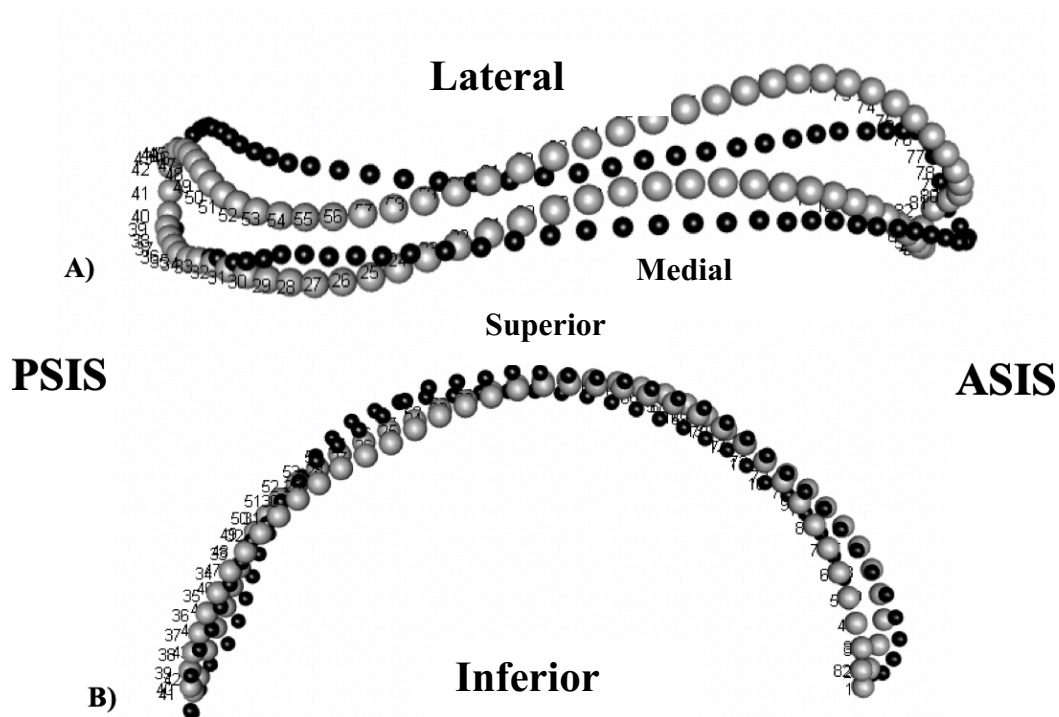


Figure 4.7. A comparison between the extreme positions shape outlines of PC1 in the combined sample; grey dots represent the minimum (negative) and the black dots represent the maximum (positive) shapes along the axis. The points represent the location of the semilandmarks and are labelled in order of placement with the first on the anterior-most aspect of the crest then continuing posteriorly along the medial aspect. The **A)** view of the superior aspect of the iliac crest; **B)** view of the lateral aspect of the iliac crest, viewed from the medial border.

Table 4.5. Results of correlation tests in both samples combined (sample size was 60 individuals). The first three principal components were analysed with respect to age and size. The significant p-values are bolded.

	PC1	PC2	PC3
Centroid Size	r = 0.3 p-value = 0.004	r = 0.6 p-value = <0.001	r = -0.1 p-value = 0.885
Age	r = 0.2 p-value = 0.057	r = 0.6 p-value = <0.001	r = 0.2 p-value = 0.233

When the minimum and maximum axes of PC2 were observed beginning at the medial ASIS, initially there is a lateral shift in landmark position (Figure 4.8). Moving posteriorly, there is significant medial movement of the landmarks. This continues along the majority of the medial border; however, the change does oscillate briefly to lateral shifting and back to medial displacement at the medial aspect of the PSIS. Along the lateral aspect of the PSIS and the border moving anteriorly, the landmarks shift laterally initially, and switch to medial displacement approximately halfway along the crest. At the lateral aspect of the ASIS, the landmarks have shifted laterally once again. As seen in LSA and IK, both PC1 and PC2 are significantly correlated with age and size.

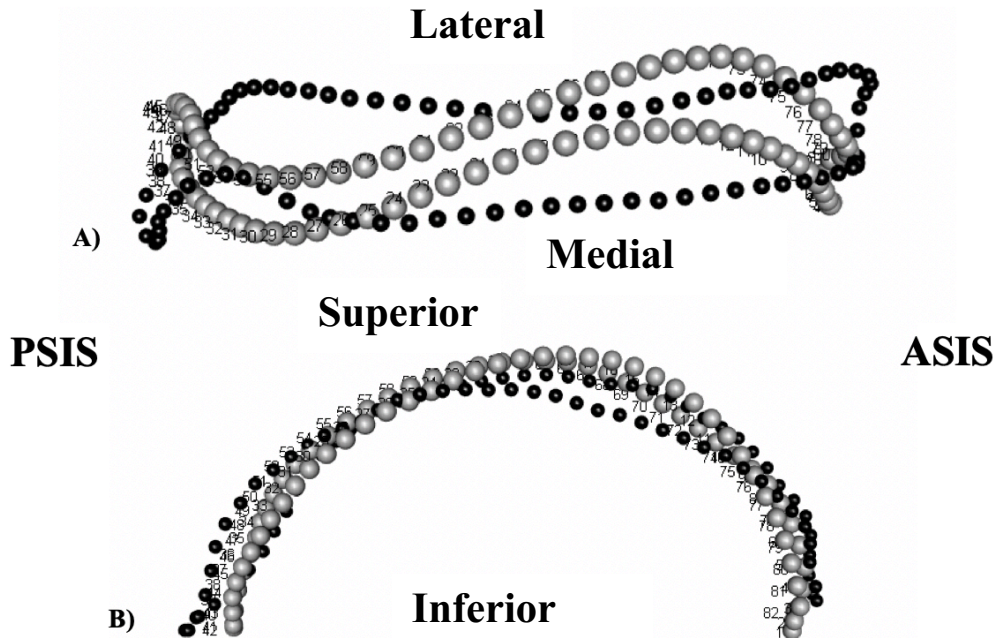


Figure 4.8. A comparison between the extreme positions shape outlines of PC2 in the combined sample; grey dots represent the minimum (negative) and the black dots represent the maximum (positive) shapes along the axis. The points represent the location of the semilandmarks and are labelled in order of placement with the first on the anterior-most aspect of the crest then continuing posteriorly along the medial aspect. The **A)** view of the superior aspect of the iliac crest; **B)** view of the lateral aspect of the iliac crest, viewed from the medial border.

Overall, the shifting of landmarks observed demonstrate the majority of landmark movement occurs in the mediolateral plane and oscillates along either aspect of the iliac crest. This trend can be seen in both the first and second principal component when looking at LSA and IK isolated, as well as when the samples are combined.

While it was important to compare and contrast patterns of shape change in each sample separately, based on the landmark movement demonstrating similar shape change on each axis, the two samples were combined to create one comprehensive dataset and the same analyses were performed, once again looking at the first three principal components which capture 50% of the total variation (Figure 4.1; Table 4.5 Figure A3; Table A3). PC3 was not significantly correlated to age or size. Combining the samples allowed more direct visual comparison between samples

and also increased sample size to improve the robusticity of statistical analysis. The principal component analysis of this combined sample can be seen in Figure 4.9. The distribution of individuals in this graph are not clearly delineated between age group, or sample. This indicates there is a coexisting source of variability acting on individuals in this sample. Since centroid size and age impacted variability, as demonstrated by correlation tests, these two values were compared. Centroid size and age are highly positively correlated ($r = 0.824$, $df = 58$, **p-value** = **<0.001**), demonstrating the expected result of increase in size of the ilium with growth.

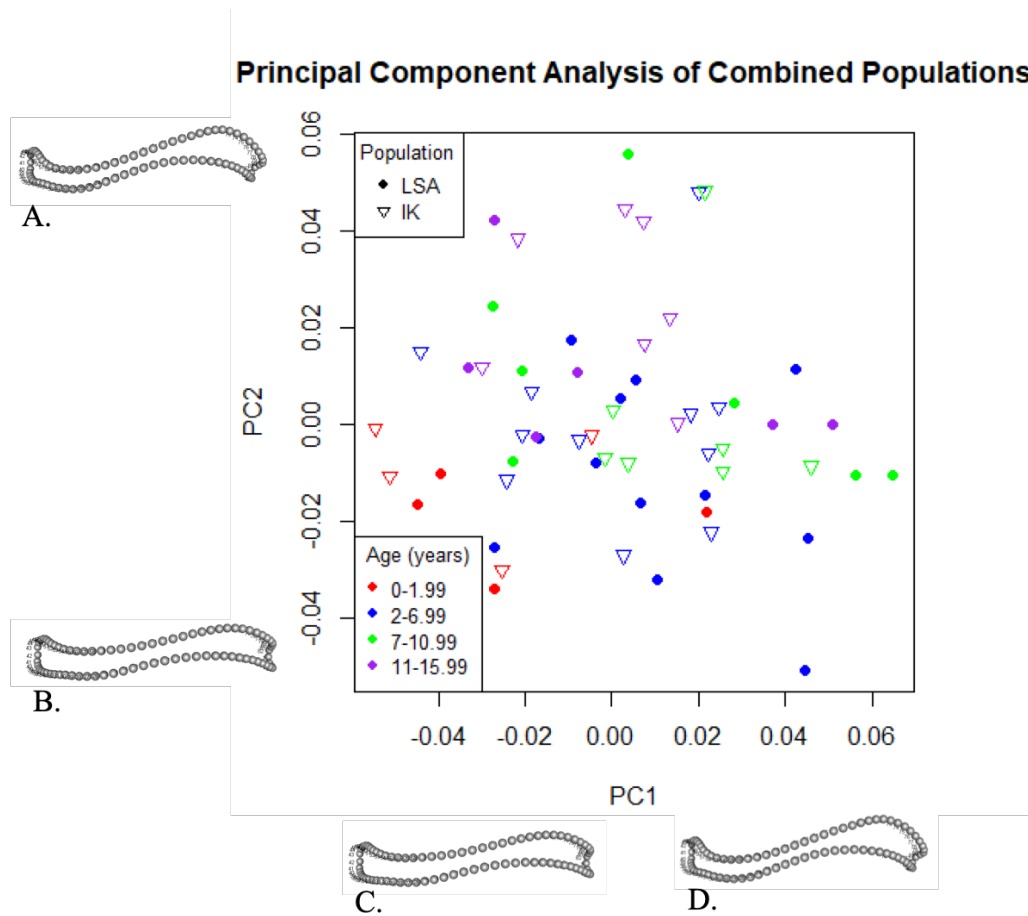


Figure 4.9. Principal Component Analysis of the combined sample visualizing shape change along the first two principal components. The extreme shapes on each principal component were displayed with **A.** representing the positive shape outline of PC2, **B.** representing the negative shape outline of PC2, **C.** the negative shape outline of PC1 and **D.** the positive shape outline of PC1.

4.3 Mean Shape

The results of the PCA allowed for the mean shapes to be analyzed at their extremes in order to understand the range of shape change that occurs within each sample. PC1 and PC2 represent the greatest proportion of shape variation present in the sample and how each individual differs moving along a given axis. The PCA captures the axes of shape variation but needed to be explored to determine if variables, such as age and size, contribute to shape variation along a given axis. With an understanding of the extreme shapes on the two most significant PCs, it is now important to consider what the mean shape of each age cohort looks like, especially in comparison to other age cohorts, in order to understand the shape change that occurs over development. In order to study size and shape maturation by comparing mean shape across age cohorts, the shape differences are related directly to age.

Both LSA and IK were observed separately before combining into one large sample in order to determine if similar or different patterns were occurring in each sample independently (Figure 4.10). In the LSA sample, there is a significant difference in mean shape between the first and second age cohort. Sinuosity in the mediolateral plane increases from the first cohort to the second cohort. There is very slight shifting in this plane when comparing the second and third, and the third and fourth. The difference is most evident in examining the comparison of the mean shape of cohort 1 to the mean shape of cohort 4. In this comparison, the increase in sinuosity in the older sample demonstrates significant shape change in the mediolateral plane.

In the IK sample, there was less movement when comparing the first and second cohort in contrast to LSA. Similar to LSA, the shape change between the means of the second and third, and third and fourth cohorts in IK demonstrate only slight medial and lateral shifting of the landmarks. When comparing the mean shape of cohort 1 to the mean shape of cohort 4, the

difference in shape once again clearly demonstrates the increase in sinuosity in the mediolateral plane as age increases.

The trends of shape change are similar in each sample. It follows that the trends in the combined sample demonstrate similar shifting in the landmarks. While there is a larger shift in the means between 1 and 2 when compared to 2 and 3, and 3 and 4, once again the change in shape is best observed in the comparison of the means between groups 1 and 4. In Table 4.5, the sinuosity observed in the samples independently is once again clearly evident in the combined sample. Therefore, based on the mean shapes of each cohort, it can be summarized that starting from the ASIS and moving posteriorly, the landmarks initially shift medially, progress along the curve moving laterally, then shift medially towards the posterior end. Following the crest on the lateral border moving anteriorly the landmarks shift laterally initially, then oscillate from medial movement to lateral movement along the curve, meeting back at the anterior end with slight medial shifting.

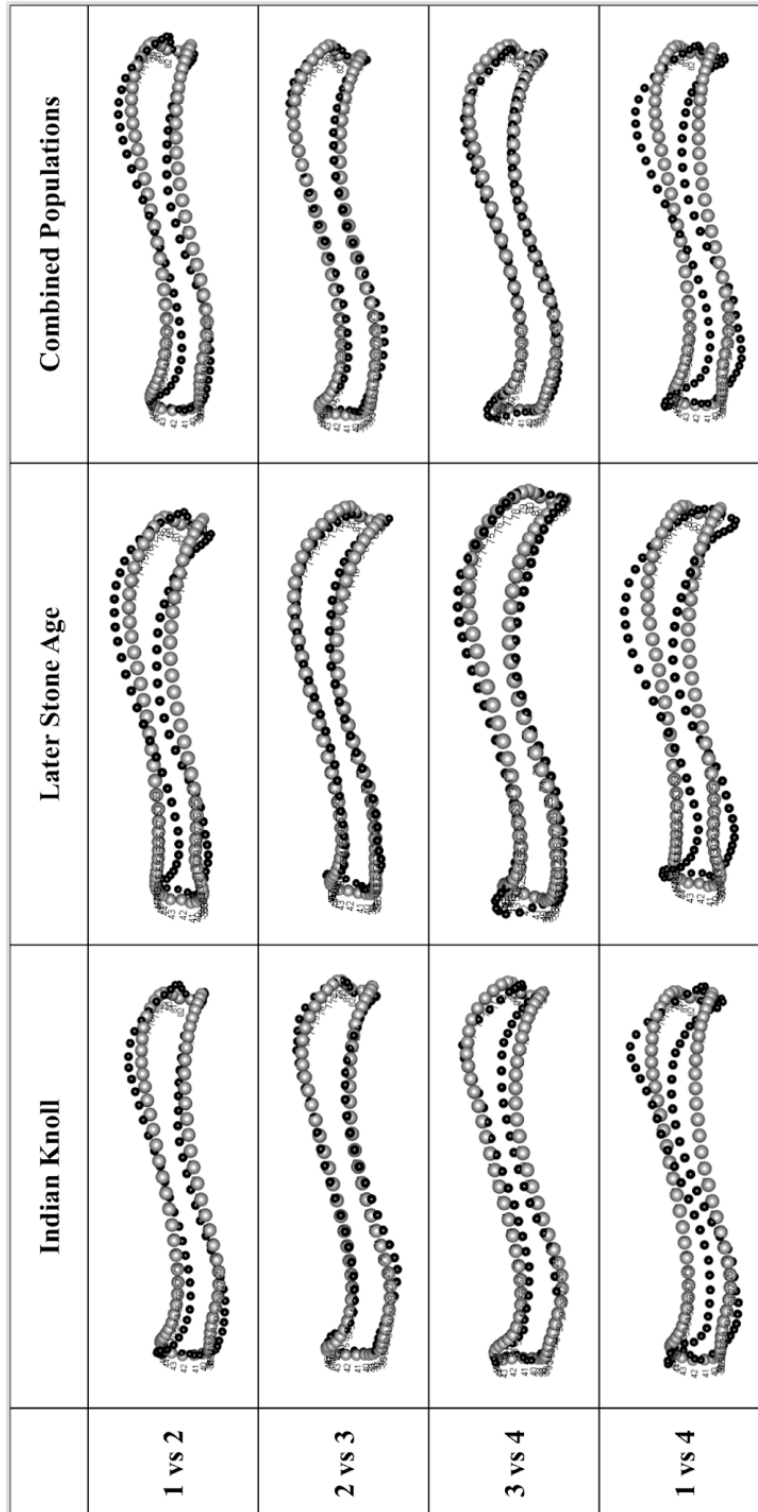


Figure 4.10 These images depict shape change between the means of each age cohort (1 = 0-1.99 years; 2 = 2-7.99 years; 3 = 8-10.99 years; 4 = 11-15.99 years) for the two samples separately and combined. Descriptions of these images can be found within the text. The gray dots represent the mean of the younger cohort in the comparison, while the black dots represent the mean of the older cohort in the comparison.

4.4 Maturation

With a better understanding of shape change in the juvenile individuals, the next question is what the trajectory of maturation looks like in the sample. In order to achieve this, it is necessary to first explore the patterns that drive adult shape change. A Generalized Procrustes Analysis of the adult sample and Principal Component Analyses were performed on the two samples separately (Figure 4.10) and then combined (Figure 4.11).

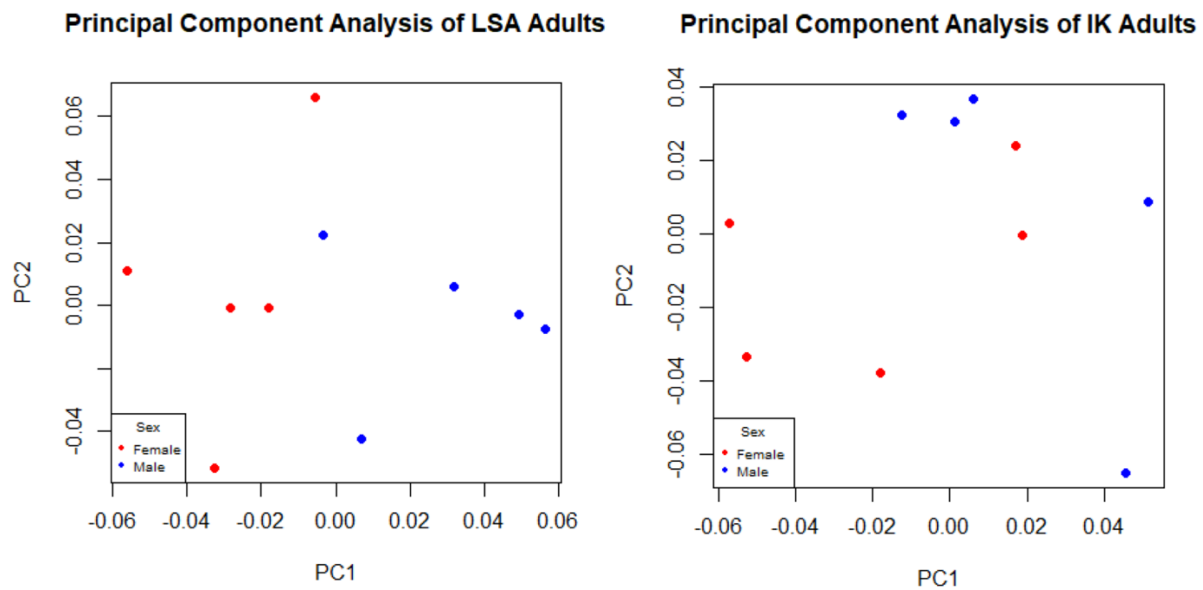


Figure 4.11. Principal Component Analysis of the LSA adults (left) and IK adults (right), visualizing shape change along PC1 and PC2. Males and females were visually separated with females as red and males as blue.

Principal Component Analysis of Combined Adults

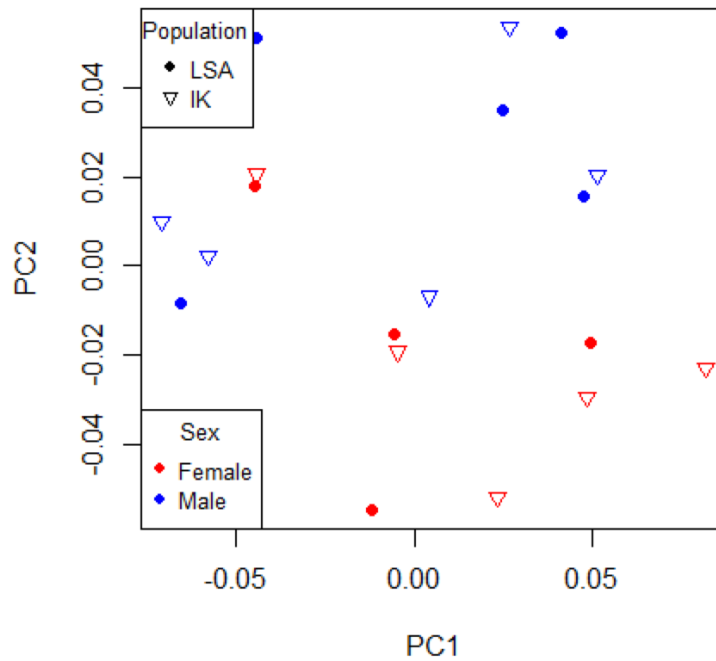


Figure 4.12. Principal Component Analysis of the combined sample visualizing shape change along PC1 and PC2. Data are separated by sex and sample cohorts. The circles represent LSA and the triangles represent IK. Red represents females and blue represents males.

Centroid size was highly correlated with PC1 but was not significantly correlated with PC2 (Table 4.6). A t-test was also performed on centroid size and the combined sample to determine if LSA and IK adults differ in centroid size. The results were significant ($t = 5.697$, $df = 18$, $p = <0.001$), indicating a difference in centroid size based on sample.

Table 4.6. Results of the correlation tests performed on the adult sample (sample size of 20 individuals). Significant correlations are bolded.

	PC1	PC2
Centroid Size	$r = -0.8$ p-value = <0.001	$r = 0.1$ p-value = 0.079

Knowing there is a correlation with centroid size, a t-test was performed to determine if there was a difference in size between males and females specifically, within either of the

samples, or the combined sample. The results indicate that there is not a significant difference in size between males and females for any of the samples (Table 4.7).

Table 4.7. Results of an independent samples t-test between males and females for centroid size. Tests were run for each sample individually (sample size of 10) and for the combined sample (sample size of 20).

	LSA	IK	Combined
t	1.209	-1.361	-0.450
df	8	8	18
p-value	0.261	0.211	0.658

Male and female shape (represented by PC scores) in each sample were subjected to a t-test to determine if there was a significant difference between male and female shape in the samples (Table 4.8). These results demonstrate that there is only a significant difference between males and females in the LSA sample. In the IK sample and combined dataset, there is not a significant difference between the mean female and mean male shape.

Table 4.8. Results of the two-sample t-test on the adult individuals, comparing male and female shape in each sample to each other. Significant results are bolded.

	LSA	IK	Combined
t	-3.925	-1.778	-0.450
df	8	8	18
p-value	0.044	0.113	0.658

4.4.1 Size Maturation

With a better understanding of the importance of centroid size in the combined study sample, the trajectory of this maturation process was further explored. The mean centroid size of

the 20 adult individuals was used to represent 100% size maturity, and an approximate age of 20 years old was assigned for graphical representation; however, the actual age of the adults may have been younger or older. The designation of “adult” was based on stage of fusion of the iliac crest epiphysis. The centroid size of each juvenile individual was then re-expressed as a percentage of this value to determine the maturity percentage of each individual. Results are graphically displayed in Figure 4.12. The linear regression is positive with an R^2 value of 0.679 ($p = <0.001$), demonstrating an increase in size with an increase in age.

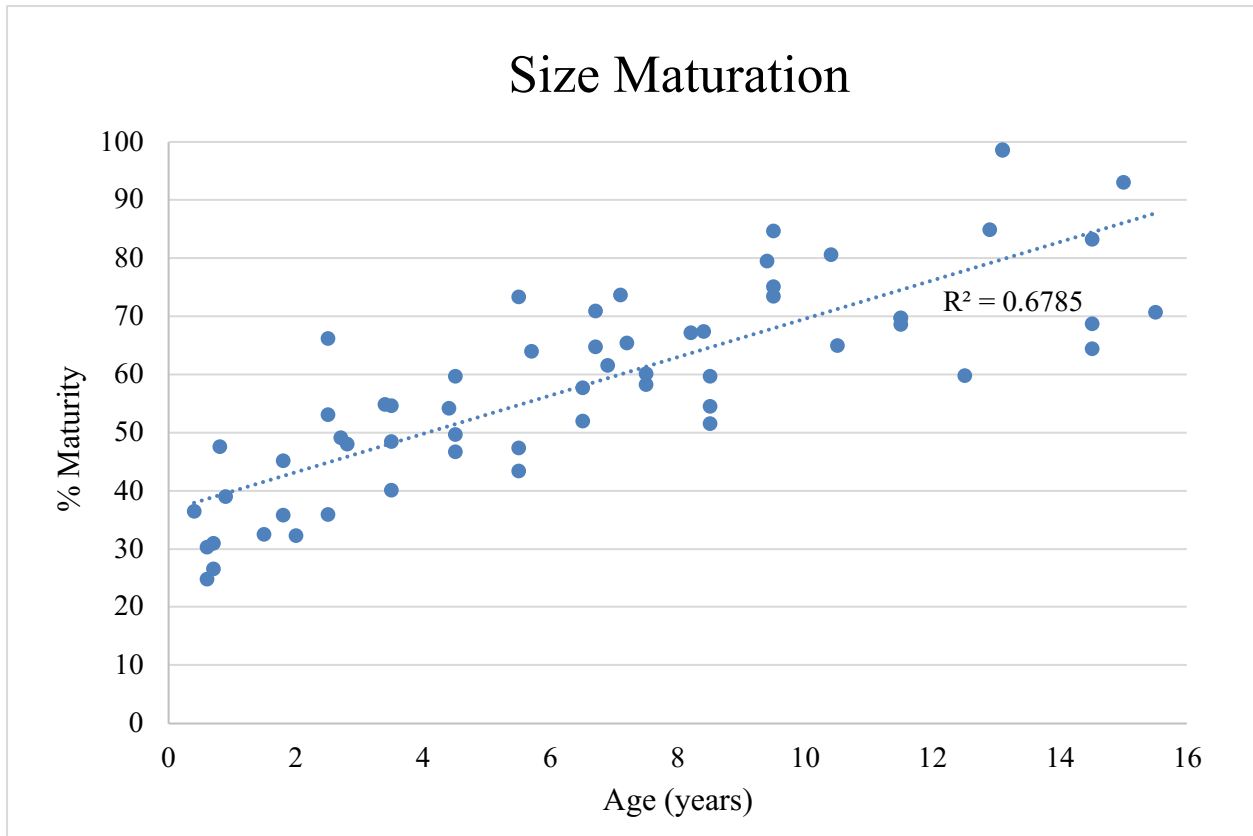


Figure 4.13. The percent size maturity of each individual in the combined sample. The linear R^2 value was 0.679 ($p = <0.001$) indicating a significant positive trend in the data.

4.4.2 Shape Maturation

Following exploring the pattern of size maturation, the progression of shape maturation was analyzed. The shape trajectory was constructed from Procrustes distance measures from the start point mean shape (5 youngest individuals) and the endpoint mean shape (the adult sample). As described in the methods, a sliding average approach was used following Wilson et al. (2015) (Appendix C) in order to reduce the potential of overestimating the true maturation trajectory. The raw Procrustes distance values were then re-expressed as a percentage of the endpoint value. Results are graphically displayed in Figure 4.13. The general trend in the data is significantly positive with a linear R^2 value of 0.979 ($p = <0.001$). The adult sample, plotted as approximately 20 years in age, was used to represent 100% maturity.



Figure 4.14 The percent shape maturity of each individual in the combined sample. The linear R^2 value was 0.979 ($p = <0.001$) indicating a significant positive trend in the data.

In order to directly compare the size and shape maturity trajectories the sliding average approach was applied to the size maturity values. These new percentages were plotted with shape maturity in Figure 4.14. Both data series produce positive trends; with increasing age there is an increase in both size and shape maturity. With both data series standardized to the same sliding average, the graph demonstrates a steeper slope for shape maturation, indicating a greater rate of increase initially. The size maturation trend is more gradual, not overlapping with shape maturation until approximately 8 years old, where the slope continues below that of the shape maturation trajectory. This may suggest individuals reach shape maturation before size maturation.

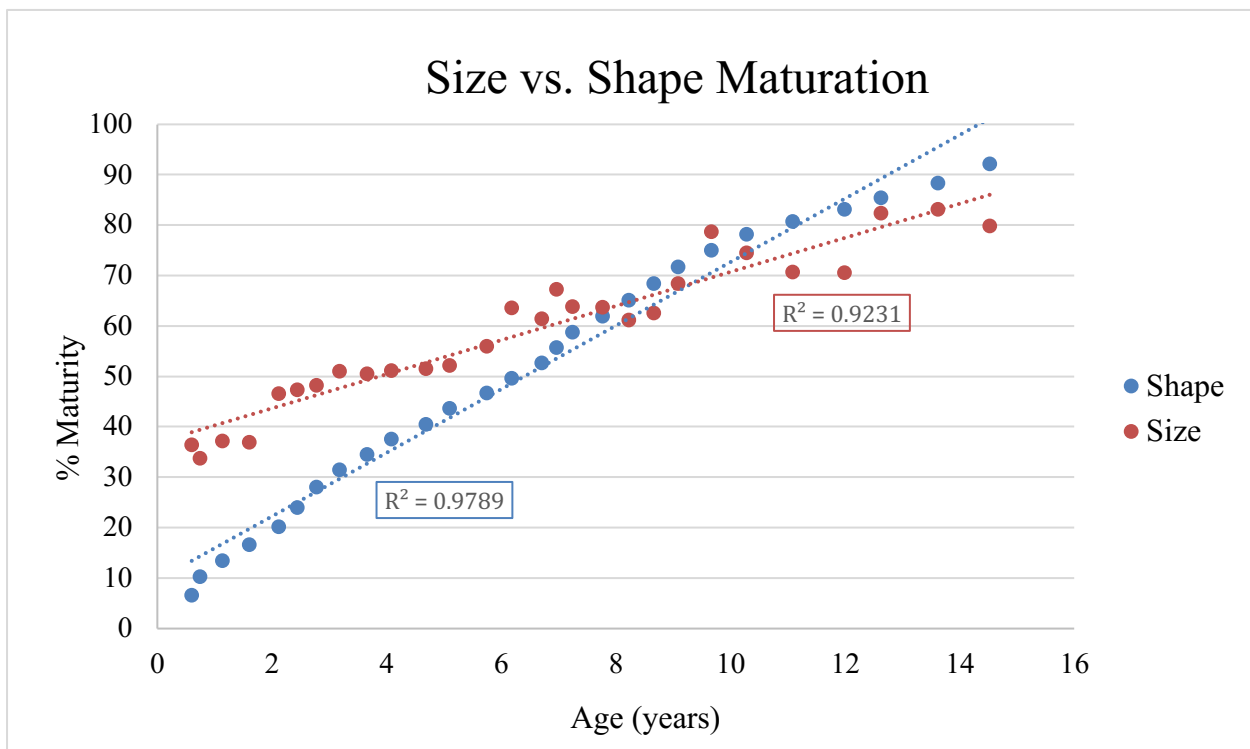


Figure 4.15. A comparison between the shape and size maturation trajectories in the combined sample. The orange series represents the average size-maturation trend. The linear R^2 is 0.923. The blue series represents the shape-maturation trend. The linear R^2 is 0.979.

Chapter 5. Discussion

The results of this thesis have demonstrated that while there are morphological differences in the shape of the iliac crest among age groups, similar trends can be seen in both samples. The shape changes occurring will be explored further to better understand the development of the ilium with respect to the potential impact of intrinsic and extrinsic variables.

5.1 Results in Context

5.1.1 Error Analysis

In order to assess the impact of landmark error the Euclidean distance between the XYZ coordinates of the first fixed landmark between the original trial and error trial was derived. The average error across the 12 specimens was 3.121 units of Euclidean distance, indicating a close placement of the first semilandmark across the specimens. Moreover, a Procrustes ANOVA was run in MorphoJ (Klingenberg 2011) to quantify measurement error in the 82 semilandmarks of each specimen using a ratio of the two variance components from the mean square values. The resultant repeatability was 0.96, or in other words, an error of 4% exists in the placement of the semilandmarks. This is a low error value, and in combination with the close placement of the first semilandmark, indicates that intraobserver error is not a significant contributor to error in this study.

5.1.2 Morphological Shape Change

The first two questions of this thesis aimed to determine the changes that occur in the morphology of the iliac crest, and what the average shape of the crest is at certain developmental stages. When examining the results of the patterns of shape change, the majority of landmark movement between the extremes of variation was in the mediolateral plane. This change in

sinuosity was seen in the LSA, IK and combined samples. Similar patterns of change were observed when comparing age cohorts. Considering LSA independently, there was a significant change in mediolateral sinuosity when comparing the first age cohort (0-1.99 years) to the second (2-7.99 years). However, comparisons between the second and third (8-10.99 years) and third to fourth (11-15.99 years) cohorts demonstrated considerably less variation. The greatest difference was observed in comparing the first and fourth cohorts, which is intuitive given the large difference in age and the expected development between these age groupings. The same results were observed in the IK sample as well as in the combined sample. Comparing the first age cohort to the last (beginning of growth to the end of growth in this sample) there is a change in sinuosity of the iliac crest in the mediolateral plane with increased lateral movement at the anterior portion of the crest and more medial displacement at the posterior aspect of the crest.

The secondary epiphysis that may impact the development of iliac shape is the iliac crest. Ossification of the iliac crest begins at 12-13 years in females and 14-15 years in males (Cunningham et al. 2016). As discussed in the introduction, ossification begins in the anterior portion followed by fusion of the anterior and posterior segments. Fusion of the crest to the ilium begins at the ASIS and progresses posteriorly, with partial fusion by 14-26 years in females and 15-24 years in males (Cunningham et al. 2016). However, if an individual displayed partial fusion of the iliac epiphysis, they were excluded from this sample. Therefore, the process of iliac crest fusion is likely not a component of the shape change being displayed in this study.

However, independent of the secondary epiphysis, there are changes that have been observed over growth between sexes in the iliac crest. For example, Coleman (1969) reported that the mean total growth of the anterior iliac crest is larger in males, while the growth of the posterior region is larger in females. As reported by Humphrey (1998), 70% of adult growth occurs by the

approximate age of 9 years. There was a significant shape change occurring between age groups 1 and 2 (by 8 years of age.) This shape change between the first two age groupings may be correlated with size increase during this ontogenetic stage. It is interesting that a high amount of change is observed between the first two age groupings and not after the initiation of puberty. Puberty is generally seen as the period of greatest developmental growth and is when the expression of secondary sexual characteristics begins to develop. The pubertal growth spurt typically initiates from 10-14 years in females and 14-19 years in males (Rissech and Malgosa 2005). Humphrey (1998) indicated the pelvis is an intermediate-late growing skeletal region, with iliac breadth reaching 70% of adult size at 9 years old and 90% of adult size by 17-18 years old. Following this trajectory, one would therefore expect to see differences between the third and fourth age cohorts of this study, as the fourth group marks the beginning of puberty and an increase in size of approximately 20%. However, a great amount of shape differences sequentially occurred between the first two age cohorts (0-1.99 years and 2-7.99 years). This may be influenced by the large sample size of the second age cohort.

There are several reasons why the signal of the growth spurt may not be apparent in this research, one of which is the osteological paradox. While this paradox will be discussed further in potential sources of error, briefly, the osteological paradox outlines the inherent problem of looking at prehistoric skeletons as they represent individuals who are deceased (Wood et al. 1992). This is especially problematic in juvenile skeletal populations as it is a clear indication of premature death, whether by disease or another manner. Moreover, several studies have found that individuals in development with poor health can result in a slight growth deficit (Saunders and Hoppa 1993) as the body allocates resources to other priorities pertinent to immediate survival. Poor health or nutrition in juveniles may impact the normal growth and development

trajectories (Wilson et al. 2017). Developmental plasticity enables an organism's body to respond to intrinsic and extrinsic factors, such as disease or poor nutrition, and make potential trade-offs to allow immediate survival (Gluckman and Hanson 2006), which may include growth of the bones of the pelvis. Several studies have demonstrated poor childhood nutrition will result in delayed puberty in expectations for better stability in the future (Gluckman and Hanson 2006). Due to the untimely death of the juveniles in the study sample, it is possible that poor health, either from nutritional deficiencies or disease, resulted in a delay in the commencement of puberty. Therefore, it is possible the individuals in this study died before the proper signals of puberty were instigated. However, due to the cross-sectional nature of this study, and the wide age ranges for the initiation of puberty, it is more likely that an averaging effect due to sampling obliterated the ability to see the timing of pubertal growth spurts.

What may be influencing the observed patterns is sexual dimorphism. In younger males, the direction of iliac growth is more lateral initially, followed by superior growth, whereas females develop more laterally later in development (Coleman 1969). The greater superior growth later in development in males and the greater lateral growth later in development in females may be due to obstetric selection by producing a wider lower iliac height in females (Coleman 1969). These growth patterns result in females having a greater point of pelvic breadth superolaterally. Considering the ASIS specifically, Coleman (1969) stated that following both lateral and superior movement, there is a difference of 60-70 degrees in both sexes, measured from the vertical. However, at the PSIS, males see 0-20 degrees of superolateral growth while females typically expand beyond this, reaching 20-30 degrees (Coleman 1969). This results in a wider and broader pelvic shape in females. Wilson et al. (2016) corroborated this observation indicating female iliac crest shape diverges from the male shape especially on the posterior half.

Wilson et al. (2016) also emphasized that curvature is more pronounced in males during development; this sinuosity, especially in the anterior half, increased with age.

Considering the observations of the individuals in this study between the first and last age groups, the change in sinuosity is evident and is consistent with the descriptions by Coleman (1969) and Wilson et al. (2016). Since the sex of the juveniles is unknown, the role of sexually divergent growth trajectories cannot be parsed out; however, the different sinuosity patterns in the anterior and posterior regions may be indicating there is an underlying sex-driven difference in morphology. The significant changes in sinuosity throughout the iliac crest may be largely driven by male patterns of change in the sample. This is further supported by the more medial movement of the posterior region of the crest. As discussed above, females tend to display more lateral growth in the posterior region. Therefore, the medial sinuosity observed between age groups may be due to a larger influence of male growth patterns in the sample. Overall, the differences between the youngest and oldest age groups in this sample are consistent with literature, demonstrating increasing sinuosity with increasing age, with the potential of underlying sex-driven changes impacting resultant movement in the posterior region.

5.1.3 Correlation Between Shape and Size

Two correlation tests were applied to the first 2 or 3 principal components in each sample. The first 2-3 were chosen due to their inclusion of more than half of the total variation in shape. For IK and LSA the first two PCs accounted for 50% of the total variation. However, for the combined sample, PC3 required inclusion to reach 50%. This is likely due to the incorporation of an additional source of variation, since any population-based shape variation was included in the combined sample. The two correlations with shape that were explored included size, with centroid size as a proxy in the analysis, and estimated age. In the LSA

sample, neither variable correlated significantly with the first principal component. However, both size and age correlated significantly with the second principal component. In comparison, the Indian Knoll (IK) sample demonstrated partial separation of the influence of size and shape. The first principal component was significantly correlated with centroid size, while the second principal component was similar to LSA, with correlations to both centroid size and age. While there are slight differences in correlations between the two samples, when combined, the correlation of the two variables on the second principal component persisted. In addition, in the combined sample the first principal component was significantly correlated to centroid size. Therefore, the overall analysis demonstrates that the most significant contributor to shape variation is size-related change, or allometric shape variation. However, the variable of size is further incorporated into the second principal component in combination with a significant correlation with age. The combined impact of size and age is likely driven by an age-size correlation; the ilium increases in size with an increase in age. There is likely significant variation in size at a given age within the sample due to differences between the samples as well. Pfeiffer and Harrington (2010) demonstrated that LSA children are smaller on average in femoral length, especially when compared to IK children. This may be impacting the signal of age-size related change.

The significant correlation of shape to size indicates patterns of ontogenetic allometry in the sample. Allometry itself is the covariation between shape and size, as defined by Gould (1966, 1975). Ontogeny is essential as it is through this process that differences in adult form are achieved (Klingenberg 2016; Terhune et al. 2013). Moreover, these resultant forms can be impacted during growth by variables such as health, nutrition, and environment, and the timing of these variables during growth between sexes can be very influential on resultant

morphological variation in adults (Freidline et al. 2015; Smith et al. 2013). Three modes of allometry have been considered including static, ontogenetic, and evolutionary (Freidline et al. 2015; Klingenberg 2016). In static allometry, shape change related to size change occurs within a single ontogenetic stage within individuals or populations of a species (Freidline et al. 2015). Evolutionary allometry also occurs within the same ontogenetic stage but occurs between several lineages (Freidline et al. 2015). The main difference in ontogenetic allometry is that the size-shape changes occur over several ontogenetic stages. In other words, it is the change associated with increased size during growth, an expected result and seen in this study.

5.1.4 Maturation Trajectory

Age, and therefore development, is a major aspect of juvenile pelvic shape variation. Morphological changes in the pelvis occur gradually and continuously over development (Olivares and Aguilera 2016) and therefore must be considered in the manifestation of shape variation. Biological processes during maturation impact shape and size of certain features at a given age, and therefore its development in this context is essential. The third question of this thesis was to determine what the maturation trajectory looked like in each population with respect to shape and size. When exploring the general trends of growth with respect to both size and shape, both resulted in a positive correlation: with an increase in age there is an increase in size and a positive trend towards adult shape (as defined by the mean shape of the adult sample). While both values demonstrate a positive correlation, there is a stronger relationship between age and shape maturation. However, this may be a result of how shape maturation was explored in the study. Instead of using the raw age and Procrustes distances, a sliding average age was used, as demonstrated by Wilson et al. (2015) (Appendix C), in order to correct for over-estimating the maturation trajectory. If a sliding average was not used, the analysis would assume that for an

individual to reach the maturation stage of an individual 5 years old, they must pass through the shapes of the individuals preceding that age. This assumption can result in the overestimation of the maturation trajectory, especially considering the data are cross-sectional. Averaging the Procrustes distances with a sliding average acts as a smoothing function, reducing the impact of such an assumption (Wilson et al. 2015). This approach was initially only applied to shape maturation. However, in order to directly compare size and shape maturation, the same procedure was applied to size maturation in a second analysis. This resulted in a significant correlation for size maturation. Therefore, both size and shape maturation demonstrate a significant positive correlation with age when using the sliding average method. Moreover, the similar trend supports the covariation of size and shape in this study. In the graphical comparison of the two maturation trajectories, the slope of size maturation is lower, not overlapping with shape maturation until approximately 8 years old. At this point the slope of size maturation continues to be positive, as does shape maturation; however, size maturation continues below the slope line of shape maturation. This demonstrates that size maturation may be occurring at a slower rate than shape maturation; individuals attain adult shape in advance of reaching mean adult size.

When examining normal development, the pubescent growth spurt is often the period of biggest growth (Coleman 1969), although pelvic remodeling does extend into adulthood (Fischer and Mitteröcker 2017). While this research did not directly examine the impact of sexual dimorphism on the development of pelvic morphology, it is a part of contrasting normal development of male and female growth patterns and can be directly correlated to both size and shape. This concept will be further explored examining sexual dimorphism and the obstetrical dilemma hypothesis in a following section, as it is important to look at adult sexual dimorphism

in the samples first. The size-driven shape changes observed in this study sample may be due to underlying sexual dimorphism in combination with growth related size changes. The resultant male and female morphology seen in adults of a given population are achieved through the development of sexually dimorphic traits through different patterns, rates, or periods of growth (Rogers 2005). However, while dimorphism may be present in juveniles, many studies have shown that reliable sex estimation is not achievable until after puberty (Boucher 1955; Hunt 1990; Mittler and Sheridan 1992; Reynolds 1945; Schutkowski 1993; Thomson 1899; Weaver 1980). Several authors have expounded on observations and methodologies of the fetal, infant, and juvenile pelvis (i.e. Boucher 1957; Choi and Trotter 1970; Reynolds 1945). Hromada (1939) observed little sexual dimorphism between fetal months 2-7; however, differences became more apparent after 7 months. Nevertheless, prior to puberty, it is more likely that males and females show similar growth trajectories due to similar functional requirements (Humphrey 1998). Various metric and morphological methods have assessed sex estimation in juveniles, each failing to provide reliable or consistently significant results (i.e. Loth and Henneberg 2001; Olivares and Aguilera 2016; Schutkowski 1993; Vlak et al. 2008; Wilson et al. 2008). If sex were a known variable for the juveniles in the samples, it is possible the results may separate variation according to sex, or that sex in combination with other variables is responsible for patterns of shape change. However, this is a postulate for future research on samples with juveniles of known sex and age.

5.2 Adult Shape Variation

The adult pelvis is a key bone in many skeletal analyses, used in two primary aspects of the biological profile: age and sex (e.g. Buikstra and Ubelaker 1994; Phenice 1969; Rogers and Saunders 1994; Sutherland and Suchey 1991). Such demographic information is imperative in

any study of an archaeological skeletal assemblage that examines human physiology or behaviour in the past. Skeletal analyses are generally more robust in adults as juveniles have not yet reached skeletal maturity, impacting analyses such as sex estimation as well as the preservation potential of skeletal elements. Moreover, the interplay of plasticity and developmental constraints during pelvic growth may further impact how variation is displayed in pelvic morphology. Several methods of juvenile sex estimation have been proposed using other skeletal elements (e.g. Cardoso 2008; Molleson and Cruse 1998; Rogers 2009); however, these tend to be population specific and therefore not applicable in assemblages of unknown origin. Due to the high accuracy in adult pelvic sex estimation (e.g. Buikstra and Ubelaker 1994; MacLaughlin and Bruce 1986; Rogers and Saunders 1994; Sutherland and Suchey 1991; Washburn 1948), many studies have focused on the potential of the juvenile pelvis in subadult sex estimation. However, pelvic traits used in adult sex estimation result in juvenile analyses with low reproducibility (e.g. Cardoso 2008; Holcomb and Konigsberg 1995; Schutkowski 1993; Sutter 2003; Weaver 1980; Wilson et al. 2008, 2011). Since juvenile sex could not be directly examined in this study, looking at adult sexual dimorphism was a way of understanding sexual dimorphism in the samples in general and the potential role it has in impacting shape variation.

A total of twenty adults (10 males and 10 females) were included from LSA and IK in order to explore the end point of growth in both samples. It is possible that by exploring the drivers of shape variation in the adults, inferences could be made on what may be happening during growth to result in these morphologies in adulthood. Since the sex of the adults were estimated, the role of sexual dimorphism could be explored despite not being able to directly assess it in the juvenile sample. It is important to note that the sex estimations were conducted by observers through visual assessment and therefore may have inaccuracies. However, studies have

shown up to 96% accuracy can be achieved through such methodologies (Phenice 1969) and therefore these estimated values were included. The results of the Principal Component Analysis of the adult sample demonstrated there was a significant correlation of PC1 with centroid size.

A t-test was run to determine if there was a significant difference in centroid size based on sample. The results of this test indicated a significant difference in centroid size between IK and LSA adults. This means centroid size is likely impacting shape variation along PC1, which may also be influenced by the fact that there are two samples. A t-test determined that the LSA are smaller in mean size. When the samples were examined independently, only the LSA adults demonstrated a weak significant difference between male and female shape, while the IK and combined samples did not demonstrate significant shape differences between sexes. The t-test exploring whether males and females were different based on centroid size was not significant. These results are slightly unexpected; in a given adult sample one would expect to see the impact of sexual dimorphism, especially when examining the pelvis as it is the most accurate bone for such analyses. Additionally, given the significant impact of size, one would expect sexual dimorphism to be underlying this difference.

There are a few reasons why sexual dimorphism may not be seen in the study sample. These samples may not display as much sexual dimorphism as other populations due to the lack of sexual dimorphism in the adults. Studies on different populations have demonstrated that populations will differ in sexually dimorphic traits based on geographic and ecological location (González et al. 2007). Kenyhercz et al. (2017) examined how different populations can vary in sexually dimorphic traits by applying a global equation of sex estimation to different groups. This global equation included samples from all temporal and geographic groups possible. While their results demonstrated a correct classification rate of 93.5%, the authors did emphasize that

population-specific equations rather than a global equation would produce higher accuracies (Kenyhercz et al. 2017). This is because by pooling populations from very different geographic locations, there is the chance that less dimorphic populations or populations with different patterns of trait expression may be impacting the applicability of the global equation (Kenyhercz et al. 2017). The following sections will further explore the major variables at play that result in population differences including the evolvability of the pelvis in light of the obstetrical dilemma hypothesis and the important role of developmental plasticity.

It is possible that there is not a strong signal of sexual dimorphism in the sample because of the pelvic region being explored. The pubic bone produces the highest accuracies in visual sex estimation, specifically, the ventral arc, the subpubic concavity, and the ischio-pubic ramus (Phenice 1969). Buikstra and Ubelaker (1994) expanded on adult pelvic sex estimation by including the size of the greater sciatic notch and the presence or absence of the preauricular sulcus. There are different hypotheses regarding which region of the pelvis is the most accurate for exploring sex-based morphological differences. Coleman (1969) postulated that the majority of sexually dimorphic growth occurs from the lateral migration of the ischium in females to expand pelvic capacity. Conversely, St. Hoyme (1984) hypothesized the significant growth occurs in the posterior portion of the pelvis. This growth occurs either on the iliac portion of the sacroiliac joint or on the sacral portion of the joint (St. Hoyme 1984). While many studies have explored the pelvic inlet and outlet (e.g. Coleman 1969; Rosengberg and Trevathan 2002; Tague 1989), which are in some dimensions defined by the ilium, the iliac crest does not necessarily differ in morphology based on sex. Shifts in the position of the iliac crest are likely the by-product of the overall position of the pelvis. Adult sex estimation methods either primarily focus on the pubic region, or the overall shape of the pelvis in anatomical position, not the shape of the

iliac crest. While studies on juvenile sex estimation have looked at the iliac crest and produced varying accuracies on sex estimation (e.g. Olivares and Aguilera 2016; Shutkowski 1993; Vlák et al. 2008; Wilson et al. 2008, 2011, 2015), few adult studies have explored this region due to the high accuracies in overall shape and pubic analyses. It is possible that during growth the iliac crest demonstrates variations between sexes, but that by adulthood, this signal is not detected due to the small sample size in this study and a potentially smaller difference in overall shape. However, it is also possible that the study samples are simply less sexually dimorphic in the region of the iliac crest, and stronger separation of the sexes may have occurred if a different pelvic region was explored. Therefore, further exploring the obstetrical dilemma hypothesis in tandem with developmental plasticity may help to explain the trends of iliac crest movement in increased sinuosity demonstrated in the study samples.

5.3 Obstetrical Dilemma Hypothesis

While the above section briefly discussed sexual dimorphism, its expression in the human pelvis is due to evolutionary processes differentially impacting each sex due to both intrinsic and extrinsic limitations. Understanding the growth of the pelvis in combination with the potential development of secondary sexual characteristics relates to the obstetrical dilemma (OD) hypothesis, which contrasts the role of bipedalism and parturition in females. This section will further explore the postulates of the hypothesis while discussing the evolvability of the pelvis and how developmental plasticity impacts shape morphology during ontogeny. It is imperative to study the postulates of the OD hypothesis in light of the results of minimal sexual dimorphism seen in the adults of this study. While testing sexual dimorphism was not one of the questions of

this thesis, it is an inherent aspect of pelvic morphological differences, and therefore its potential impact on pelvic morphology is important to consider.

The OD hypothesis states that sex differences exist in the human pelvis due to sex-specific solutions to selective pressures such as bipedal locomotion and safe parturition. Considering overall pelvic shape rather than specific regions, it has been previously hypothesized that males have greater external dimensions, while females have greater internal dimensions to facilitate childbirth (Coleman 1969). One reason for this that has been proposed is males have a slightly larger pelvic complex before the adolescent growth spurt. On the other hand, it may be attributable to the earlier age at which the growth spurt occurs in females; this ceases growth earlier than in males, allowing for continued growth in males (Coleman 1969). However, Coleman (1969) emphasizes that differences in the pelvic inlet are due to functional demands. Lower iliac height in females is directly related to the second functional role of the pelvic complex: parturition (Coleman 1969). However, more recent studies contradict this hypothesis and demonstrate a weak relationship that pelvic inlet shape differs significantly by sex (e.g. Delprete 2017; Gluckman and Hanson 2006; Tague 1994). While there is evidence for different growth trajectories between males and females, Delprete (2017) emphasizes that pelvic morphology is extremely variable during growth. This does not mean that sexual differences do not exist between male and female pelvis. Countless studies have shown statistical significance in various pelvic elements, including overall pelvic shape. For example, Koļesova and Vetra (2011) concluded the female pelvic cavity is statistically wider in females, especially in the transverse diameter (also supported by Correia et al. 2005). What this does mean is that there are more variables than sex-driven growth that impact resultant pelvic morphology (Brown 2015). Humans have been shown to display a reduced integration within the birth canal and between the

birth canal and other traits (Brown 2015; Grabowski et al. 2011). Betti (2017) explored population-based variation of the pelvis and concluded females did not display less variation than males, which would not be expected if strong evolutionary forces due to obstetrics were at play.

If obstetrics does not play as influential of a role in pelvic evolvability, the other component of the OD hypothesis must be further explored: bipedal locomotion. Recent research has heavily focused on further exploring the OD hypothesis in light of other selective pressures in order to better understand pelvic shape within and between populations. The OD as a driving force for morphological variation in the pelvis is no longer considered sufficient (Dunsworth et al. 2012; Dunsworth and Eccleston 2015; Kurki 2013; Roberts and Thorpe 2014). Dunsworth (2018) emphasized that modern experimental designs on pelvic efficiency in walking and running have been unable to demonstrate that the female pelvis is evolutionarily constrained by the balance between bipedalism and childbirth. Furthermore, bony pelvic anatomy demonstrates considerable variability (Betti and Manica 2018; Betti 2017) while not impacting bipedal locomotion (Warrener et al. 2015). Wall-Scheffler and Myers (2017) further explored the kinematics of locomotion in humans. The plane in which females are wider than males is primarily the mediolateral plane, and it is this expansion that is often attributed to locomotor constraints on females (Wall-Scheffler and Myers 2017). However, Wall-Scheffler and Myers (2017) have argued parturition is more related to the dimensions of the anteroposterior plane. Ruff (1995) has also supported the greater role of the anteroposterior plane in obstetrics. Ruff (1995) emphasized that further expansion of the mediolateral plane is restricted by climatic and thermoregulatory reasons in addition to bipedalism, while expansion in the anteroposterior plane would not have significant impacts on such considerations. Moreover, the expansion of the true

pelvis in the anteroposterior plane, while the inlet remains relatively wide mediolaterally, is associated with the development of rotational birth: the narrow lateral walls of the midplane result in the rotation of the fetal head to the anteroposterior plane, which is the largest diameter in modern human's lower true pelvis (Ruff 1995).

Understanding the OD hypothesis and postulates that have been challenged is essential to consider in a study that is exploring juvenile pelvic ontogeny and morphological change. Even though this thesis did not directly explore sex estimation in juveniles, understanding the OD hypothesis outlines the potential changes that may appear in morphology over ontogeny. This section emphasizes that there are more factors that impact shape morphology, which may be impacting the results seen in this study. Moreover, the fact that this study only explored the iliac crest may explain why patterns of sexual dimorphism were not detected. The iliac crest is only one morphological component of the obstetric pelvis. It is the iliac crest in relation to other proportions of the pelvis that create the wider inlet in females than in males. By studying the crest in isolation, it is not possible to study the overall pelvic shape. In light of what drives sexual dimorphism in the pelvis according to the OD, examining the crest alone may explain why differences were not detected between the males and females of this study.

5.4 Revisiting the Question: Differences Between Populations

The fourth question of this thesis was whether there is a difference in the patterns of growth between two different populations. The results of this study found that there were similar trends of iliac crest shape change in both populations. These results are slightly surprising given that the developmental constraints believed to be present on pelvic morphology due to the OD hypothesis are more relaxed, resulting in higher plasticity, so we might expect different habitual

activities in the two study samples to perhaps result in differing pelvic morphology.

Developmental plasticity is the ability of a genotype to alter both developmental processes and phenotype in response to differential environmental pressures and a relaxation in evolutionary limitations and is a potential source of variation in pelvic shape during development (Betti 2017; Hochberg et al. 2011; Moczek et al. 2011; Wells et al. 2012; Wilson et al. 2015). In other words, developmental plasticity can result in pelvic variation because it facilitates the alteration of phenotypic expression of traits. Developmental plasticity is essential in the study of growth as adult pelvic shape is achieved through the developmental constraints present during growth that influence its response to external pressures. Lower covariance and high evolvability of the pelvis may explain its phenotypic plasticity and resulting population-specific differences in morphology (Betti 2017). Lower evolutionary constraints help explain why, despite obstetric pressures, variation can be seen in both male and female pelvises (Betti 2017). In comparison to non-human primates, the human pelvis is described as less constrained, resulting in its susceptibility to morphological change (Betti 2017; Grabowski et al. 2011; Grabowski and Roseman 2015). Considering the human pelvis, Betti (2017) reported that geographic distance is responsible for 30-35% of the variation between human populations, while climatic adaptation is responsible for approximately 43% of variation. Therefore, one may expect to see morphological differences in pelvic shape between populations of different geographic regions due to genetic reasons. There are both genetic and non-genetic processes that impact how pelvic variation manifests. Non-plasticity factors, such as geography-based differences caused by genetic drift and natural selection, may underlie pelvic differences. However, pelvic morphological differences are not seen in the results of this study despite the two samples being in different geographic regions. It is possible that both samples were experiencing similar stressors that resulted in similar plastic

responses during growth regardless of any pre-existing genetic differences in pelvic shape. The factors that can impact plastic pelvic morphology during the lifetime can be extrinsic or intrinsic and may impact growth (size and age) or development (shape and age) of the pelvis (Wilson et al. 2017). These pathways of plasticity can be driven by genetic and non-genetic processes, impacting how a bony component responds in morphological change. Extrinsic factors include but are not limited to cultural processes, climate, prenatal and postnatal nutrition, levels of physical activity, health/disease, and endocrine-disruptive chemicals (Betti 2017; Hochberg et al. 2011; Wilson et al. 2017). Intrinsic factors can include variation in the length or patterns of size or shape maturity trajectories (Wilson et al. 2017) and specifically target physiological processes through leptin, the GH-IGF-I axis, ghrelin, thyroid hormones, insulin, and the cortisone-cortisol shuttle (Hochberg et al. 2011).

Bone is able to demonstrate phenotypic plasticity during growth because bone formation and remodelling respond to mechanical stimuli (Abel and Macho 2011). Studying this process during growth is important as the susceptibility of bones to strain is more acute during childhood (Stock 2006). Cunningham and Black (2009) have argued that such mechanical stimuli begin in utero through early reflexive limb movement. The ability of bone to respond to stimuli indicates that bone morphology is a reflection of genetic, epigenetic, and extragenetic factors (Cunningham and Black 2009). It has long been accepted that the geographic environment of an individual is typically reflected in body proportions (Ruff 1991). Body breadth should be larger in colder environments and smaller in warm environments due to thermoregulatory constraints on body shape and size (Ruff 1991). However, these geographic clines in body size and shape are compromised by many other factors, such as individual variation in response to intrinsic and extrinsic variables during growth (Ruff 1991). It is through the integration of genetic and

environmental influences working with plasticity over development that variation arises in a population (Grabowski and Roseman 2015) and both natural selection and evolutionary forces may influence within-group variation (Betti et al. 2013; Roseman and Auerbach 2015). Lewontin (1972) described how phenotypic clusters in population dynamics are the outcome of evolutionary processes acting on individual variation that is inherent genetically within a population. Besides natural selection acting on ecogeographic patterns of body form, random genetic drift, mutation, and gene flow are also at play (Roseman and Auerbach 2015). This demonstrates the complicated factors that impact pelvic variability. There is a genetic component as well as the plastic response of bone to stimuli unique to individuals.

The strength of developmental plasticity lies in the fact that the phenotype is able to alter in response to environmental conditions (Moczek et al. 2011). This plasticity acts as a buffer against potentially harmful environmental and genetic disturbances, and therefore, cryptic genetic variation accumulates in a population (Moczek et al. 2011). These genetic variations are considered neutral and therefore hidden from selection unless acted upon specifically (Moczek et al. 2011). In other words, having this plasticity allows a range of phenotypes to exist in a given population that are triggered for survival in a variety of scenarios (Gluckman and Hanson 2006). Therefore, one would expect in a study examining two or more populations, there is the potential for genotypes giving rise to a range of phenotypes in differing environmental contexts. While one would therefore expect major differences between the two given populations this is not necessarily true and is demonstrated in the results of this study. The two samples experienced similar shape changes and had similar mean shapes. The role of individual variation has demonstrated that the majority of genetic diversity exists at the local population level (Betti et al.

2013; Lewontin 1972). Exploring a larger sample of one population in this study may better demonstrate pelvic variation than comparing two different populations.

Examples of variation within populations have been demonstrated in many studies of archaeological human populations as well. The application of sex estimation in different populations has demonstrated the role of both genetics and environment. This is due to the fact that one method of sex estimation can produce varying accuracies depending on the population at hand as well as within population variation (e.g. LaVelle 1995; MacLaughlin and Bruce 1996; Weaver 2002; Weaver and Hublin 2009). Kurki (2013) found that pelvic geometry may vary among populations due to climatic or demographic pressures on body shape and size. Higher latitude populations had a transversally wider mid-plane pelvic shape and a shallower anterior-posterior inlet than lower latitude populations (Kurki 2013). This follows patterns of the overall human body, which has been described to vary based on ecogeographic location: colder climates result in shorter limb proportions and larger, broader bi-iliac breadths (Holliday 1997; Kurki 2013; Ruff 1994). Variation in the pelvis among different populations has been demonstrated through pelvic shape analysis in several studies (e.g. Betti et al. 2014; Kimura 1982; Kurki 2013; LaVelle 1995; MacLaughlin and Bruce 1996; Weaver 2002; Weaver and Hublin 2009). It is important to emphasize this shape variation is at the population level and is partially attributable to genetics. Betti et al. (2012) corroborated this by stating pelvic variation within a population suggests a phylogenetic history of genetic and selective pressures impacting shape through genetic drift, excluding the possibility of plasticity. On the other hand, Kurki (2013) also demonstrated that because growth is related to pelvic capacity, poor health and childhood nutrition can impact body size and consequently pelvic capacity, which is plasticity. Therefore, conditions experienced during growth can influence pelvic shape. It is essential to understand the

developmental constraints experienced during growth in order to acknowledge external pressures and any resulting pelvic variation.

Therefore, it is evident that populations can vary in pelvic morphology beyond sexual dimorphism due to external factors impacting comparative assessments of sex estimation. While these genetic and evolutionary factors can impact pelvic variation at the population level, there are several other factors that can impact pelvic shape. These factors include individual plastic response to differences in health, diet, lifestyle, or other factors. This may help to explain the lack of difference seen between the populations in this study. Despite varying temporal contexts, geographical regions, and subsistence strategies, similar patterns of development were observed in the IK and LSA populations. If developmental plasticity best describes differences between individuals instead of variation between populations, it is possible for similar trends to be seen when comparing two different ecogeographic populations. This does not mean that there were not differences between the two populations, but that the differences may have resulted in similar pressures and resultant maturation trajectories in both populations and that exploring a larger sample of one population may better explain pelvic shape variation within the population. Moreover, only one aspect of the bony pelvis was considered in this research: the iliac crest. By examining a specific region, many signals of overall pelvic differences may not be included in the results of this study.

5.5 Research Evaluation

As briefly discussed above, one of the inherent issues in studying skeletal populations is the osteological paradox (Wood et al. 1992). The individuals being studied represent non-survivors, and therefore they likely do not represent the whole population (Wilson et al. 2017). Moreover, by studying deceased children, it is probable they experienced prolonged illness or

inadequate nutrition during life, either of which could impact growth and development. As this study directly explored growth, such an impact may have significantly affected the results by underestimating the full growth potential. This potential growth deficit is an inherent bias in subadult skeletal samples (Saunders and Hoppa 1993). However, this is more likely for the IK sample than LSA sample due to the lack of observed long-term health defects in LSA (Pfeiffer and Harrington 2018). Moreover, while the samples had approximately the same distribution, each sample's population distribution of life expectancy may be different. While attempts were made to study as many individuals throughout growth, it is possible the high number of infants in IK may have impacted the results. Studies of the IK population have indicated a high infant mortality, with 20% of skeletal individuals under one year old in the entirety of the IK sample (Johnston and Snow 1961). While not every infant was included in this study, the high mortality of infants in the sample may be indicating severe health issues in the sample, which could impact growth and development trajectories. The burials themselves may also be a potential source of error. Both populations were seasonal foragers, moving across the landscape during the year. The burials included cannot represent the entire mortuary population and may represent biased seasonal or socially defined subsets. This is especially true from LSA due to the fact that burials were collected from different site types over a large spatial area, while Indian Knoll burials were from one burial type in a focused area.

Another potential source of error in this study is the application of age estimation. The method used for dental estimation is developed using mandibular dentition; however, to increase sample size in the samples, the same developmental patterns were used on maxillary teeth in the absence of mandibular dentition. While the same application of developmental patterns was applied to both samples, it is possible that potential error effect is different for each sample.

There may be slight discrepancies in eruption and development between maxillary and mandibular teeth, which may have impacted the age estimations. However, while there is population variation in dental eruption timing, the sequence is usually consistent. Dentition is less sensitive than skeletal elements to environmental impacts on development (Liversidge et al. 1998; Van Der Linden 1966). Moreover, some individuals of the LSA sample did not have teeth, and therefore a regression formula created using those with dentition and long bone lengths was applied. While this succeeded in increasing sample size, one cannot assume that every individual follows the same growth trajectory. This method acts under the assumption that there is a general pattern of dental growth in relation to long bone length growth, which may be significantly biased depending on the individuals of the sample in question. However, this bias was minimized by the creation of population specific formulae for LSA and IK, respectively. This privileges the identification of relative development of individuals in the sample rather than specific age estimates. However, since this study explored general developmental patterns between age groups and not specific individual age-based comparisons, the chance of misclassifying age is lessened.

While left ilia were preferentially used, to increase sample size, reflected right ilia of individuals lacking a left were included. Some authors (Bytheway and Ross 2010) have stated it is better to avoid reflectivity due to the potential of asymmetry in the pelvis. Kurki (2017) explored asymmetry in canal and non-canal aspects of the pelvis. Asymmetry can occur due to genetics, but it is typically seen as a plastic response to biomechanical loading (Kurki 2017). The low levels of morphological integration found in pelvic traits increase the likelihood of variability in asymmetry at an individual and population level; however, Kurki (2017) concluded that there were low levels of directional asymmetries in all pelvic traits, which is also consistent

with previous research. It is still possible that asymmetry may have impacted the morphological results in this study, but research such as that conducted by Kurki (2017) demonstrate there is likely a low influence of asymmetry on pelvic traits. This is further supported by the overall low asymmetry in the lower limbs (Auerbach and Ruff 2006).

Furthermore, while geometric morphometrics is considered to be more repeatable than visual assessment of skeletal elements and can provide a more nuanced examination of shape variation, there is the possibility for human error in the placement of landmarks. This can be very influential in studies using traditional landmarks; however, since this study used semilandmarks, the impact is likely less notable due to the reliance on the placement of only one homologous landmark. Only the first landmark was placed at the exact same location between individuals. The placement of this initial landmark may have varied due to intraobserver error. However, although the landmarks placed along the iliac crest became sliding semilandmarks in the analysis, there is the possibility for discrepancies in the crest location and therefore general outline of the iliac crest. Young individuals have very amorphous crests, making demarcating the crest border challenging, potentially impacting the comparison between such age cohorts and older individuals with more defined iliac crest outlines. Moreover, the statistical analysis on intra-observer error did not demonstrate significant differences and therefore a high accuracy and repeatability of both deriving the semilandmarks and the placement of the original homologous landmark on the ASIS. Nevertheless, considering the time required to landmark the individuals, a future research design could explore an alternative method of obtaining the outline of the iliac crest to derive semilandmarks from.

Finally, this research was limited by only examining the iliac crest. The iliac crest is only one component of the bony human pelvis. While morphological change was observable in the

iliac crest, drawing its broader connection to aspects such as the OD hypothesis and developmental plasticity in response to intrinsic and extrinsic factors is limited to a section of the pelvis rather than the pelvis overall. This may have impacted results such as those exploring sexual dimorphism in the adult population. It also limits the ability to compare the two populations as differences within or between may be better highlighted in examining the entire pelvic shape or another pelvic region.

6.0 Conclusion and Future Directions

The goal of this thesis was to explore pelvic variability of the iliac crest during growth between two archaeological human skeletal collections in order to understand the development of the iliac crest. The first two questions postulated were 1) What morphological changes occur in the iliac crest? and 2) What is the average shape of the iliac crest at developmental stages?

Landmark movement occurred primarily in the mediolateral plane of the iliac crest in each study sample. This sinuosity was especially notable when comparing the first two age cohorts, and the first and last age cohorts. Increased lateral movement at the anterior portion of the iliac crest was observed, with contrasting medial displacement at the posterior portion of the iliac crest. Further tests explored the cause of morphological variation, testing centroid size as a proxy for size and age. In the LSA sample neither variable correlated with principal component one; however, both correlated significantly with principal component two. In comparison, IK principal component one correlated significantly with centroid size while principal component two correlated with centroid size and age. These results support that the most significant contributor to morphological shape variation is allometric shape variation, or size-related change.

The third question was 3) What is the maturation trajectory in each population? Both size and shape demonstrated a positive correlation with age. A stronger relationship was observed between age and shape maturation; however, both size and shape demonstrate a highly significant positive correlation with age. Size maturation is more gradual, not overlapping with shape maturation until 8 years of age, at which point shape maturation occurs at a faster rate. This indicates individuals may reach adult shape before attaining mean adult size.

The fourth question was 4) Is there a difference in growth patterns between two populations? The results of this study concluded there were similar trends of iliac crest shape

change in both populations. This growth is largely impacted by an increase in size but can also likely be attributable to external factors such as individual plasticity and sexual dimorphism. These similar patterns are likely due to the fact that the majority of genetic variation exists within populations rather than between. With the impact of individual plasticity, is it likely a high degree of variation exists within a given population. Future research should consider studying a larger subset of a population sample in order to better understand the individual variation in addition to studying the potential intrinsic and extrinsic factors that might influence pelvic variation. Moreover, while sexual dimorphism was not directly observed or tested for in this study, it is also an area for future research. It is possible the mean shapes observed in these results were influenced by sex-driven changes in pelvic shape. A future study on juveniles of known sex could better illuminate the influence of sexual dimorphism during pelvic growth while continuing to explore individual pelvic variation.

There are several future avenues of research that could develop from this study. Further statistical tests could be applied to the data. For example, Freidlinem et al. (2015) expanded their study by exploring the percentage of shape variation explained by allometry. Such an analysis could also be applied to this research to potentially explore the allometric growth patterns in this study. Wilson et al. (2015) used such allometric studies to explore different types of growth trajectories and where in pelvic growth such trajectories could be seen. A study of allometric patterns could be furthered by computing the angles between allometric trajectories to use in comparison (Klingenberg 2016). Moreover, Smith et al. (2013) looked at the relationship between ontogenetic patterns and molecular distance in order to explore population history. Their analysis included exploring differences in adult size between populations to explore the possible differences in timing and or rate of growth (Smith et al. 2013). Furthermore, while this

study mentioned the potential influence of underlying sex differences driving some patterns of shape change, it could not be explored as the juveniles were of unknown sex. This research could be taken further by applying a similar methodology to a juvenile population with known sex. While many studies have looked at shape sexual dimorphism, the importance of size in development was important in this study and may be better at sexual dimorphism in juveniles. It would also be beneficial to employ this methodology to more populations to better understand how population differences impact pelvic morphology.

Overall, this study has demonstrated that patterns of morphological change can be observed over growth. Examining changes in morphology of the iliac crest over ontogeny, there was a consistent pattern of increased mediolateral sinuosity, especially within the first two age groupings, which demonstrates 70% of pelvic growth (Humphrey 1998). This change in sinuosity was especially pronounced when comparing infants to older children in the last cohort, demonstrating the change in iliac crest shape with growth. Similar trends were found in both samples. A significant correlation between size and shape indicates patterns of ontogenetic allometry. A positive correlation was found for both size and shape maturation over growth. Once again, these trends were similar in both samples. There was an overall similarity in growth patterns between the two different populations for all analyses. Moreover, future research is required to better understand the interplay of sexual dimorphism and developmental plasticity and the importance of looking at pelvic variation both within and between different populations.

Works Cited

- Abel, R. and G. A. Macho. (2011). Ontogenetic changes in the internal and external morphology of the ilium in modern humans. *Journal of Anatomy* 218: 324-335.
- Adams, D. C., M. L. Collyer, and A. Kaliontzopoulou. (2019). Geomorph: Software for geometric morphometric analyses. R package version 3.1.0.
<https://cran.r-project.org/package=geomorph>.
- Aiello, L. and C. Dean. (1990). *An Introduction to Human Evolutionary Anatomy*. Elsevier Ltd.
- Auerbach, B. M. and C. B. Ruff. 2006. Limb bone bilateral asymmetry: Variability and commonality among modern humans. *Journal of Human Evolution* 50: 203– 218.
- Baab, K. L., K. P. McNulty and F. J. Rohlf. (2012). The Shape of Human Evolution: A Geometric Morphometrics Perspective. *Evolutionary Anthropology* 21: 151-165.
- Bastir, M., P. Godoy and A. Rosas. (2011). Common Features of Sexual Dimorphism in the Cranial Airways of Different Human Populations. *American Journal of Physical Anthropology* 146: 414-422.
- Betti, L. (2017). Human Variation in Pelvic Shape and the Effects of Climate and Past Population History. *The Anatomical Record* 300: 687-697.
- Betti, L. and A. Manica. 2018. Human variation in the shape of the birth canal is significant and geographically structured. *Proceedings of the Royal Society B* 285: 1-9.
- Betti, L., N von Cramon-Taubadel and S. J. Lycett. (2012). Human pelvis and long bones reveal differential preservation of ancient population history and migration out of Africa. *Human Biology* 84: 139-152.
- Betti, L., N. von Cramon-Taubadel and S. J. Lycett. (2014). The interaction of neutral evolutionary processes with climatically driven adaptive changes in the 3D shape of the human os coxae. *Journal of Human Evolution* 73: 64-74.
- Betti, L., N. von Cramon-Taubadel, A. Manica, and S. J. Lycett. (2013). Global Geometric Morphometric Analyses of the Human Pelves Reveal Substantial Neutral Population History Effects, Even across Sexes. *PLOS ONE* 8(2): e55909.
- Bookstein, F. L. (1989). “Size and Shape”: A Comment on Semantics. *Systematic Zoology* 38(2): 173-180.
- Bookstein, F. L. (1991). *Morphometric tools for landmark data: Geometry and biology*. Cambridge University Press.

- Bookstein, F. L. (1996). Biometric, biomathematics and the morphometric synthesis. *Bulletin of Mathematical Biology* 58(2): 313-365.
- Bookstein, F. L. (1996/7). Landmark methods for forms without landmarks: morphometrics of group differences in outline shape. *Medical Image Analysis* 1(3): 225-243.
- Boucher, B. J. (1957). Sex Differences in the Foetal Pelvis. *American Journal of Physical Anthropology*: 581-600.
- Brooks, S. and J. M. Suchey. (1990). Skeletal age determination based on the os pubis: a comparison of the Acsádi-Nemeskéri and Suchey-Brooks methods. *Human Evolution* 5(3): 227-238.
- Brown, K. M. (2015). Selective Pressures in the Human Bony Pelvis: Decoupling Sexual Dimorphism in the Anterior and Posterior Spaces. *American Journal of Physical Anthropology* 157: 428-440.
- Buckberry, J. L. and A. T. Chamberlain. (2002). Age Estimation from the Auricular Surface of the Ilium: A Revised Method. *American Journal of Physical Anthropology* 119: 231-239.
- Buikstra, J. E. and D. H. Ubelaker. (1994). Standards for Data Collection from Human Skeletal Remains: Proceeding of a Seminar at the Field Museum of Natural History. Arkansas Archaeology Survey.
- Bytheway, J. A. and A. H. Ross. (2010). A Geometric Morphometric Approach to Sex Determination of the Human Adult Os Coxa. *Journal of Forensic Sciences* 55(4): 859-864.
- Cardoso, H. F. V. (2008). Sample-specific (universal) metric approaches for determining the sex of immature human skeletal remains using permanent tooth dimensions. *Journal of Archaeological Science* 35: 158-168.
- Choi, S. C. and M. Trotter. (1970). A statistical study of the multivariate structure and race-sex differences of American White and Negro fetal skeletons. *American Journal of Physical Anthropology* 33(3): 307-312.
- Classen, C. (2019). The beads of Indian Knoll. *Southeastern Archaeology* 38(2): 95-112.
- Coleman, W. H. (1969). Sex Differences in the Growth of the Human Bony Pelvis. *American Journal of Physical Anthropology* 31: 125-152.
- Correia, H., S. Balseiro and M. De Areia. (2005). Sexual dimorphism in the human pelvis: Testing a new hypothesis. *Journal of Comparative Human Biology* 56: 153-160.
- Cowgill, L. W. (2010). The ontogeny of Holocene and Late Pleistocene human postcranial strength. *American Journal of Physical Anthropology* 141(1): 16-37.

- Cunningham, C. A. and S. M. Black. (2009). Development of the fetal ilium - challenging concepts of bipedality. *Journal of Anatomy* 214: 91-99.
- Cunningham, C., L. Scheuer and S. Black. (2016). *Developmental Juvenile Osteology*. Second Edition. Elsevier Ltd.
- D. Wiley and the Institute of Data Analysis and Visualization. (2006). Landmark Editor.
- Deacon, H. J. (1976). Where hunters gathered: a study of Holocene Stone Age people in the eastern Cape. (Vol. 1). South African Archaeological Society.
- Deacon, H. J. and J. Deacon. (1999). *Human Beginnings in South Africa: Uncovering the Secrets of the Stone Age*. New Africa Books.
- Delprete, H. (2017). Pelvic Inlet Shape is Not as Dimorphic as Previously Suggested. *The Anatomical Record* 300: 706-715.
- Dunsworth, H. M. (2018). There is no “obstetrical dilemma”: towards a braver medicine with fewer childbirth interventions. *Perspectives in Biology and Medicine* 61(2): 249-263.
- Dunsworth, H. M., A. G. Warrener, T. Deacon, P. T. Ellison and H. Pontzer. (2012). Metabolic hypothesis for human altriciality. *PNAS* 109(38): 15212-15216.
- Dunsworth, H. and L. Eccleston. (2015). The Evolution of Difficult Childbirth and Helpless Hominin Infants. *Annual Review of Anthropology* 44: 55-69.
- Editors of Encyclopaedia Britannica. “Pelvis.” *Encyclopedia Britannica*, Encyclopedia Britannica, Inc., 1 Apr. 2019, www.britannica.com/science/pelvic-girdle.
- Freidline S. E., P. Gunz, and J.-J. Hublin. (2015). Ontogenetic and Static Allometry in the Human Face: Contrasting Khoisan and Inuit. *American Journal of Physical Anthropology* 1-16.
- Fischer, B. and P. Mitteroecker. (2017). Allometry and Sexual Dimorphism in the Human Pelvis. *The Anatomical Record* 300: 698-705.
- Gayzik, F. S., M. M. Yu, K. A. Danelson, D. E. Slice, J. D. Stitzel. (2008). Quantification of age-related shape change of the human rib cage through geometric morphometrics. *Journal of Biomechanics* 41: 1545-1554.
- 3D Systems Inc. (2019). Geomagic Design X.
- Gluckman, P. D. and M. A. Hanson. (2006). Changing times: The evolution of puberty. *Molecular and Cellular Endocrinology* 254-255: 26-31.

- González, P. N., V. Bernal, S. I. Perez and G. Barrientos. (2007). Analysis of dimorphic structures of the human pelvis: its implications for sex estimation in samples without reference collections. *Journal of Archaeological Science* 34: 1720-1730.
- González, P. N., V. Bernal and S. I. Perez. (2009). Geometric morphometric approach to sex estimation of human pelvis. *Forensic Science International* 189: 68-74.
- Gould, S. J. (1966). Allometry and size in ontogeny and phylogeny. *Biological Reviews* 41: 587-640.
- Gould, S. J. (1975). Allometry in primates, with emphasis on scaling and the evolution of the brain. *Contributions to Primatology* 5: 244-292.
- Grabowski, M. W., J. D. Polk and C. C. Roseman. Divergent patterns of integration and reduced constraint in the human hip and the origins of bipedalism. *Evolution* 65(5): 1336-1356.
- Grabowski, M. and C. C. Roseman. (2015). Complex and changing patterns of natural selection explain the evolution of the human hip. *Journal of Human Evolution* 85: 94-110.
- Gunz, P., P. Mitteröcker and F. L. Bookstein. Semilandmarks in Three Dimensions. *Modern Morphometrics in Physical Anthropology*. Edited by: Slice, D. E. 2005.
- Gunz, P. and P. Mitteröcker. (2013). Semilandmarks, a new method for quantifying curves and surfaces. *Italian Journal of Mammalogy* 2013: 1-7.
- Hammond, A. S., S. Almécija, Y. Libsekal, L. Rook and R. Macchiarelli. (2018). A partial *Homo* pelvis from the Early Pleistocene of Eritrea. *Journal of Human Evolution* 123: 109-128.
- Harrington, L. (2010). Ontogeny of Postcranial Robusticity among Holocene Hunter-Gatherers of Southernmost Africa.
- Hochberg, Z., R. Feil, M. Constancia, M. Fraga, C. Junien, J.-C. Carel, P. Boileau, Y. Le Bouc, C. L. Deal, K. Lillycrop, R. Scharfmann, A. Sheppard, M. Skinner, M. Szyf, R. A. Waterland, D. J. Waxman, E. Whitelaw, K. Ong and K. Albertsson-Wikland. (2011). Child Health, Developmental Plasticity, and Epigenetic Programming. *Endocrine Reviews* 32: 159-224.
- Holcomb, S. M. C, and L. W. Konigsberg. (1995). Statistical Study of Sexual Dimorphism in the Human Fetal Sciatic Notch. *American Journal of Physical Anthropology* 97: 113-125.
- Holliday, T. W. (1997). Body proportions in Late Pleistocene Europe and modern human origins. *Journal of Human Evolution* 32: 423 - 447.
- Hromada, J. (1939). Contribution to the study of the growth of the fetal pelvis. *Anthropologie* 18: 129-170.

- Hunt, D. R. (1990). Sex Determination in the Subadult Iliac Crest: An Indirect Test of Weaver's Nonmetric Sexing Method. *Journal of Forensic Sciences* 35(4): 881-885.
- Humphrey, L. T. (1998). Growth Patterns in the Modern Human Skeleton. *American Journal of Physical Anthropology* 105: 57-72.
- Johnston, F. E. (1962). Growth of Long Bones of Infants and Young Children at Indian Knoll. *American Journal of Physical Anthropology*: 249-254.
- Johnston, F. E. and C. E. Snow. (1961). The Reassessment of the Age and Sex of the Indian Knoll Skeletal Population: Demographic and Methodological Aspects. *American Journal of Physical Anthropology*: 237-244.
- Kenyhercz, M. W., A. R. Hlales, K. E. Stull, K. A. McCormick and S. J. Cole (2017). Worldwide population variation in pelvic sexual dimorphism: A validation and recalibration of the Klales et al. method. *Forensic Science International* 277: 259.e1-259.e8.
- Kimura, K. (1982). Sex Differences of the Hip Bone Among Several Populations. *Okajimas Folia Anat. Jpn.* 58(4-6): 265-276. _
- Klingenberg, C. P. 2011. MorphoJ: an integrated software package for geometric morphometrics. *Molecular Ecology Resources* 11:353-357
- Klingenberg, C. P. (2013). Visualizations in geometric morphometrics: how to read and how to make graphs showing shape changes. *Italian Journal of Mammalogy* 24(1): 15-24.
- Klingenberg, C. P. (2016). Size, shape and form: concepts of allometry in geometric morphometrics. *Dev Genes Evol* 266(3): 113-137.
- Koļesova, O. (2014). The Sexual Dimorphism and Age-Related Changes of the Lesser Pelvis in Humans. Doctoral Dissertation, Rīga Stradiņš University
- Koļesova, O. and J. Vētra. (2011). Sexual dimorphism of pelvic morphology variation in live humans. *Papers on Anthropology* 209-217.
- Kurki, H. K. (2013). Bony Pelvic Canal Size and Shape in Relation to Body Proportionality in Humans. *American Journal of Physical Anthropology* 151: 88-101.
- Kurki, H. K. (2017). Bilateral Asymmetry in the Human Pelvis. *The Anatomical Record* 300: 653-665.
- LaVelle, M. (1995). Natural Selection and Developmental Sexual Variation in the Human Pelvis. *American Journal of Physical Anthropology* 98: 59-72.

- Lewis, C. L., N. M. Laudicina, A. Khuu and K. L. Loverro. (2017). The Human Pelvis: Variation in Structure and Function During Gait. *The Anatomical Record* 300: 633-642.
- Lewontin, R. C. The Apportionment of Human Diversity. 381-398. In *Evolutionary Biology Volume 6*. Theodosius Dobzhansky, M. K. Hecht and W. C. Steere. 1972. Meredith Corporation, New York.
- Lewton, K. L. (2010). Locomotor function and the evolution of the primate pelvis. Doctoral Dissertation, Arizona State University.
- Liversidge, H. M. and T. Molleson. (2004). Variation in Crown and Root Formation and Eruption of Human Deciduous Teeth. *American Journal of Physical Anthropology* 123: 172-180.
- Loth, S. R. and M. Henneberg. (2001). Sexually dimorphic mandibular morphology in the first few years of life. *American Journal of Physical Anthropology* 115(2): 179-186.
- Lovejoy, C. O., R. S. Meindl, T. R. Pryzbeck and R. P. Mensforth. (1985). Chronological Metamorphosis of the Auricular Surface of the Ilium: A New Method for the Determination of Adult Skeletal Age at Death. *American Journal of Physical Anthropology* 68: 15-28.
- Lycett, S. J. and N. von Cramon-Taubadel. (2013). Understanding the comparative catarrhine context of human pelvic form: A 3D geometric morphometric analysis. *Journal of Human Evolution* 64: 300-310.
- MacLaughlin, S. M. and M. F. Bruce. (1986). Population variation in sexual dimorphism in the human innominate. *Human Evolution* 1(3): 221-231.
- Mitchell, P. (2002). *The Archaeology of Southern Africa*. Cambridge University Press.
- Mitteröcker, P. and P. Gunz. (2009). Advances in Geometric Morphometrics. *Evol Biol* 36: 235-247.
- Mittler, D. M. and S. G. Sheridan. (1992). Sex Determination in Subadults Using Auricular Surface Morphology: A Forensic Science Perspective. *Journal of Forensic Sciences* 37(4): 1068-1075.
- Moczek, A. P., S. Sultan, S. Foster, G. Ledón-Rettig, I. Dworkin, H. F. Nijhout, E. Abouheif and D. W. Pfennig. (2011). The role of developmental plasticity in evolutionary innovation. *Proceedings of the Royal Society B* 278: 2705-2713.
- Mokrane, F-H., F. Dedouit, S. Gellée, N. Sans, H. Rousseau, D. Rougé and N. Telmon. (2013). Sexual Dimorphism of the Fetal Ilium: A 3D Geometric Morphometric Approach with Multislice Computed Tomography. *Journal of Forensic Sciences* 58(4): 851-858.

- Molleson, T. and K. Cruse. (1998). Some Sexually Dimorphic Features of the Human Juvenile Skull and their Value in Sex Determination in Immature Skeletal Remains. *Journal of Archaeological Science* 25: 719-728.
- Morey, D. F., G. M. Crothers, J. K. Stein, J. P. Fenton and N. P. Herrmann. (2002). The fluvial and geomorphic context of Indian Knoll, an Archaic shell midden in West-Central Kentucky. *Geoarchaeology: An International Journal* 17(6): 521-553.
- NextEngine, Inc. (2015).
- Nielsen, R., J. M. Akey, M. Jakobsson, J. K. Pritchard, S. Tishkoff and E. Willerslev. (2017). Tracing the peopling of the world through genomics. *Nature* 541: 302 - 310.
- Olivares, J. I. and I. A. Aguilera. (2016). Validation of the sex estimation method elaborated by Schutkowski in the Granada Osteological Collection of identified infant and young children: Analysis of the controversy between the different ways of analyzing and interpreting the results. *Int. J. Legal Med.* 130: 1623-1632.
- Perez, S. I., V. Bernal and P. N. Gonzalez. (2006). Differences between sliding semi-landmark methods in geometric morphometrics, with an application to human craniofacial and dental variation. *Journal of Anatomy* 208: 769-784.
- Phenice, T. W. (1969). A Newly Developed Visual Method of Sexing the Os Pubis. *American Journal of Physical Anthropology* 30: 297-302.
- Pfeiffer, Susan and L. Harrington. (2018). Regional Continuity and Local Challenges to Resilience among Holocene Hunter-Gatherers of the Greater Cape Floristic Region, South Africa. In, Temple, D. Howard, & Stojanowski, C. M. Hunter-gatherer adaptation and resilience: a bioarchaeological perspective. Cambridge, United Kingdom: Cambridge University Press. 2019.
- Pfeiffer, Susan and L. Harrington. (2010). Child Growth among Southern African Foragers in the Past. In, Moffat, Tina and Prowse, T. Human Diet and Nutrition in Biocultural Perspective. Berghahn Books, 2010.
- Reynolds, E. L. (1945). The bony pelvic girdle in early infancy: A roentgenometric study. *American Journal of Physical Anthropology* 3(4): 321-354.
- Rissech, C. and A. Malgosa. (2005). Ilium growth study: applicability in sex and age diagnosis. *Forensic Science International* 147: 165-174.
- Roberts, A. M., and S. K. S. Thorpe. (2014). Challenges to human uniqueness: bipedalism, birth and brains. *Journal of Zoology* 292: 281-289.
- Rogers, T. L. (1991). Sex Determination and Age Estimation: Skeletal Evidence from St. Thomas' Cemetery Belleville, Ontario. Doctoral dissertation, McMaster University

- Rogers, T. L. (2005). Determining the Sex of Human Remains Through Cranial Morphology. *Journal of Forensic Sciences* 50(3): 1-8.
- Rogers, T. L. (2009). Sex Determination of Adolescent Skeletons Using the Distal Humerus. *American Journal of Physical Anthropology* 140: 143-148.
- Rogers, T. and S. Saunders. (1994). Accuracy of Sex Determination Using Morphological Traits of the Human Pelvis. *Journal of Forensic Sciences* 39(4): 1047-1056.
- Rohlf, F. J. and D. Slice. (1990). Extensions of the Procrustes Method for the Optimal Superimposition of Landmarks. *Systematic Biology* 39(1): 40-59.
- Rosenberg, K. R. and W. R. Trevathan. (1995). Bipedalism and Human Birth: The Obstetrical Dilemma Revisited. *Evol Anthropol* 4(5): 161-68.
- Roseman, C. C. and B. M. Auerbach. (2015). Ecogeography, genetics, and the evolution of human body form. *Journal of Human Evolution* 78: 80-90.
- RStudio Team (2016). RStudio: Integrated Development for R. RStudio, Inc., Boston, MA. <http://www.rstudio.com/>
- Rothschild, N. A. (1979) Mortuary Behavior and Social Organization at Indian Knoll and Dickson Mounds. *American Antiquity* 44(4): 658-675.
- Ruff, C. (2002). Variation in Human Body Size and Shape. *Annual Review of Anthropology* 31: 211-232.
- Ruff, C. R. (1991). Climate and body shape in hominid evolution. *Journal of Human Evolution* 21: 81-105.
- Ruff, C. B. (1995). Biomechanics of the Hip and Birth in Early *Homo*. *American Journal of Physical Anthropology* 98: 527-574.
- Ruff, C. B. (1994). Morphological adaptation to climate in modern and fossil hominids. *Yearbook of Physical Anthropology* 37: 65-107.
- Saunders, S. R. and R. D. Hoppa. (1993). Growth deficit in survivors and non-survivors: Biological mortality bias in subadult skeletal samples. *American Journal of Physical Anthropology* 36: 127-151.
- Scholtz, Y., M. Steyn and E. Pretorius. (2010). A geometric morphometric study into the sexual dimorphism of the human scapula. *HOMO Journal of Comparative Human Biology* 61: 253-270.

- Schutkowski, H. (1993). Sex Determination of Infant and Juvenile Skeletons: I. Morphognostic Features. *American Journal of Physical Anthropology* 90: 199-205.
- Slice, D. E. (2007). Geometric Morphometrics. *Annual Review of Anthropology* 36: 261-281.
- Slizewski, A., M. Friess and P. Semal. (2010). Surface scanning of anthropological specimens: nominal-actual comparison with low cost laser scanner and high end fringe light projection surface scanning systems. *Quartär* 57: 179-187.
- Smith, B. H. (1991). Standards of human tooth formation and dental age assessment. Wiley-Liss Inc.
- Smith, H. F., T. Ritzman, E. Otárola-Castillo and C. E. Terhune. (2013). A 3-D geometric morphometric study of intraspecific variation in the ontogeny of the temporal bone in modern *Homo sapiens*. *Journal of Human Evolution* xxx: 1-11.
- Snow, C. E. (1948) Indian Knoll Skeletons of Site Oh 2 Ohio County Kentucky. *Reports in Anthropology* 4(3) part 2. Department of Anthropology, University of Kentucky, Lexington.
- Sutter, R. C. (2003). Nonmetric Subadult Skeletal Traits: I. A Blind Test of the Accuracy of Eight Previously Proposed Methods Using Prehistoric Known-Sex Mummies from Northern Chile. *Journal of Forensic Sciences* 48(5): 1-9.
- Steyn, M., E. Pretorius and L. Hutten. (2004). Geometric morphometrics analysis of the greater sciatic notch in South Africans. *HOMO* 54(3): 197-206.
- St. Hoyme, L. E. (1984). Sex Differentiation in the Posterior Pelvis. *Collegium Anthropologica* 8: 139-153.
- Stock, J. T. (2006). Hunter-Gatherer Postcranial Robusticity Relative to Patterns of Mobility, Climatic Adaptation, and Selection for Tissue Economy. *American Journal of Physical Anthropology* 131: 194-204.
- Sutherland, L. and J. Suchey. (1991). Use of the Ventral Arc in Pubic Sex Determination. *Journal of Forensic Sciences* 36(2): 501-511.
- Tague, R. G. (1989). Variation in pelvic Size Between Males and Females. *American Journal of Physical Anthropology* 80: 59-71.
- Tague, R. G. (1994). Maternal Mortality or Prolonged Growth: Age at Death and Pelvic Size in Three Prehistoric Amerindian Populations. *American Journal of Physical Anthropology* 95: 27-40.

- Terhune, C. E., W. H. Kimbel and C. A. Lockwood. (2013). Postnatal Temporal Bone Ontogeny in *Pan*, *Gorilla*, and *Homo*, and the Implications for Temporal Bone Ontogeny in *Australopithecus afarensis*. *American Journal of Physical Anthropology* 151: 630-642.
- Thomson, A. (1896). The Sexual Differences of the Foetal Pelvis. *Journal of Anatomy and Physiology* 33: 359-380.
- Todd, T. W. (1920). Age Changes in the Pubic Bone. *American Journal of Physical Anthropology* 3(8): 285-334.
- Van Der Linden, F. P. (1966). Genetic and environmental factors in dentofacial morphology. *American Journal of Orthodontics* 52(8): 576-583.
- Villa, C., D. Gaudio, C. Cattaneo, J. Buckberry, A. S. Wilson and N. Lynnerup. (2015). Surface Curvature of Pelvic Joints from Three Laser Scanners: Separating Anatomy from Measurement Error. *Journal of Forensic Sciences* 60(2): 374 - 381.
- Vlak, D., M. Roksandic, and M. A. Schillaci. (2008). Greater Sciatic Notch as a Sex Indicator in Juveniles. *American Journal of Physical Anthropology* 137: 309-315.
- Wall-Scheffler, C. M. and M. J. Myers. (2017). The Biomechanical and Energetic Advantages of a Mediolaterally Wide Pelvis in Women. *The Anatomical Record* 300: 764-775.
- Warrener, A. G., K. L. Lewton, H. Pontzer and D. E. Lieberman. (2015). A Wider Pelvis Does Not Increase Locomotor Cost in Humans, with Implications for the Evolution of Childbirth. *PLoS ONE* 10(3): e0118903.
- Washburn, S. L. (1948). Sex Differences in the Pubic Bone. *American Journal of Physical Anthropology* 6: 199-208.
- Washburn, S. L. (1960). Tools and Human Evolution. *Science America* 203: 3-15
- Weaver, D. S. (1980). Sex Differences in the Iliac of Known Sex and Age Sample of Fetal and Infant Skeletons. *American Journal of Physical Anthropology* 52: 191-195.
- Weaver, T. D. (2002) A Multi-causal Functional Analysis of Hominid Hip Morphology. Doctoral dissertation, Stanford University.
- Weaver, T. D. and J.-J. Hublin. (2009). Neanderthal birth canal shape and the evolution of human childbirth. *PNAS* 106(20): 8151-8156.
- Webb, W. S. (1946). Indian Knoll, Site Oh 2, Ohio County Kentucky: The University of Kentucky Reports in Anthropology and Archaeology. *Lexington: Department of Anthropology*, 111-365.

- Webster, M. and H. D. Sheets. (2010). A practical introduction to landmark-based geometric morphometrics. *The Paleontological Society Papers* 16: 163-188.
- Wells, J. C., S. C. Dumith, U. Ekelund, F. F. Reichert, A. M. Menezes, C. G. Victora, and P. C. Hallal. (2012). Associations of intrauterine and postnatal weight and length gains with adolescent body composition: Prospective birth cohort study from Brazil. *Journal of Adolescent Health*, 51(6), S58–S64.
- Wells, J. C. K. (2016). Worldwide variability in growth and its association with health: Incorporating body composition, developmental plasticity, and intergenerational effects. *American Journal of Human Biology* 29: 1-16.
- White, T. D., M. T. Black and P. A. Folkens. (2011). *Human Osteology*. 3rd Ed. Elsevier Science and Technology.
- Wilson, L. A., N. MacLeod and L. T. Humphrey. (2008). Morphometric Criteria for Sexing Juvenile Human Skeletons Using the Ilium. *Journal of Forensic Science* 53(2): 269-278.
- Wilson, L. A. B., H. F. V. Cardoso and L. T. Humphrey. (2011). On the reliability of a geometric morphometric approach to sex determination: A blind test of six criteria of the juvenile ilium. *Forensic Science International* 206: 35-42.
- Wilson, L. A. B., R. Ives, H. F. V. Cardoso and L. T. Humphrey. (2015). Shape, Size and Maturity Trajectories of the Human Ilium. *American Journal of Physical Anthropology* 2014: 1-16.
- Wilson, L. A. B., R. Ives and L. T. Humphrey. (2016). Quantification of 3D curvature in the iliac crest: Ontogeny and implications for sex determination in juveniles. *American Journal of Physical Anthropology* 2016: 1-12.
- Wilson, L. A. B. and L. T. Humphrey. (2017). Voyaging into the third dimension: A perspective on virtual methods and their application to studies of juvenile sex estimation and the ontogeny of sexual dimorphism. *Forensic Science International* 278: 32-46.
- Wood, J. W., G. R. Milner, H. C. Harpending, K. M. Weiss. (1992). The Osteological Paradox: Problems of Inferring Prehistoric Health from Skeletal Samples. *Current Anthropology* 33(4): 343-370.
- Yusof, N. A., R. W. Soames, C. A. Cunningham and S. M. Black. (2013). Growth of the human ilium: the anomalous sacroiliac junction. *Anatomical Record* 296: 1688-1694.
- Zelditch, M. L., D. L. Swiderski and H. D. Sheets. (2012). *Geometric Morphometrics for Biologists: A Primer*. Second Edition. Elsevier Inc.

Appendix A: Tables and Figures

Table A1. Juvenile Later Stone Age sample. Age at death estimations are based on dental age. Site the individual was found was included where possible, as well as the radiocarbon date. Each individual was given a classifier that identifies the number of the individual, the population, the side of the ilium used (left or reflected right) and the age cohort (1, 2, 3 or 4).

Individual	Classifier	Age (years)	Site	Radiocarbon Date (years BP)
Isaa0029911		0.6		
Isaa0013511		1.1	Spitzkop	4900 ± 60
Isaa0026511		1.6		
Isaa0116b11		1.8		
Isas0022312		2.5		
Isaa0030012		2.5	St. Francis Bay	80 ± 27
Isaa0017612		3.5	Kleinpoort	350 ± 60
Isaa0019312		3.5	Kleinpoort	230 ± 60
Isaa0010812		3.5		
Isaa00138r2		3.6	Spitzkop	4800 ± 80
Isaa00137r2		4.2	Spitzkop	4750 ± 60
Isam0022212		4.5		
Isaa0023612		4.8	Mitford Park	2010 ± 60
Isaa00175r2		5.5	Kleinpoort	
Isas04207r2		5.9	Dury's Cave	
Isas0605212		6.0	Byneskranskop 3	360 ± 50
Isaa0013212		6.5	Spitzkop	4720 ± 70
Isaa00181r2		6.5	Kleinpoort	450 ± 50
Isaa0026612		6.5	Delamare Frm	580 ± 50

Isaa0018313	6.5	Dunbrody	220 ± 50
Isaa0013313	6.7	Spitzkop	4860 ± 70
Isam00230r3	7.5	Koffiefontein	
Isas06053r3	7.5	Byneskranskop 1	
Isau00247r3	8.5	Klein Brakrivier	510 ± 40
Isaa0018213	8.5		
Isaa0023813	10.1		
Isaa0151b13	10.9		
Isaa00051r3	10.9	Plettenberg Bay	
Isaa0029514	11.5		
Isaa0035114	11.2		
Isas6054a14	12.2		
Isaa0024514	12.5		
Isaa00152r4	13.1		
Isam00248r4	14.5		

Table A2. Juvenile individuals from the Indian Knoll sample. Age estimations are based on dental age. Each individual was given a classifier that identifies the number of the individual, the population, the side of the ilium used (left or reflected right) and the age cohort (1, 2, 3 or 4).

Individual Classifier Age (years)

inkn0006211	0.4
inkn00008r1	0.6
inkn0002911	0.7
inkn0003311	0.7
inkn0013911	0.8
inkn0027111	0.9
inkn00196r1	1.8
inkn00286r2	2.7
inkn0022512	2.8
inkn0051512	3.4
inkn00530r2	4.4
inkn0072412	5.7
inkn0017212	6.7
inkn0078512	6.7
inkn0085512	6.9
inkn0059913	7.1
inkn0024413	7.2
inkn0082613	8.2
inkn0044413	8.4
inkn00232r3	9.4
inkn0047213	9.5

inkn00138r3	10.4
inkn0012514	12.9
inkn00302r4	13.1
inkn0004714	13.1
inkn00127r4	15

Table A3. Adult individuals from both the Indian Knoll and Later Stone Age populations. Adult classification was assigned for completed growth. Sex is an estimated value. Each individual was given a classifier that identified the number of the individual, the population, the side of the ilium used (left or reflected right) and the estimated sex.

Individual Classifier Estimated Sex Population

inkn000171f	Female	IK
inkn000221f	Female	IK
inkn008501f	Female	IK
inkn005361f	Female	IK
inkn001401f	Female	IK
lsaa002931f	Female	LSA
lsan012711f	Female	LSA
lsas018711f	Female	LSA
lsaa001781f	Female	LSA
lsan016401f	Female	LSA
inkn002171m	Male	IK
inkn003471m	Male	IK
inkn004471m	Male	IK
inkn004541m	Male	IK
inkn004621m	Male	IK
lsaa002001m	Male	LSA
lsas1878A1m	Male	LSA
lsaa002221m	Male	LSA
lsas050751m	Male	LSA
lsan012731m	Male	LSA

Variance Explained by PCs in Later Stone Age Population

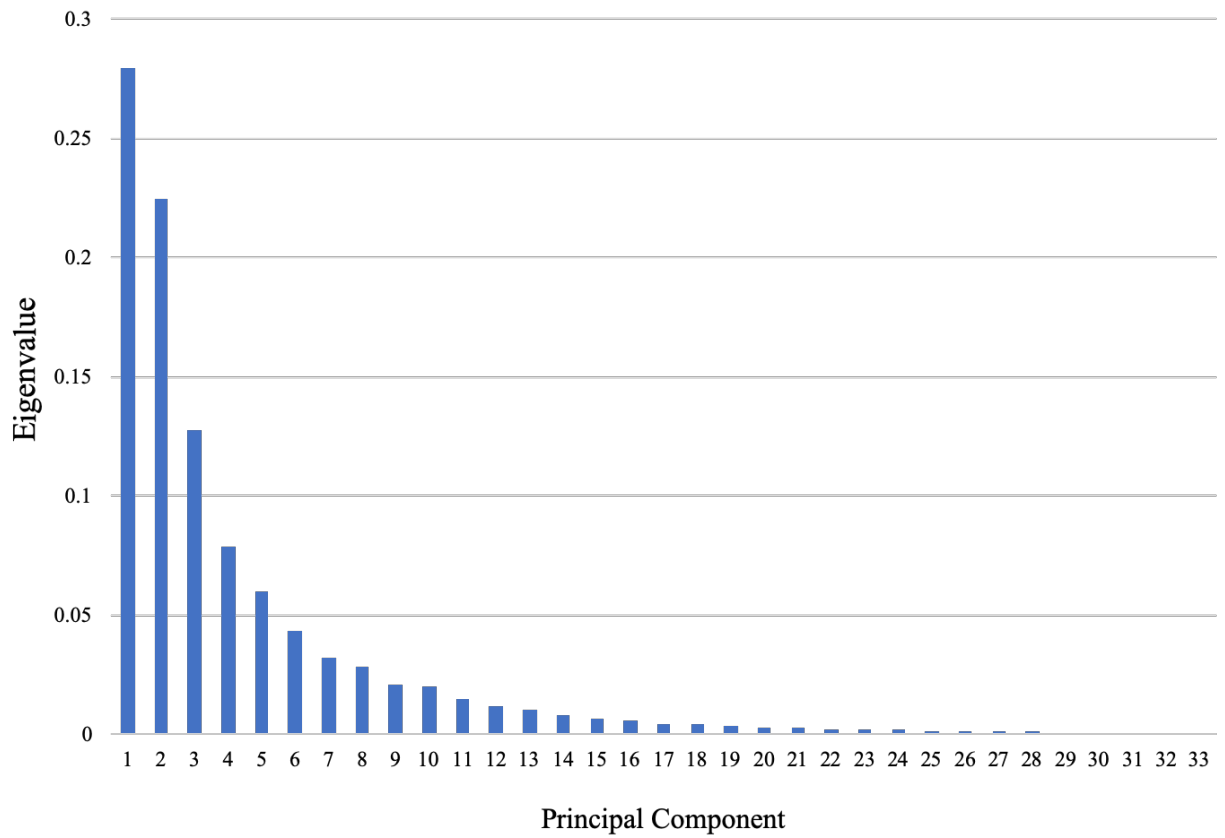


Figure A1. The percent of variance explained by each principal component in the Later Stone Age sample.

Table A4. The proportion of variance explained by each PC as well as its cumulative proportion given as a percentage for Later Stone Age. The stop-point was 50%; this point is highlighted and indicates at which PC analyses were cut off.

PC	Proportion of Variance	Cumulative Proportion (%)
PC1	0.28003	28.003
PC2	0.22456	50.46
PC3	0.12759	63.219
PC4	0.07847	71.066
PC5	0.0596	77.026
PC6	0.0432	81.346
PC7	0.03203	84.549
PC8	0.02834	87.382
PC9	0.02094	89.476
PC10	0.01988	91.465
PC11	0.01463	92.928
PC12	0.01148	94.077
PC13	0.01035	95.112
PC14	0.00775	95.886
PC15	0.0062	96.506
PC16	0.00561	97.067
PC17	0.00452	97.519
PC18	0.00402	97.921
PC19	0.00354	98.275
PC20	0.0029	98.565
PC21	0.00243	98.808

PC22 0.00204	99.011
PC23 0.0019	99.202
PC24 0.00168	99.37
PC25 0.00136	99.506
PC26 0.00107	99.613
PC27 0.00091	99.704
PC28 0.00088	99.792
PC29 0.00071	99.863
PC30 0.00064	99.927
PC31 0.00049	99.976
PC32 0.00016	99.992
PC33 0.00008	100

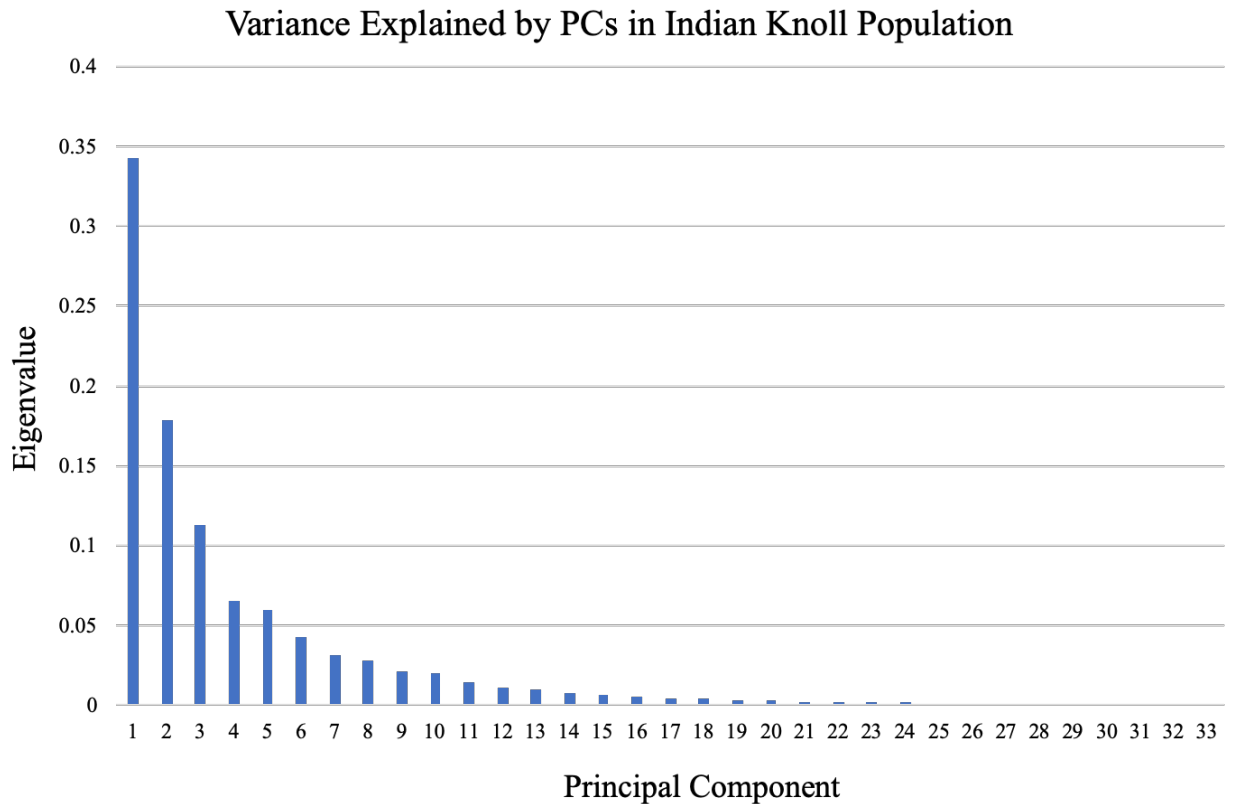


Figure A2. The percent of variance explained by each principal component in the Indian Knoll sample.

Table A5. The proportion of variance explained by each PC as well as its cumulative proportion given as a percentage for Indian Knoll. The stop-point was 50%; this point is highlighted and indicates at which PC analyses were cut off.

PC	Proportion of Variance	Cumulative Proportion (%)
PC1	0.34251	34.251
PC2	0.17907	52.158
PC3	0.11362	63.519
PC4	0.06534	70.053
PC5	0.06258	76.311
PC6	0.04392	80.703
PC7	0.03666	84.369
PC8	0.02713	87.082
PC9	0.02681	89.763
PC10	0.02203	91.966
PC11	0.01578	93.544
PC12	0.01411	94.955
PC13	0.01064	96.019
PC14	0.00805	96.824
PC15	0.00607	97.432
PC16	0.00477	97.909
PC17	0.00451	98.36
PC18	0.00418	98.777
PC19	0.00325	99.102
PC20	0.00271	99.373
PC21	0.00194	99.567

PC22	0.00177	99.744
PC23	0.00147	99.891
PC24	0.00076	99.967
PC25	0.00033	100

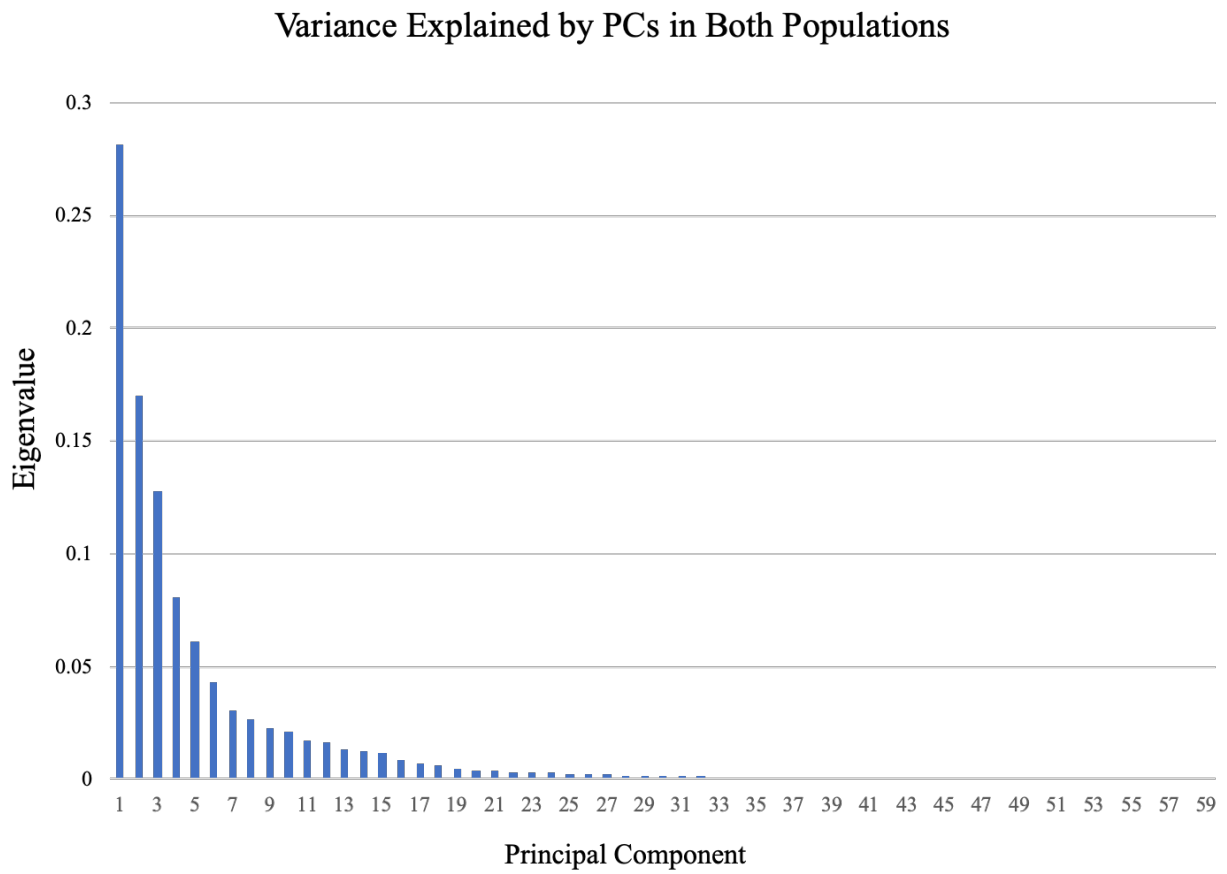


Figure A3. The percent of variance explained by each principal component in the combined sample.

Table A6. The proportion of variance explained by each PC as well as its cumulative proportion given as a percentage for the combined sample. The stop-point was 50%; this point is highlighted and indicates at which PC analyses were cut off.

PC	Proportion of Variance	Cumulative Proportion (%)
PC1	0.28107	28.107
PC2	0.17001	45.108
PC3	0.12745	57.853
PC4	0.08032	65.885
PC5	0.06121	72.006
PC6	0.04298	76.304
PC7	0.03072	79.376
PC8	0.02645	82.021
PC9	0.02295	84.316
PC10	0.02137	86.453
PC11	0.01702	88.155
PC12	0.01665	89.82
PC13	0.01311	91.131
PC14	0.01218	92.349
PC15	0.01153	93.502
PC16	0.00838	94.34
PC17	0.00669	95.009
PC18	0.0059	95.599
PC19	0.00421	96.02
PC20	0.00406	96.426
PC21	0.00367	96.794

PC22 0.00323	97.117
PC23 0.00306	97.422
PC24 0.00265	97.687
PC25 0.00242	97.93
PC26 0.00198	98.128
PC27 0.00188	98.315
PC28 0.00167	98.482
PC29 0.00149	98.631
PC30 0.00134	98.765
PC31 0.00129	98.894
PC32 0.00115	99.009
PC33 0.00104	99.113
PC34 0.00089	99.201
PC35 0.00074	99.276
PC36 0.0007	99.346
PC37 0.00067	99.412
PC38 0.00062	99.474
PC39 0.00057	99.531
PC40 0.0005	99.581
PC41 0.00046	99.627
PC42 0.00041	99.668
PC43 0.00039	99.708
PC44 0.00039	99.747
PC45 0.00033	99.78

PC46 0.00031	99.811
PC47 0.00028	99.839
PC48 0.00022	99.861
PC49 0.00022	99.883
PC50 0.00021	99.904
PC51 0.00019	99.923
PC52 0.00016	99.939
PC53 0.00013	99.952
PC54 0.00012	99.964
PC55 0.00011	99.975
PC56 0.0001	99.984
PC57 0.00007	99.992
PC58 0.00006	99.998
PC59 0.00002	100

Appendix B: R Code

Code B1. Code used to landmark ilia. Parts in italics indicate where information would be personalized to an individual's study. A specimen was used, *Isaa0010812* throughout this example. This would be unique to an individual's study as well.

```
> install.packages("geomorph")
> library(geomorph)
> setwd("C:/Users/datalocationfolder")

# In order to run in R, the ply file must be in Ascii format.
> Isaa0010812 <- read.ply("Isaa0010812.ply", ShowSpecimen = TRUE, addNormals = TRUE)

# The function digit.fixed was used to derive 100 landmarks to capture the outline of the iliac crest. Landmark 1 is the most anterior point of the pelvis (ASIS).
> landmarks = digit.fixed(spec = Isaa0010812, fixed = 100, index = FALSE, ptsize = 1, center = TRUE)
# If enter "landmarks" into console following this step, will see the 100 landmarks outlining the iliac crest.

# The 100 outline landmarks were exported as a csv file.
> write.csv(landmarks, "Isaa0010812landmarks.csv")

# The function digit.curves was used to derive 82 sliding semilandmarks from the 100 outline landmarks. The "1" placed after "landmarks" indicates to use this landmark as the first of the 82 landmarks and to keep it fixed.
> semilandmarks = digit.curves(start = landmarks[1,], curve = landmarks, nPoints = 81, closed = TRUE)
# If enter "semilandmarks" into console following this step, will see the 82 sliding semilandmarks derived from the outline "landmarks".

# The 82 semilandmarks were exported as a csv file.
> write.csv(semilandmarks, "Isaa0010812semilandmarks.csv")
```

Code B2. Code used to run analyses in geomorph such as Generalized Procrustes analysis and Principal Component Analysis. Throughout this example, I have left my populations as "LSA", "IK" and "CMB", for combined samples. These values and names would change depending on an individual's study.

```
> install.packages("geomorph")
> library(geomorph)
> setwd("C:/Users/datalocationfolder")

# The first step is to read in the csv file containing the principal components from the digit.curve function. This csv file would have all the PCs from the given sample, organized by age cohort.
```



```

> plot(pca.CMB$pc.scores[,plotted_axes], main = 'Principal Component Analysis of Combined
Populations', pch = c(19,6,19,6,19,6,19,6), xlab = "PC1", ylab = "PC2", col =
c('red','blue','green','purple')[GPA_CMB_col2])
#text(pca.CMB$pc.scores[,plotted_axes], rownames(pca.CMB$pc.scores[,1:2]), pos = 4, cex =
.5)
legend('bottomleft',cex = 0.8,legend = c('0-1.99','2-6.99','7-10.99','11-15.99'),pch = 19,title =
'Age (years)',col = c('red','blue','green','purple'))
legend('topleft', cex = 0.8, legend = c('LSA','IK'), pch = c(19,6), title = "Population", col =
'black')

```

Code B3. Code used to compare minimum and maximum shapes along the PC axes. To run these tests, the GPA analysis must have been previously run.

```

# This code allows the minimum and maximum shape of each PC to be visualized in a plot of the
82 landmarks.

```

```

> plotRefToTarget(PC1_min_LSA, PC1_min_LSA, method = "points", label = TRUE)
> plotRefToTarget(PC1_max_LSA, PC1_max_LSA, method = "points", label = TRUE)
> plotRefToTarget(PC2_max_LSA, PC2_max_LSA, method = "points", label = TRUE)
> plotRefToTarget(PC2_min_LSA, PC2_min_LSA, method = "points", label = TRUE)

```

```

> PC1_min_LSA = pca.LSA$pc.shapes$PC1min
> PC1_max_LSA = pca.LSA$pc.shapes$PC1max
> PC2_min_LSA = pca.LSA$pc.shapes$PC2min
> PC2_max_LSA = pca.LSA$pc.shapes$PC2max

```

```

# This code compared the minimum and maximum shapes along a PC axis. A magnification of 2
was used to better see the difference between the minimum and maximum shape (mag = ). The
target landmarks are in black (second matrix) and the reference is in gray (first matrix).

```

```

> plotRefToTarget(PC1_max_LSA, PC1_min_LSA, method = "points", mag = 2, label = TRUE)
> plotRefToTarget(PC2_max_LSA, PC2_min_LSA, method = "points", mag = 2, label = TRUE)

```

```

# The same analyses run with the IK sample.

```

```

> plotRefToTarget(PC1_min_IK, PC1_min_IK, method = "points", label = TRUE)
> plotRefToTarget(PC1_max_IK, PC1_max_IK, method = "points", label = TRUE)
> plotRefToTarget(PC2_max_IK, PC2_max_IK, method = "points", label = TRUE)
> plotRefToTarget(PC2_min_IK, PC2_min_IK, method = "points", label = TRUE)

```

```

> PC1_min_IK = pca.IK$pc.shapes$PC1min
> PC1_max_IK = pca.IK$pc.shapes$PC1max
> PC2_min_IK = pca.IK$pc.shapes$PC2min
> PC2_max_IK = pca.IK$pc.shapes$PC2max

```

```

> plotRefToTarget(PC1_max_IK, PC1_min_IK, method = "points", mag = 2, label = TRUE)

```

```
> plotRefToTarget(PC2_max_IK, PC2_min_IK, method = "points", mag = 2, label = TRUE)
```

```
# The same analyses run with the combined (CMB) sample.
```

```
> plotRefToTarget(PC1_min_CMB, PC1_min_CMB, method = "points", label = TRUE)
> plotRefToTarget(PC1_max_CMB, PC1_max_CMB, method = "points", label = TRUE)
> plotRefToTarget(PC2_min_CMB, PC2_min_CMB, method = "points", label = TRUE)
> plotRefToTarget(PC2_max_CMB, PC2_max_CMB, method = "points", label = TRUE)
```

```
> PC1_min_CMB = pca.CMB$pc.shapes$PC1min
> PC1_max_CMB = pca.CMB$pc.shapes$PC1max
> PC2_min_CMB = pca.CMB$pc.shapes$PC2min
> PC2_max_CMB = pca.CMB$pc.shapes$PC2max
```

```
> plotRefToTarget(PC1_max_CMB, PC1_min_CMB, method = "points", mag = 2, label = TRUE)
> plotRefToTarget(PC2_max_CMB, PC2_min_CMB, method = "points", mag = 2, label = TRUE)
```

Code B4. Code used to compare mean shapes along the PC axes based on age cohort. To run these tests, the GPA analysis must have been previously run.

```
> LSA_mean = mshape(GPA_LSA$coords)
> LSAgroup1_mean = mshape(GPA_LSA$coords[,1:4])
> LSAgroup2_mean = mshape(GPA_LSA$coords[,4:22])
> LSAgroup3_mean = mshape(GPA_LSA$coords[,23:27])
> LSAgroup4_mean = mshape(GPA_LSA$coords[,28:34])
```

```
> onetwo_LSA <- plotRefToTarget(LSAgroup1_mean, LSAgroup2_mean, mag = 2, method = "points", label = TRUE)
> twothree_LSA <- plotRefToTarget(LSAgroup2_mean, LSAgroup3_mean, mag = 2, method = "points", label = TRUE)
> threefour_LSA <- plotRefToTarget(LSAgroup3_mean, LSAgroup4_mean, mag = 2, method = "points", label = TRUE)
> onefour_LSA <- plotRefToTarget(LSAgroup1_mean, LSAgroup4_mean, mag = 2, method = "points", label = TRUE)
```

```
# The same analyses run with the IK sample.
```

```
> IK_mean = mshape(GPA_IK$coords)
> IKgroup1_mean = mshape(GPA_IK$coords[,1:7])
> IKgroup2_mean = mshape(GPA_IK$coords[,8:15])
> IKgroup3_mean = mshape(GPA_IK$coords[,16:21])
```

```

> IKgroup4_mean = mshape(GPA_IK$coords[,22:26])

> onetwo_IK <- plotRefToTarget(IKgroup1_mean, IKgroup2_mean, mag = 2, method =
"points", label = TRUE)
> twothree_IK <- plotRefToTarget(IKgroup2_mean, IKgroup3_mean, mag = 2, method =
"points", label = TRUE)
> threefour_IK <- plotRefToTarget(IKgroup3_mean, IKgroup4_mean, mag = 2, method =
"points", label = TRUE)
> onefour_IK <- plotRefToTarget(IKgroup1_mean, IKgroup4_mean, mag = 2, method =
"points", label = TRUE)

```

The same analyses run with the combined (CMB) sample.

```

> CMB_mean = mshape(GPA_CMB$coords)
> CMBgroup1_mean = mshape(GPA_CMB$coords[,1:10])
> CMBgroup2_mean = mshape(GPA_CMB$coords[,11:33])
> CMBgroup3_mean = mshape(GPA_CMB$coords[,34:47])
> CMBgroup4_mean = mshape(GPA_CMB$coords[,48:60])

> onetwo_CMB <- plotRefToTarget(CMBgroup1_mean, CMBgroup2_mean, method = "points",
mag = 2, label = TRUE)
> twothree_CMB <- plotRefToTarget(CMBgroup2_mean, CMBgroup3_mean, method =
"points", mag = 2, label = TRUE)
> threefour_CMB <- plotRefToTarget(CMBgroup3_mean, CMBgroup4_mean, method =
"points", mag = 2, label = TRUE)
> onefour_CMB <- plotRefToTarget(CMBgroup1_mean, CMBgroup4_mean, method =
"points", mag = 2, label = TRUE)

```

Code B5. Code used to run correlation and t-tests.

Correlation tests were run on age and centroid size. The c() function was used to indicate the raw ages of the individuals in the sample.

```

> LSANew_Ages =
c(0.6,1.11,1.58,1.8,2.5,2.5,3.5,3.5,3.5,3.55,4.15,4.5,4.8,5.5,5.91,5.95,6.45,6.5,6.5,6.5,6.7,7.5,7.5
3,8.5,8.5,10.07,10.85,10.9,11.5,11.2,12.2,12.5,13.1,14.5)

> cor.test(LSANew_Ages, pca.LSA$pc.scores[,1], method = "pearson", conf.level = 0.95)
> cor.test(GPA_LSA$Csize, pca.LSA$pc.scores[,1], method = "pearson", conf.level = 0.95)

```

The same analyses run with the IK sample.

```

> IK2_Ages =
c(0.8,1.8,0.9,0.6,0.7,0.7,0.4,6.7,2.8,2.7,3.4,4.4,5.7,6.9,6.7,10.4,7.2,8.4,9.5,7.1,8.2,9.4,12.9,13.1,1
5,13.1)
> cor.test(IK2_Ages, pca.IK$pc.scores[,1], method = "pearson", conf.level = 0.95)
> cor.test(GPA_IK$Csize, pca.IK$pc.scores[,1], method = "pearson", conf.level = 0.95)

```

The same analyses run with the combined (CMB) sample.

```

> CMB2_Ages =
c(1.8,1.5,0.6,0.8,1.8,0.9,0.6,0.7,0.7,0.4,2.5,2.5,4.5,3.5,4.5,5.5,3.5,6.5,3.5,5.5,2,6.5,2.5,5.5,4.5,6.7
,2.8,2.7,3.4,4.4,5.7,6.9,6.7,10.5,7.5,8.5,9.5,7.5,8.5,9.5,8.5,10.4,7.2,8.4,9.5,7.1,8.2,9.4,11.5,14.5,1
4.5,11.5,14.5,15.5,11.5,12.5,12.9,13.1,15,13.1)
> cor.test(CMB2_Ages, pca.CMB$pc.scores[,1], method = "pearson", conf.level = 0.95)
> cor.test(GPA_CMB$Csize, pca.CMB$pc.scores[,1], method = "pearson", conf.level = 0.95)

```

An additional correlation test was run with the combined sample comparing centroid size to age.

```

> CMB_cor = cor.test(GPA_CMB$Csize, CMB2_Ages, method = "pearson", conf.level = 0.95)

```

Code B6. Code used for adult sample analysis. For later use in maturation trajectory analysis, a GPA was also conducted on the youngest five individuals of the LSA, IK and CMB samples from the juvenile database.

A similar code as above was followed except using the 20 adult individuals to perform GPA and PCA analyses.

```

> LSAadults = read.csv("LSAadults.csv", header = TRUE, sep = ",")
> LSAadults_mtx = as.matrix(LSAadults[,2:4])
> LSAadults_arr = arrayspecs(LSAadults_mtx, 82, 3)
> GPA_LSAadults = gpagen(LSAadults_arr, PrinAxes = TRUE, max.iter = NULL, ProcD =
TRUE, Proj = TRUE, print.progress = TRUE)

> LSAadults_mean = mshape(GPA_LSAadults$coords)
> LSAadults_CS = GPA_LSAadults$Csize

```

Code for the youngest five LSA individuals from the juvenile subset.

```

> LSAyoungest = read.csv("LSAyoungest.csv", header = TRUE, sep = ",")
> LSAyoungest_mtx = as.matrix(LSAyoungest[,2:4])
> LSAyoungest_arr = arrayspecs(LSAyoungest_mtx, 82, 3)

```

```
> GPA_LSAyoungest = gpagen(LSAyoungest_arr, PrinAxes = TRUE, max.iter = NULL, ProcD = TRUE, Proj = TRUE, print.progress = TRUE)
```

```
> LSAyoungest_mean = mshape(GPA_LSAyoungest$coords)
```

```
> LSAyoungest_CS = GPA_LSAyoungest$Csize
```

```
# The same analyses run with the IK sample.
```

```
> IKadults = read.csv("IKAdults.csv", header = TRUE, sep = ",")
```

```
> IKadults_mtx = as.matrix(IKadults[,2:4])
```

```
> IKadults_arr = arrayspecs(IKadults_mtx, 82, 3)
```

```
> GPA_IKadults = gpagen(IKadults_arr, PrinAxes = TRUE, max.iter = NULL, ProcD = TRUE, Proj = TRUE, print.progress = TRUE)
```

```
> IKadults_mean = mshape(GPA_IKadults$coords)
```

```
> IKadults_CS = GPA_IKadults$Csize
```

```
# Code for the youngest five IK individuals from the juvenile subset.
```

```
> IKyoungest = read.csv("IKyoungest.csv", header = TRUE, sep = ",")
```

```
> IKyoungest_mtx = as.matrix(IKyoungest[,2:4])
```

```
> IKyoungest_arr = arrayspecs(IKyoungest_mtx, 82, 3)
```

```
> GPA_IKyoungest = gpagen(IKyoungest_arr, PrinAxes = TRUE, max.iter = NULL, ProcD = TRUE, Proj = TRUE, print.progress = TRUE)
```

```
> IKyoungest_mean = mshape(GPA_IKyoungest$coords)
```

```
> IKyoungest_CS = GPA_IKyoungest$Csize
```

```
# The same analyses run with the combined (CMB) sample.
```

```
> CMBadults = read.csv("AdultIndividuals.csv", header = TRUE, sep = ",")
```

```
> CMBadults_mtx = as.matrix(CMBadults[,2:4])
```

```
> CMBadults_arr = arrayspecs(CMBadults_mtx, 82, 3)
```

```
> GPA_CMBadults = gpagen(CMBadults_arr, PrinAxes = TRUE, max.iter = NULL, ProcD = TRUE, Proj = TRUE, print.progress = TRUE)
```

```
> CMBadults_mean = mshape(GPA_CMBadults$coords)
```

```
> CMBadults_CS = GPA_CMBadults$Csize
```

```
# Code for the youngest five CMB individuals from the juvenile subset.
```

```
> CMByoungest = read.csv("CMByoungest.csv", header = TRUE, sep = ",")
```

```
> CMByoungest_mtx = as.matrix(CMByoungest[,2:4])
```

```
> CMByoungest_arr = arrayspecs(CMByoungest_mtx, 82, 3)
```

```

> GPA_CMByoungest = gpagen(CMByoungest_arr, PrinAxes = TRUE, max.iter = NULL,
ProcD = TRUE, Proj = TRUE, print.progress = TRUE)

> CMByoungest_mean = mshape(GPA_CMByoungest$coords)
> CMByoungest_CS = GPA_CMByoungest$Csize

# Code for PCA combined adults sample and customized PCA plot

> pca.CMBadults = plotTangentSpace(GPA_CMBadults$coords, warpgrids = TRUE, label =
TRUE)
> plotted_axes = c(1,2)
> GPA_CMBadults_col = c(1,1,1,1,1,1,1,1,1,2,2,2,2,2,2,2,2,2)
> GPA_CMBadults_shp = c(1,1,1,1,1,2,2,2,2,2,3,3,3,3,4,4,4,4,4)
> par(mar=c(6,4,4,4)+0.8)
> plot(pca.CMBadults$pc.scores[,plotted_axes], main = 'Principal Component Analysis of
Combined Adults', pch = c(19,6,19,6), xlab = "PC1", ylab = "PC2", col =
c('red','blue')[GPA_CMBadults_col])
#text(pca.CMBadults$pc.scores[,plotted_axes], rownames(pca.CMBadults$pc.scores[,1:2]), pos
= 4, cex = .5)
legend('bottomleft',cex = 0.8,legend = c('Female','Male'),pch = 19,title = 'Sex',col = c('red','blue'))
legend('topleft', cex = 0.8, legend = c('LSA','IK'), pch = c(19,6), title = "Population", col =
'black')

# A PCA was run to determine if the mean shape distribution is different between the male and
female PC scores in each sample.

> pca.LSAadults = plotTangentSpace(GPA_LSAadults$coords, warpgrids = TRUE, label =
TRUE)

> plotted_axes = c(1,2)
> GPA_LSAadults_col = c(1,1,1,1,1,2,2,2,2,2)
> GPA_LSAadults_shp = c(1,1,1,1,1,2,2,2,2,2)

> plot(pca.LSAadults$pc.scores[,plotted_axes], main = 'Principal Component Analysis of LSA
Adults', pch = c(19), xlab = "PC1", ylab = "PC2",col = c('red','blue')[GPA_LSAadults_col])
#text(pca.LSAadults$pc.scores[,plotted_axes], rownames(pca.LSAadults$pc.scores[,1:2]), pos =
4, cex = 0.5)

> legend('bottomleft',cex = 0.6,legend = c('Female','Male'),pch = 19,title = 'Sex',col =
c('red','blue'))

```

```

# The same analyses run with the IK sample.

> pca.IKadults = plotTangentSpace(GPA_IKadults$coords, warpgrids = TRUE, label = TRUE)

```

```

> plotted_axes = c(1,2)
> GPA_IKadults_col = c(1,1,1,1,1,2,2,2,2,2)
> GPA_IKadults_shp = c(1,1,1,1,1,2,2,2,2,2)
> plot(pca.IKadults$pc.scores[,plotted_axes], main = 'Principal Component Analysis of IK
Adults', pch = c(19), xlab = "PC1", ylab = "PC2",col = c('red','blue')[GPA_IKadults_col])
#text(pca.IKadults$pc.scores[,plotted_axes], rownames(pca.IKadults$pc.scores[,1:2]), pos = 4,
cex = 0.5)
> legend('bottomleft',cex = 0.6,legend = c('Female','Male'),pch = 19,title = 'Sex',col =
c('red','blue'))

```

Code B7. Code used for correlation and t-tests of adult population. Code in B6 required for certain parameters of the statistical tests.

```

> cor.test(GPA_CMBadults$Csize, pca.CMBadults$pc.scores[,1], method = "pearson",
conf.level = 0.95)
> cor.test(GPA_CMBadults$Csize, pca.CMBadults$pc.scores[,2], method = "pearson",
conf.level = 0.95)

```

A t-test to determine if IK and LSA differ in size.

```

> t.test(GPA_LSAadults$Csize, GPA_IKadults$Csize, var.equal = TRUE)

```

A t-test to determine whether females and males differ in centroid size based on each sample.

```

> LSAadults_Sex = c(1,1,1,1,1,2,2,2,2,2)
> LSA_CSt.test = t.test(GPA_LSAadults$Csize ~ LSAadults_Sex, var.equal = TRUE)

```

```

> IKadults_Sex = c(1,1,1,1,1,2,2,2,2,2)
> IK_CSt.test = t.test(GPA_IKadults$Csize ~ IKadults_Sex, var.equal = TRUE)

```

```

> CMBadults_Sex = c(1,1,1,1,1,1,1,1,1,2,2,2,2,2,2,2,2,2,2)
> CMB_CSt.test = t.test(GPA_CMBadults$Csize ~ CMBadults_Sex, var.equal = TRUE)

```

A t-test to determine whether the combined sample was significantly different based on sample

```

> CMB_Sample = c(1,1,1,1,1,2,2,2,2,2,1,1,1,1,1,2,2,2,2,2)
> CMB_Samplet.test = t.test(GPA_CMBadults$Csize ~ CMB_Sample, var.equal = TRUE)

```

Code B8. Code used for maturation trajectories. The code in B6 was required to be run before running this code. A new GPA analysis was run on the combined juvenile subset with the individuals in increasing age.

```
# Code for size maturity calculations.
```

```
> CMBage = read.csv("CombinedDataAscendingAge.csv", header = TRUE, sep = ",")
> CMBage_mtx = as.matrix(CMBage[,2:4])
> CMBage_arr = arrayspecs(CMBage_mtx, 82, 3)
> GPA_CMBage = gpagen(CMBage_arr, PrinAxes = TRUE, max.iter = NULL, ProcD = TRUE,
Proj = TRUE, print.progress = TRUE)
> pca.CMBadults = plotTangentSpace(GPA_CMBadults$coords, warpgrids = TRUE, label =
TRUE)

> plotted_axes = c(1,2)
> GPA_CMBadults_col = c(1,1,1,1,1,1,1,1,1,1,2,2,2,2,2,2,2,2,2,2)
> GPA_CMBadults_shp = c(1,1,1,1,1,2,2,2,2,2,3,3,3,3,3,4,4,4,4,4)
> par(mar=c(6,4,4,4)+0.8)
> plot(pca.CMBadults$pc.scores[,plotted_axes], main = 'Principal Component Analysis of
Combined Adults', pch = c(19,6,19,6), xlab = "PC1", ylab = "PC2", col =
c('red','blue')[GPA_CMBadults_col])
#text(pca.CMBadults$pc.scores[,plotted_axes], rownames(pca.CMBadults$pc.scores[,1:2]), pos
= 4, cex = .5)
legend('bottomleft',cex = 0.8,legend = c('Female','Male'),pch = 19,title = 'Sex',col = c('red','blue'))
legend('topleft', cex = 0.8, legend = c('LSA','IK'), pch = c(19,6), title = "Population", col =
'black')

> CMBadults_CS = GPA_CMBadults$Csize
> CMBadults_CSmean = mean(CMBadults_CS)

#Mean CS value of each specimen, then re-expressed as percentage of CMBadults_CSmean
GPA_CMBage$Csize in an excel document
> write.csv(GPA_CMBage$Csize, "CombinedPopulationCSAscendingAge.csv")
> write.csv(CMBadults_CSmean, "AdultMeanCS.csv")
```

```
# Code for shape maturity calculations.
```

```
# Loading the package "shapes" is required for this part of analysis.
```

```
> library(shapes)
```

```
> CMBage = read.csv("CombinedDataAscendingAge.csv", header = TRUE, sep = ",")
> CMBage_mtx = as.matrix(CMBage[,2:4])
> CMBage_arr = arrayspecs(CMBage_mtx, 82, 3)
> GPA_CMBage = gpagen(CMBage_arr, PrinAxes = TRUE, max.iter = NULL, ProcD = TRUE,
Proj = TRUE, print.progress = TRUE)
> CMBage_mean = mshape(GPA_CMBage$coords)
```

```

> CMByoungest = read.csv("CMByoungest.csv", header = TRUE, sep = ",")
> CMByoungest_mtx = as.matrix(CMByoungest[2:4])
> CMByoungest_arr = arrayspecs(CMByoungest_mtx, 82, 3)
> GPA_CMByoungest = gpagen(CMByoungest_arr, PrinAxes = TRUE, max.iter = NULL,
ProcD = TRUE, Proj = TRUE, print.progress = TRUE)
> CMByoungest_mean = mshape(GPA_CMByoungest$coords)

> CMBoldest = read.csv("AdultIndividuals.csv", header = TRUE, sep = ",")
> CMBoldest_mtx = as.matrix(CMBoldest[2:4])
> CMBoldest_arr = arrayspecs(CMBoldest_mtx, 82, 3)
> GPA_CMBoldest = gpagen(CMBoldest_arr, PrinAxes = TRUE, max.iter = NULL, ProcD =
TRUE, Proj = TRUE, print.progress = TRUE)
> CMBoldest_mean = mshape(GPA_CMBoldest$coords)

> PD0 = procdist(CMByoungest_mean, GPA_CMBage$coords[,1], type = "full", reflect =
FALSE)
> PD1 = procdist(GPA_CMBage$coords[,1], GPA_CMBage$coords[,2], type = "full", reflect =
FALSE)
> PD2 = procdist(GPA_CMBage$coords[,2], GPA_CMBage$coords[,3], type = "full", reflect =
FALSE)
> PD3 = procdist(GPA_CMBage$coords[,3], GPA_CMBage$coords[,4], type = "full", reflect =
FALSE)
> PD4 = procdist(GPA_CMBage$coords[,4], GPA_CMBage$coords[,5], type = "full", reflect =
FALSE)
> PD5 = procdist(GPA_CMBage$coords[,5], GPA_CMBage$coords[,6], type = "full", reflect =
FALSE)
> PD6 = procdist(GPA_CMBage$coords[,6], GPA_CMBage$coords[,7], type = "full", reflect =
FALSE)
> PD7 = procdist(GPA_CMBage$coords[,7], GPA_CMBage$coords[,8], type = "full", reflect =
FALSE)
> PD8 = procdist(GPA_CMBage$coords[,8], GPA_CMBage$coords[,9], type = "full", reflect =
FALSE)
> PD9 = procdist(GPA_CMBage$coords[,9], GPA_CMBage$coords[,10], type = "full", reflect
= FALSE)
> PD10 = procdist(GPA_CMBage$coords[,10], GPA_CMBage$coords[,11], type = "full",
reflect = FALSE)
> PD11 = procdist(GPA_CMBage$coords[,11], GPA_CMBage$coords[,12], type = "full",
reflect = FALSE)
> PD12 = procdist(GPA_CMBage$coords[,12], GPA_CMBage$coords[,13], type = "full",
reflect = FALSE)
> PD13 = procdist(GPA_CMBage$coords[,13], GPA_CMBage$coords[,14], type = "full",
reflect = FALSE)
> PD14 = procdist(GPA_CMBage$coords[,14], GPA_CMBage$coords[,15], type = "full",
reflect = FALSE)

```

```
> PD15 = procdist(GPA_CMBage$coords[,15], GPA_CMBage$coords[,16], type = "full",
reflect = FALSE)
> PD16 = procdist(GPA_CMBage$coords[,16], GPA_CMBage$coords[,17], type = "full",
reflect = FALSE)
> PD17 = procdist(GPA_CMBage$coords[,17], GPA_CMBage$coords[,18], type = "full",
reflect = FALSE)
> PD18 = procdist(GPA_CMBage$coords[,18], GPA_CMBage$coords[,19], type = "full",
reflect = FALSE)
> PD19 = procdist(GPA_CMBage$coords[,19], GPA_CMBage$coords[,20], type = "full",
reflect = FALSE)
> PD20 = procdist(GPA_CMBage$coords[,20], GPA_CMBage$coords[,21], type = "full",
reflect = FALSE)
> PD21 = procdist(GPA_CMBage$coords[,21], GPA_CMBage$coords[,22], type = "full",
reflect = FALSE)
> PD22 = procdist(GPA_CMBage$coords[,22], GPA_CMBage$coords[,23], type = "full",
reflect = FALSE)
> PD23 = procdist(GPA_CMBage$coords[,23], GPA_CMBage$coords[,24], type = "full",
reflect = FALSE)
> PD24 = procdist(GPA_CMBage$coords[,24], GPA_CMBage$coords[,25], type = "full",
reflect = FALSE)
> PD25 = procdist(GPA_CMBage$coords[,25], GPA_CMBage$coords[,26], type = "full",
reflect = FALSE)
> PD26 = procdist(GPA_CMBage$coords[,26], GPA_CMBage$coords[,27], type = "full",
reflect = FALSE)
> PD27 = procdist(GPA_CMBage$coords[,27], GPA_CMBage$coords[,28], type = "full",
reflect = FALSE)
> PD28 = procdist(GPA_CMBage$coords[,28], GPA_CMBage$coords[,29], type = "full",
reflect = FALSE)
> PD29 = procdist(GPA_CMBage$coords[,29], GPA_CMBage$coords[,30], type = "full",
reflect = FALSE)
> PD30 = procdist(GPA_CMBage$coords[,30], GPA_CMBage$coords[,31], type = "full",
reflect = FALSE)
> PD31 = procdist(GPA_CMBage$coords[,31], GPA_CMBage$coords[,32], type = "full",
reflect = FALSE)
> PD32 = procdist(GPA_CMBage$coords[,32], GPA_CMBage$coords[,33], type = "full",
reflect = FALSE)
> PD33 = procdist(GPA_CMBage$coords[,33], GPA_CMBage$coords[,34], type = "full",
reflect = FALSE)
> PD34 = procdist(GPA_CMBage$coords[,34], GPA_CMBage$coords[,35], type = "full",
reflect = FALSE)
> PD35 = procdist(GPA_CMBage$coords[,35], GPA_CMBage$coords[,36], type = "full",
reflect = FALSE)
> PD36 = procdist(GPA_CMBage$coords[,36], GPA_CMBage$coords[,37], type = "full",
reflect = FALSE)
> PD37 = procdist(GPA_CMBage$coords[,37], GPA_CMBage$coords[,38], type = "full",
reflect = FALSE)
```

```
> PD38 = procdist(GPA_CMBage$coords[,38], GPA_CMBage$coords[,39], type = "full",
reflect = FALSE)
> PD39 = procdist(GPA_CMBage$coords[,39], GPA_CMBage$coords[,40], type = "full",
reflect = FALSE)
> PD40 = procdist(GPA_CMBage$coords[,40], GPA_CMBage$coords[,41], type = "full",
reflect = FALSE)
> PD41 = procdist(GPA_CMBage$coords[,41], GPA_CMBage$coords[,42], type = "full",
reflect = FALSE)
> PD42 = procdist(GPA_CMBage$coords[,42], GPA_CMBage$coords[,43], type = "full",
reflect = FALSE)
> PD43 = procdist(GPA_CMBage$coords[,43], GPA_CMBage$coords[,44], type = "full",
reflect = FALSE)
> PD44 = procdist(GPA_CMBage$coords[,44], GPA_CMBage$coords[,45], type = "full",
reflect = FALSE)
> PD45 = procdist(GPA_CMBage$coords[,45], GPA_CMBage$coords[,46], type = "full",
reflect = FALSE)
> PD46 = procdist(GPA_CMBage$coords[,46], GPA_CMBage$coords[,47], type = "full",
reflect = FALSE)
> PD47 = procdist(GPA_CMBage$coords[,47], GPA_CMBage$coords[,48], type = "full",
reflect = FALSE)
> PD48 = procdist(GPA_CMBage$coords[,48], GPA_CMBage$coords[,49], type = "full",
reflect = FALSE)
> PD49 = procdist(GPA_CMBage$coords[,49], GPA_CMBage$coords[,50], type = "full",
reflect = FALSE)
> PD50 = procdist(GPA_CMBage$coords[,50], GPA_CMBage$coords[,51], type = "full",
reflect = FALSE)
> PD51 = procdist(GPA_CMBage$coords[,51], GPA_CMBage$coords[,52], type = "full",
reflect = FALSE)
> PD52 = procdist(GPA_CMBage$coords[,52], GPA_CMBage$coords[,53], type = "full",
reflect = FALSE)
> PD53 = procdist(GPA_CMBage$coords[,53], GPA_CMBage$coords[,54], type = "full",
reflect = FALSE)
> PD54 = procdist(GPA_CMBage$coords[,54], GPA_CMBage$coords[,55], type = "full",
reflect = FALSE)
> PD55 = procdist(GPA_CMBage$coords[,55], GPA_CMBage$coords[,56], type = "full",
reflect = FALSE)
> PD56 = procdist(GPA_CMBage$coords[,56], GPA_CMBage$coords[,57], type = "full",
reflect = FALSE)
> PD57 = procdist(GPA_CMBage$coords[,57], GPA_CMBage$coords[,58], type = "full",
reflect = FALSE)
> PD58 = procdist(GPA_CMBage$coords[,58], GPA_CMBage$coords[,59], type = "full",
reflect = FALSE)
> PD59 = procdist(GPA_CMBage$coords[,59], GPA_CMBage$coords[,60], type = "full",
reflect = FALSE)
> PD60 = procdist(GPA_CMBage$coords[,60], CMBage_mean, type = "full", reflect = FALSE)
```

```
> PD61 = procdist(GPA_CMBage$coords[,60], CMBadults_mean, type = "full", reflect = FALSE)
```

Appendix C: Sliding Average Approach

Example C1. Example of sliding trajectory as outlined by Wilson et al. (2015). This method was applied to the data to reduce overestimating the true maturation trajectory.

A = juvenile mean shape

B = adult mean shape

1-5 are individual juveniles in order youngest to oldest.

Cumulative trajectory length (**X**) is the Procrustes Distance (->) between each parameter.

$$\mathbf{X} = (A \rightarrow 1) + (1 \rightarrow 2) + (2 \rightarrow 3) + (3 \rightarrow 4) + (4 \rightarrow 5) + (5 \rightarrow 6) \dots (y \rightarrow B)$$

Each juvenile will have a single distance representing its position along trajectory “x”. For example, individual three:

$$\text{Distance 3} = (A \rightarrow 1) + (1 \rightarrow 2) + (2 \rightarrow 3)$$

In order to avoid overestimating the maturation trajectory, the individual distances and associated ages were averaged, acting as a smoothing function:

Individual	Age	Procrustes Distance
A	Mean	0.008
1	0.05	0.08
2	0.5	0.8
3	1	0.81
4	1.5	0.811
5	2	1.0
Etc.		

Groups are created by averaging the values of age and Procrustes Distance.

Group 1 = A (the mean of the five youngest)

Group 2 = mean of individual 1-5

Group 3 = mean of individuals 3-7

Group 4 = mean of individuals 5-9

Etc.

Group	Age (cumulative)	Procrustes Distance (cumulative)
1	$(0.05 + 0.5 + 1 + 1.5 + 2) / 5$	$(0.008 + 0.08 + 0.8 + 0.81 + 0.811 + 1.0) / 5$
Etc.		

Once this information is obtained, re-express the group average Procrustes Distances relative to the last group (as a percentage of your last group). For group 1 maturity:

$$\text{Maturity 1} = [(0.008 + 0.08 + 0.8 + 0.81 + 0.811 + 1.0) / 5] / \mathbf{X}$$

Etc.

This calculation is performed for each maturity group.